2017

Assessing Interactions between Estuary Water Quality and Terrestrial Land Cover in Hurricane Events with Multi-sensor Remote Sensing

Chandan Mostafiz
University of Central Florida

ASSESSING INTERACTIONS BETWEEN ESTUARY WATER QUALITY AND TERRESTRIAL LAND COVER IN HURRICANE EVENTS WITH MULTI-SENSOR REMOTE SENSING

by

CHANDAN MOSTAFIZ
B.S. Bangladesh University of Engineering and Technology, 2014

A thesis submitted in partial fulfillment of the requirements
for the degree of Master of Science
in the Department of Civil, Environmental, and Construction Engineering
in the College of Engineering and Computer Science
at the University of Central Florida
Orlando, Florida

Fall Term
2017

Major Professor: Ni-Bin Chang

ABSTRACT

Estuaries are environmentally, ecologically and environmentally important places as they act as a meeting place for land, freshwater and marine ecosystems. They are also called nurseries of the sea as they often provide nesting and feeding habitats for many aquatic plants and animals. These estuaries also withstand the worst of some natural disasters, especially hurricanes. The estuaries as well as the harbored ecosystems undergo significant changes in terms of water quality, vegetation cover etc. and these components are interrelated. When hurricane makes landfall it is necessary to assess the damages as quickly as possible as restoration and recovery processes are time-sensitive. However, assessment of physical damages through inspection and survey and assessment of chemical and nutrient component changes by laboratory testing are time-consuming processes. This is where remote sensing comes into play. With the help of remote sensing images and regression analysis, it is possible to reconstruct water quality maps of the estuary affected. The damage sustained by the vegetation cover of the adjacent coastal watershed can be assessed using Normalized Difference Vegetation Index (NDVI) The water quality maps together with NDVI maps help observe a dynamic sea-land interaction due to hurricane landfall. The observation of hurricane impacts on a coastal watershed can be further enhanced by use of tasseled cap transformation (TCT). TCT plots provide information on a host of land cover conditions with respect to soil moisture, canopy and vegetation cover. The before and after TCT plots help assess the damage sustained in a hurricane event and also see the progress of recovery. Finally, the use of synthetic images obtained by use of data fusion will help close the gap of low temporal resolution of Landsat satellite and this will create a more robust monitoring system.

ACKNOWLEDGMENTS

First and foremost praise is to Allah, the Most Gracious, the Most Merciful. I am thankful to Allah, the Almighty; who has given me the opportunity to pursue my Master's degree at a prestigious university like UCF. I am also grateful to Him for the courage, guidance and mercy that He has bestowed upon me to complete the research works as well as complete the degree requirements.

Secondly, I would like to express my deepest gratitude to my adviser, Dr. Ni-bin Chang for providing me with valuable instructions and guidance in every step of the research works. Without his impressive kindness and most importantly, his unwavering patience, this research work would not have materialized. I would also like to express my thanks to Dr. Martin Wanielista and Dr. Kelly Kibler for their advice on the improvement of the research. Special thanks to Dr. Sanaz Imen for going to painstaking lengths to mentor me during my initial days of conducting research and to my group members of the lab namely Dan Wen, Qi Lu and Justin Joyce for their encouragement and support throughout my time here.

Lastly, I would like to express my deep gratitude to my parents, my brother and close friends and seniors for their support. Special thanks and gratitude to my mother who has been the pillar of my strength throughout my Masters career here at UCF. Thanks also to all office members of CECE department who has always helped me promptly and with a smile whenever I required help to complete various official tasks.

TABLE OF CONTENTS

LIST OF FIGURES

LIST OF TABLES

CHAPTER 1: INTRODUCTION

1.1 Impacts of Hurricanes on Estuaries and Coastal Watersheds

Estuaries harbor ecosystems that are among the most diverse, economically and environmentally significant, productive and hydrologically variable (Paerl et al., 2006; Nilson and Cronin, 1981). The reason for their productive nature is that these estuarine ecosystems receive the bulk of riverine and coastal watershed discharge (Paerl et al., 2006). It is also important to note that these estuarine ecosystems support about 75% of the world's population (Vitousek et al., 1997). Due to these natural and anthropogenic activities, they receive a host of land based nutrients via the surface runoff, atmospheric deposition and groundwater discharge. A large percentage of these nutrients are transported to the estuaries via the rivers running through urban and agricultural watersheds (Howarth et al., 1996, Jarowski et al., 1997; Paerl et al., 2002).

These estuaries and the aquatic ecosystems that the estuaries harbor are subject to various natural hazards. The most prominent among them are the hurricanes. Hurricanes are swiftly rotation storm systems accompanied by strong winds, thunderstorms and heavy rains. The disturbances generated by hurricanes can cause abrupt and extensive disturbances in coastal estuaries (Greening et al., 2006). The disturbances affect the water quality parameters such as total nitrogen, total phosphorus, dissolved oxygen, dissolved organic carbon, salinity etc. (Edmiston et al., 2008; Mallin et al., 2002; Mallin et al., 1999; Steward et al., 2006). In addition, the hurricanes cause significant damage to the coastal forests and vegetation cover by way of large-scale tree felling, trunk snapping and defoliation (Valeila et al., 1996, Loope et al., 1994).

After a hurricane impact, the speed of recovery and relief efforts depends on how quickly the damage was assessed, where the most damage occurred and the areas where relief effort takes priority. Onsite assessment of damages may take weeks to investigate and finally obtain the results.

That is why there is a need for development of a much quicker method of assessment that, in a broad sense may help local and federal authorities to prioritize relief and rescue operations as well as conduct environmental restoration works so that the disturbances suffered by the ecosystems in the estuaries as well as water quality changes may be mitigated in the shortest possible time.

The need for real time monitoring and assessment has brought remote sensing and GIS to the forefront for this purpose. Remote sensing has been in use to monitor the estuarine ecosystems for quite a while now and models have been developed to predict future changes in them (Noremberg et al., 2006.), Remote sensing is also being used in the estuarine water quality monitoring (Yang, 2005). Remote sensing makes near real time retrieval of data, which makes it an important tool in the assessment of water quality and vegetation cover of coastal watersheds and estuaries.

1.2 Research objectives.

This thesis will demonstrate how the assessment of water quality and vegetation cover in the event of hurricane event can be done through the help of remote sensing by the following: (1) Developing models from remotely sensed and ground truth data for parameter prediction and using the predicted results to observe the dynamics of sea-land interaction with earth systems process (Chapter 2); (2) Using tasseled cap transformation to assess and compare vegetation cover condition of two hurricane events and (3) Incorporating the use of data fusion along with tasseled cap transformation to assess hurricane impact on a watershed.

The research objectives indicated here introduce three remote sensing tools. These tools will be used in completion of the research works. The work flow can be shown in the flow chart below:

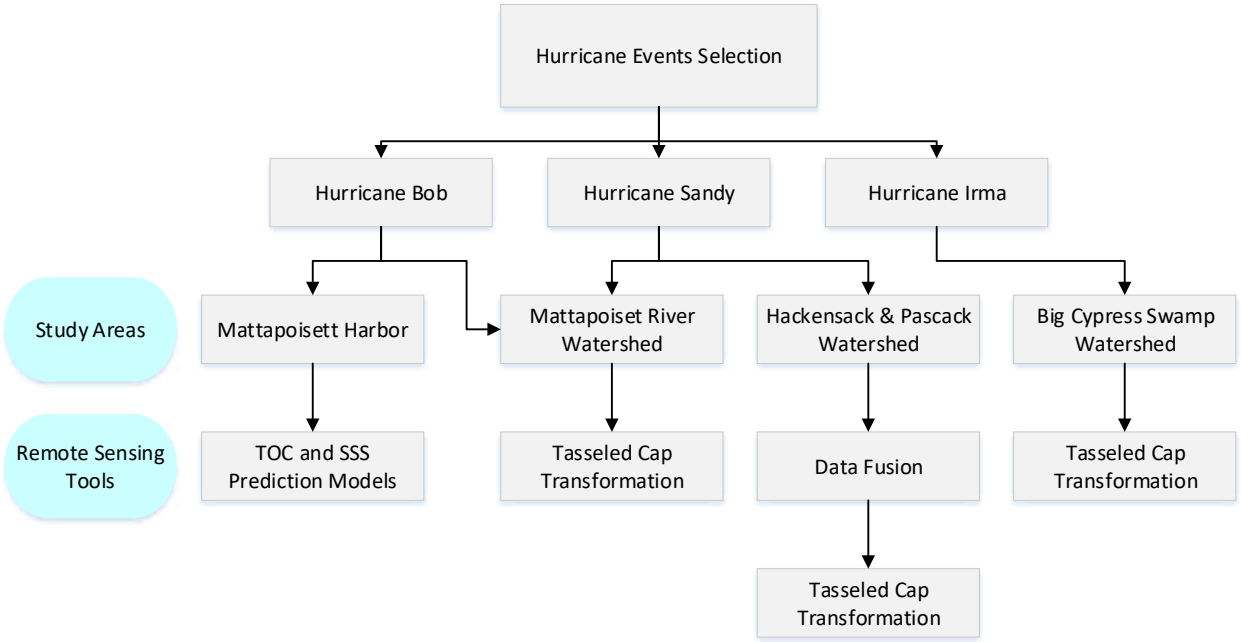

Figure 1-1: Workflow of the research presented in the thesis.

1.3 Limitations

The works presented in this thesis is limited to coastal watershed boundaries near estuaries and individual hurricane events. The works are also limited to observation of two water quality parameters and vegetation cover of the watersheds.

1.4 References

Edmiston, H. L., Fahrny, S. A., Lamb, M. S., Levi, L. K., Wanat, J. M., Avant, J. S., ... & Selly, N. C. (2008). Tropical storm and hurricane impacts on a Gulf Coast estuary: Apalachicola Bay, Florida. *Journal of Coastal Research*, 38-49.

Greening, H., Doering, P., & Corbett, C. (2006). Hurricane impacts on coastal ecosystems. *Estuaries and Coasts*, *29*(6), 877-879.

Howarth, R. W., Billen, G., Swaney, D., Townsend, A., Jaworski, N., Lajtha, K., ... & Berendse, F. (1996). Regional nitrogen budgets and riverine N & P fluxes for the drainages to the

North Atlantic Ocean: Natural and human influences. In *Nitrogen cycling in the North Atlantic Ocean and its watersheds* (pp. 75-139). Springer Netherlands.

Jaworski, N. A., Howarth, R. W., & Hetling, L. J. (1997). Atmospheric deposition of nitrogen oxides onto the landscape contributes to coastal eutrophication in the northeast United States. *Environmental Science & Technology*, *31*(7), 1995-2004.

Loope, L., Duever, M., Herndon, A., Snyder, J., & Jansen, D. (1994). Hurricane impact on uplands and freshwater swamp forest. *BioScience*, *44*(4), 238-246.

Mallin, M. A., Posey, M. H., Shank, G. C., McIver, M. R., Ensign, S. H., & Alphin, T. D. (1999). Hurricane effects on water quality and benthos in the Cape Fear watershed: natural and anthropogenic impacts. *Ecological Applications*, *9*(1), 350-362.

Mallin, M. A., Posey, M. H., McIVER, M. R., Parsons, D. C., Ensign, S. H., & Alphin, T. D. (2002). Impacts and Recovery from Multiple Hurricanes in a Piedmont–Coastal Plain River System: Human development of floodplains greatly compounds the impacts of hurricanes on water quality and aquatic life. *AIBS Bulletin*, *52*(11), 999-1010.

Neilson,B, Cronin,L (Eds.), Estuaries and Nutrients, Humana Press, Clifton, NY (1981)

Paerl, H. W., Dyble, J., Twomey, L., Pinckney, J. L., Nelson, J., & Kerkhof, L. (2002). Characterizing man-made and natural modifications of microbial diversity and activity in coastal ecosystems. *Antonie van Leeuwenhoek*, *81*(1-4), 487-507.

Noernberg, M. A., Lautert, L. F. C., Araújo, A. D., Marone, E., Angelotti, R., Netto Jr, J. P. B., & Krug, L. A. (2006). Remote sensing and GIS integration for modelling the Paranaguá estuarine complex-Brazil. *Journal of Coastal Research*, 1627-1631.

Paerl, H. W. (2006). Assessing and managing nutrient-enhanced eutrophication in estuarine and coastal waters: Interactive effects of human and climatic perturbations. *Ecological Engineering*, *26*(1), 40-54.

Steward, J. S., Virnstein, R. W., Lasi, M. A., Morris, L. J., Miller, J. D., Hall, L. M., & Tweedale, W. A. (2006). The impacts of the 2004 hurricanes on hydrology, water quality, and seagrass in the central Indian River Lagoon, Florida. *Estuaries and Coasts*, *29*(6), 954-965.

Valiela, I., Peckol, P., D'Avanzo, C., Lajtha, K., Kremer, J., Geyer, W. R., ... & Crawford, R. (1996). Hurricance Bob on Cape Cod. *American Scientist*, *84*(2), 154-165.

Vitousek, P. M., Mooney, H. A., Lubchenco, J., & Melillo, J. M. (1997). Human domination of Earth's ecosystems. *Science*, *277*(5325), 494-499.

Yang, X. (2005). Remote sensing and GIS applications for estuarine ecosystem analysis: an overview. *International Journal of Remote Sensing*, *26*(23), 5347-5356.

CHAPTER 2: RECONSTRUCTION OF SEA-LAND INTERACTION BETWEEN VEGETATION COVER AND WATER QUALITY CONSTITUENTS IN MATTAPOISETT HARBOR AREA DURING 1991 HURRICANE BOB EVENT

2.1 Introduction

Total Organic Carbon (TOC) can be defined as the measure of organic molecules of carbon in water. It is the sum of dissolved organic carbon (DOC) and particulate organic carbon (POC); it is an important water quality parameter because of its effects on pH, redox reactions, and bioavailability of metals and sorption capacity of suspended solids with regard to hydrophobic organic chemicals. Both natural and anthropogenic sources introduce TOC to surface waters (Schumacher, 2002). TOC can occur naturally due to degraded vegetation and animal matter. Anthropogenic sources may include fertilizers washed down by storm run-off, irrigation return flows, pesticides, solvents from water treatment plants etc. Salinity refers to the measurement of the concentration of dissolved salts in water. It is usually expressed in psu (practical salinity unit). The Practical Salinity Scale defines salinity in terms of the conductivity ratio of a sample to that of a solution of 32.4356 g of KCl at 15°C in a 1 kg solution. A sample of seawater at 15°C with a conductivity equal to this KCl solution has a salinity of exactly 35 practical salinity units (psu).

Earth systems processes such as tidal waves, the wind, precipitation etc. can have a huge influence on the distribution behavior of water quality parameters such as TOC and SSS Particularly for coastal areas, earth system processes can have drastic effects on TOC and SSS concentrations. Precipitation can impact coastal waters by having an increasing or decreasing effect on both TOC and Sea Surface Salinity (SSS) concentrations (Delcroix et al., 1996; Meyer et al., 1983). Subsequently, runoff from precipitation over coastal watersheds can affect larger

coastal waterbodies such as bays and harbors due to downstream flows causing changes in TOC and SSS concentrations (Nuttle et al, 2000).

Given the impacts of earth system processes on water quality parameters such TOC and SSS, it is important to monitor their changes temporally and spatially. Sources of TOC are both natural and anthropogenic in form while the source of salinity is solely natural such as from coastal waterbodies. Particularly for coastal areas, many of the changes in TOC and SSS can be attributed to not only earth system processes but via pathways for which those processes interact. A primary example of such interaction between earth system processes and pathways between them are watersheds. Watersheds are areas where major sources of water such as lakes, rivers, wetlands estuaries, streams drain to a linked water body (Environmental Protection Agency, 1998). As a result, watersheds are considered necessary convergence points for management of water resources for sustainable life. For coastal areas, these drainage pathways may empty into estuaries, which are also affected by nearby coastal waterbodies. Estuaries provide a habitat for a large group of organisms. Estuaries function as a breeding and feeding ground for a variety of aquatic and terrestrial animals whom are affected by changes in water quality such as TOC and SSS. Drainage pathways such as rivers and channels flow to large bodies of water and transport with organic matter from natural and anthropogenic sources such as farming, housing and transportation. Several earth system processes such as tides, waves and winds can also transport SSS for coastal areas. Monitoring of such interactions and pathways is of importance, environmentally.

Monitoring of TOC and SSS is typically time-consuming and very expensive. TOC analysis typically takes 2-4 weeks to obtain results (Chang et al., 2014) and can be exacerbated by lack of point sources. Salinity is determined from empirical relationships between temperature and the conductivity ratio of a sample to International Association for the Physical Sciences of the

Ocean (IAPSO) Standard Seawater. To compare results with other laboratories, all scientists and researchers are required to use IAPSO Standard Seawater for calibration.

Remote sensing provides the solution to monitor real-time TOC by less expensive means (Chang et al., 2014). The use of satellite images to map SSS distributions in estuaries was first brought forward in the year 1982 (Swift et al., 1983). Subsequently, other studies emerged. Salts have no strong color signals but salinity levels can be estimated using the close relations of salinity levels with Colored Dissolved Organic Matter (CDOM) and/or TSS (Total Suspended Solids). These parameters can be easily observed from satellite color observation and both parameters are major colorant of seawater in the harbor area. Different studies have shown an empirical correlation between SSS and CDOM light absorption. In addition, a relationship between CDOM absorption and reflectance have been identified in various studies. So the strong correlation among SSS, reflectance and CDOM absorption and accurate remote sensing of CDOM can be employed to indirectly predict SSS in coastal waters. A very recent study has proven the existence strong correlation between SSS and CDOM (Keith et al., 2016). Using this correlation, Keith et al. (2016) have been able to formulate a regression model that can be used to derive salinity maps of coastal areas and estuaries on the East Coast.

Since TOC in a waterbody is impacted by the level of organic matter that interacts with a waterbody of concern, changes in vegetation surrounding a waterbody may reveal insights into changes in TOC. An example of such consideration is the Normalized Difference Vegetative Index (NDVI). The NDVI is a numerical index that employs the visible and near-infrared bands of the electromagnetic spectrum and is used to analyze the remote sensing environment and to survey whether the area of interest contains live green vegetation or not (i.e., organic matter). Rouse et al.

(1974) initially utilized NDVI as a part of 1973 study. Since then, NDVI has had a wide range of applicability in vegetation estimation studies (Carlson et al., 1997; Hurcom et al., 1998). It has been used in the assessment of crop yields (Quarmby et al., 1993; Mkhabela 2011; Prasad et al., 2006), rangelands conveyance capacities (Yengoh et al., 2014) etc. It is often directly identified with other ground parameters such as ground cover percentage (Scanlon et al., 2002; Lukina et al., 1999), photosynthetic movement of the plant (Penuelas et al., 1995; Pettorelli et al., 2005), surface water (Fu et al., 2015; Chandrasekar et al., 2010), leaf territory record which is alos known as leaf area index (LAI) (Carlson et al., 1997; Wang et al., 2005) and the measure of biomass (Anderson et al., 1993). However, it is worthwhile to couple SSS and TOC in an estuary study in comparison against the NDVI variations at the watershed scale simultaneously during a hurricane landfall event. Reconstruction of such environmental history must count on using remotes sensing technologies.

2.2 Case Study and Study Objectives

An important case study of such monitoring of TOC and SSS is Mattapoisett Harbor. Mattapoisett Harbor typical receives discharge from an upstream pathway via the Mattapoisett River, which contains both low concentrations of salinity and high-concentrations of TOC combined with existing salinity in the harbor. Of concern, with respect to Mattapoisett Harbor, is the potential for salt-water intrusion, which could subsequently affect nearby freshwater water resources for sustainable life. Earth system processes such tides, winds, waves and rainfall can have potential impacts on water quality in the harbor and land cover in nearby inland areas. One example of such earth system processes occurring simultaneously are tropical cyclones such as hurricanes, which often cause high tides, waves, fast winds and bring heavy rainfall. Mattapoisett Harbor is all too sensitive to tropical cyclone activity such as the event during the Hurricane Bob

in August of 1991, which made landfall southwest of the harbor. Hurricane Bob not only had visual impacts to the harbor and surrounding inland areas, but possible unknown effects that have environmental implications. Efforts to relate changes of water quality parameters of TOC and SSS of an estuary with the changes of vegetation cover due to a major natural disaster with the help of remote sensing has not been seen in the works of past. There are, however, efforts to connect water quality parameters of estuaries with remote sensing data. Some of the efforts are tabulated below:

Table 2-1:Literature Review of Relevant Studies

Water Quality Parameters	**Study Area**	**Satellite**	**Reference**
Chlorophyll, Turbidity, Total Suspended Solids (TSS)	Neuse River Estuary, NC, USA	Landsat MSS	Khprram et al., 1985
Chlorophyll-a	Augusta Bay, Sicily, Italy	Landsat-4 TM	Khorram et al., 1991
TSS, Chlorophyll, Turbidity	Breydon Water Estuary, UK	Landsat TM	Baban, 1997
Salinity, TSS, Chlorophyll etc.	Pamlico Sound, NC, USA	AVHRR	Woodruff et al., 1999
TSS	San Francisco Bay, USA	AVHRR	Ruhl et al., 2001
Suspended Particulate Matter (SPM)	Gironde Estuary, France	SPOT	Doxoran et al., 2002

Water Quality Parameters	**Study Area**	**Satellite**	**Reference**
Chlorophyll, CDOM, Tripton	Moreton Bay, Australia	Hyperion	Brando et al., 2003
Pigment concentration, SSS	Southwestern Australia estuaries	Landsat TM	Ritchie et al., 2003
Chlorophyll, TSS	New York Harbor, NY, USA	Landsat TM, MODIS	Hellweger et al., 2004
Chlorophyll, CDOM	Tampa Bay, FL, USA	MODIS Ocean Color	Hu et al., 2004
Composite Pollution Index (CPI) (derived from chemical oxygen demand and nutrient concentration measurement)	Pearl River Estuary, China	SeaWiFS	Chen et al., 2007

The literature review above indicates that the use of remote sensing data to connect it to various water quality parameter is a case-specific study. The models, although case-specific, can also be used for other estuaries in the monitoring and determination of water quality parameters having the same optical conditions. The research that is going to be presented in this paper will also include an algorithm that will be used to determine TOC and use a derived algorithm from Keith et al., 2016 to determine the SSS of Mattapoisett harbor. However, the novelty lies in the

fact that in addition to modelling of algorithms, the models will be used to observe the behavior of the water quality parameters in the bay area before and after the landfall of Hurricane Bob. In addition, the remote sensing technology will be used to observe the condition of vegetation cover of the Mattapoisett river watershed. The Mattapoisett River drains directly into the Mattapoisett bay. The observation of vegetation cover, coupled with the water quality parameters of TOC and SSS will help forge a dynamic sea-land interaction, which will help us understand better how major natural events such as hurricanes can impact not only the area of landfall but also the waterbody associated with it. Another important aspect of the study is the investigation of the impact of the water quality parameters on the drinking water wells that are present in the watershed.

The objectives of this study are: 1) to explore sea-land interaction between Mattapoisett Harbor and the coastal watershed on monthly basis during 1991-92, and 2) investigate how vegetation cover and water quality change over time during Hurricane Bob landfall event. In addition to exploring these objectives, we also wish to investigate a) how were the concentrations of TOC and SSS affected during Hurricane Bob landfall? b) how the surge of freshwater discharge from the Mattapoisett River to the harbor due to excessive precipitation affected the concentration of the earlier mentioned parameters? c) how the vegetation cover of the coastal watershed changed over time driven by the hurricane landfall? and d) what interaction did it have with respect to the changes of the TOC and SSS concentration in the harbor?

2.3 Study Area and Hurricane Event

2.3.1 Study Area

The study area is the Mattapoisett harbor, located in the southeastern Massachusetts along the shores of Buzzard's Bay (Fig. 1). Our area of interest is the coastal watershed surrounding

Mattapoisett Harbor (Fig. 2). As evident in Fig. 3, the lowest elevation is at the mouth of the river with 6 m elevation. The elevation increases as the watershed moves inland. The highest elevation of the watershed is 39 m. This highest elevation is situated to the northwestern side of the watershed. The average elevation of the watershed is 22.5 m. The average area of the watershed is 66.85 square kilometers. The total perimeter of the watershed is 72 kilometers. The Mattapoisett River discharges at the harbor from the northwest. The river stretches approximately 16 km (10 miles) from its headwaters at the 2.87 km^2 Snipatuit Pond to the Mattapoisett harbor. The river basin has eight public water supply wells and many private wells that serve the needs of multiple municipalities.

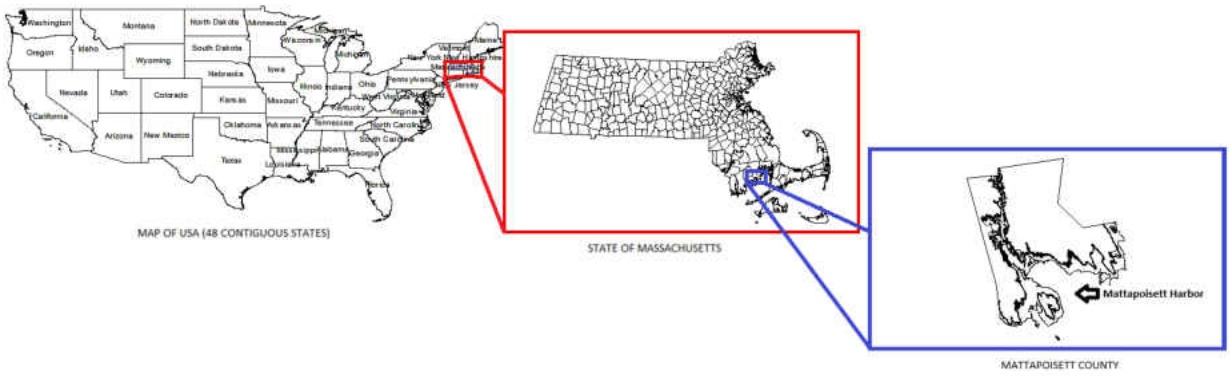

Figure 2-1: Geographical location of Mattapoisett Harbor.

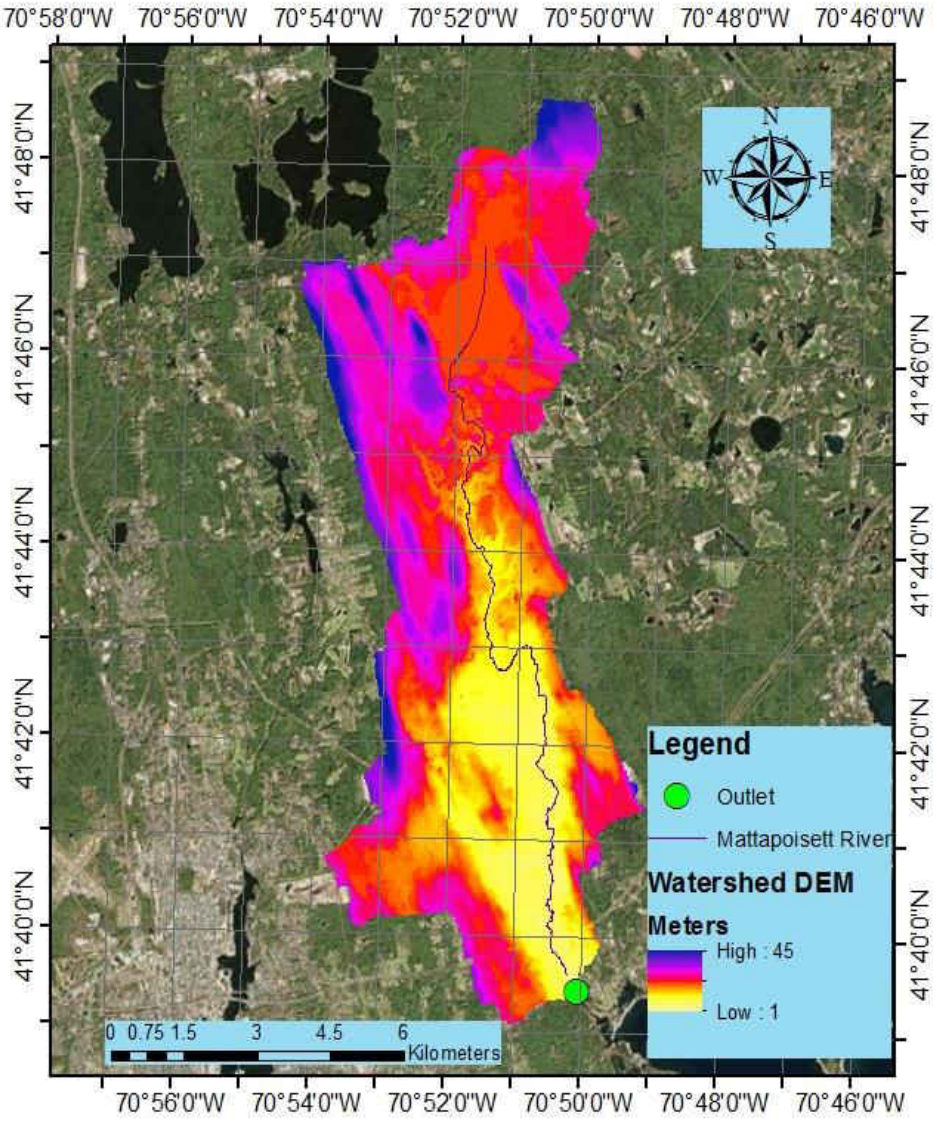

Figure 2-2: Digital Elevation Model (DEM) of the Mattapoisett River watershed

2.3.2 Hurricane Bob Event

Hurricane Bob was one of the costliest hurricanes in New England history was the first hurricane of the 1991 Atlantic hurricane season. The hurricane made landfall twice, first on Block Island Rhode Island and then in Newport, Rhode Island. The hurricane weakened as it moved further inland and emerged in the Gulf of Maine. The hurricane was initially declared a Category 3 hurricane with a maximum sustained wind speed of 184 Km per hour (115 mph) weakening as

it approached the coast of New England. Hurricane Bob caused extensive damage throughout New England in its wake. The estimated total damage is approximate $1.5 billion USD of 1991 USD, equivalent to $2.61 billion of 2016 USD. This was termed as the second costliest hurricane at that time. In addition, seventeen people died in the event. The fatalities and most of the damage occurred due to high winds and rough seas. Due to its devastating nature, we have taken an interest as to what the environmental implications were before and after the event.

2.4 Materials and Methods

2.4.1 Study Framework

The first phase of the study involved developing a real-time monitoring tool that encompasses the use of modern remote sensing technologies. Ground truth data and the corresponding reflectance values of Landsat satellite images were used to formulate an algorithm for determining both TOC and SSS concentrations using statistical regression analysis. The algorithm can then be used to generate real-time, predictive maps of TOC and SSS concentrations. The following methods explain the development of algorithms necessary for TOC and SSS map was formulated from the ground-truth data provided by the US EPA and Landsat-5 satellite. The procedures for the development of TOC and SSS predictive model are summarized in a flowchart in Fig. 2-3

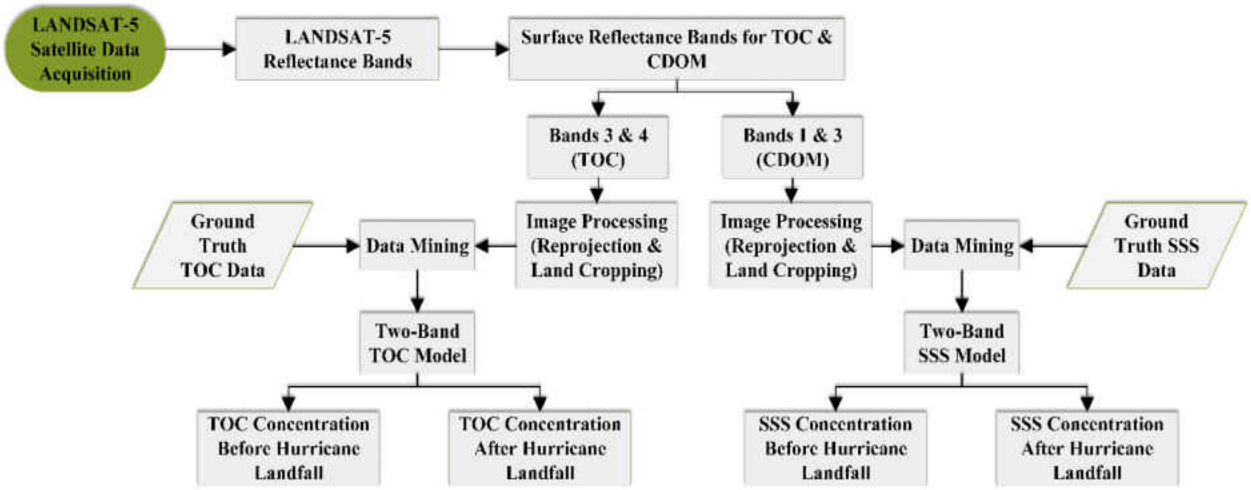

Figure 2-3: Methodological flowchart in the TOC & SSS concentration retrieval model development

2.4.2 Satellite Data Collection and Image Processing

Accurate image acquisition and processing is the key to creating genuine TOC and SSS maps. At first, a polygonal shapefile was created for the Mattapoisett harbor area. The shapefile was created in Ground Control System (GCS) system. Then the shapefile was projected from GCS to Universal Transverse Mercator (UTM) system to get the actual shape of the image. After that, a raster image was created from the projected shapefile. The number of rows and columns of the raster image was recorded. The LANDSAT-5 images of the Mattapoisett area were downloaded from the United States Geological Survey data center (http://earthexplorer.usgs.gov). The images for bands 1-7 were selected. The raw LANDSAT images were processed using MATLAB scripts. From the raster image of the projected shapefile, the pixel numbers where the stations are located are recorded and from the corresponding pixel numbers, the corresponding surface reflectance values for all seven bands were extracted and recorded.

2.4.3 Ground Truth Data Collection (TOC & SSS)

The detail of the study area is shown in Fig. 2-4. The black line shows the enclosed area of the Mattapoisett harbor. The red dots indicate the stations where data for TOC were collected during low tide. The yellow dot represents stations where TOC data was collected for both high and low tides. For SSS, data are available for all stations for both high and low tide events. The data collection campaign was run by the EPA Region-1 working with National Risk Research Management Laboratory during the month of October in the year 2015. Table 1 indicates that the TOC values range from 0.11 mg/L to 0.65 mg/L. The lowest value was obtained from the station that is out to the sea and the highest value was obtained at the station situated at the mouth of the river. This is logical since the river carries organic matter from the watershed during storm and rainfall events and eventually deposits it into the bay area.

The SSS values range from a low of 26.52 psu at the mouth of the Mattapoisett River to 31.46 psu that is out to the harbor during high tide (Table 2-3). In case of low tide, the same trend is noticeable i.e. the SSS value is 30.22 psu for the station at the mouth of the Mattapoisett River and 31.32 psu for the station ANEL, which is out to the bay. Therefore, the variation in the concentration values is logical as there is fresh water input at the mouth of the river, the SSS concentration will be relatively low. The concentration of SSS will increase as freshwater concentration dissipates out to the bay as noticed in the values for stations located in the outer bay.

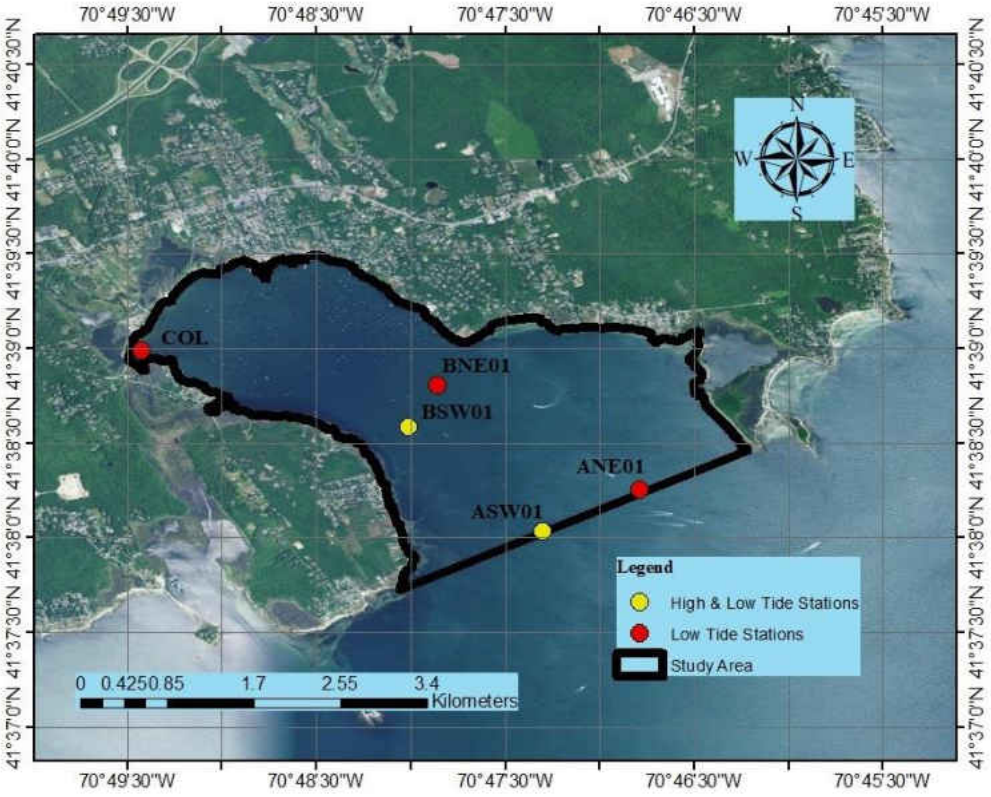

Figure 2-4: Study area and stations for TOC & SSS data collection

Table 2-2: Sampling locations and schedule of TOC data.

Station	Depth (Ft)	Tide	Latitude	Longitude	Date	TOC (mg/L)
ASW01	1.00	High tide	41.6340	-70.78840057	10/15/2015	0.2046
BSW01	1.00	High tide	41.6432	-70.80018751	10/15/2015	0.2226
ANE01	1.00	Low tide	41.6376	-70.77979104	10/15/2015	0.1185
ASW01	1.00	Low tide	41.6339	-70.78833364	10/15/2015	0.1702
BSW01	1.00	Low tide	41.6431	-70.80017281	10/15/2015	0.2575
BNE01	1.00	Low tide	41.6467	-70.79766413	10/15/2015	0.2256

Station	Depth (Ft)	Tide	Latitude	Longitude	Date	TOC (mg/L)
COL	1.00	Low tide	41.6498	-70.82376848	10/15/2015	0.6594

Table 2-3: Sampling locations and schedule of SSS data.

Stations	Date	Time	Depth (Feet)	Temperature (°C)	Salinity (psu)	Tidal Mode
ANEH	10/15/2015	9:52	0.90	---	31.46	High
ASWH	10/15/2015	10:15	0.45	16.337	31.33	High
BSWH	10/15/2015	10:40	0.69	16.417	31.09	High
BNEH	10/15/2015	10:56	0.52	16.392	31.08	High
COH	10/15/2015	11:20	0.34	15.870	26.52	High
DOH	10/15/2015	12:03	0.20	14.406	00.12	High
DOH	10/15/2015	12:06	1.68	15.348	21.66	High
DOL	10/15/2015	14:33	0.55	14.920	00.05	Low
DOL	10/15/2015	14:38	1.17	14.880	00.05	Low
ANEL	10/15/2015	15:10	0.37	16.806	31.32	Low
ASWL	10/15/2015	15;29	0.34	16.819	31.11	Low
BSWL	10/15/2015	15;45	0.42	16.821	30.91	Low
BNEL	10/15/2015	16:02	0.24	16.968	30.98	Low
COL	10/15/2015	16:31	0.44	17.525	30.22	Low
DOL	10/15/2015	17:05	0.181	14.667	00.05	Low

Stations	Date	Time	Depth (Feet)	Temperature (°C)	Salinity (psu)	Tidal Mode
DOL	10/15/2015	17:07	1.221	14.673	00.05	Low

2.4.4 Feature Extraction

Regression analysis can be referred to the art and science of fitting straight lines to patterns of data. In a linear regression model, the variable of interest, which is also known as the dependent variable, is predicted from known other variables or independent variables using a linear equation. If Y denotes the dependent variable, and $X_1,\ldots,X_k$, are the independent variables, then the assumption is that the value of Y at time t (or row t) in the data sample is determined by the linear equation

$$Y = \beta_0 + \beta_1 X_{1t} + \beta_2 X_{2t} + \ldots + \beta_k X_{kt} + \varepsilon_t \quad (2\text{-}1)$$

where the betas are constants and epsilons are independent and identically distributed normal random variables with mean zero. β_0 is called the intercept of the model, the expected value of Y when all the X's are zero and β_i is the coefficient of the variable X_i The betas together with the mean and standard deviation are the parameters of the model. The corresponding equation for the prediction of Y_t from corresponding values of X's is therefore

$$\hat{Y}_t = b_0 + b_1 X_{1t} + b_2 X_{2t} + \ldots + b_k X_{kt} \quad (2\text{-}2$$

where the b's are the estimates of betas obtained by least-squares, i.e. minimizing the squared prediction error within the sample. This is one of the simplest possible model for predicting one variable from a group of others. It rests on the basic assumptions (see Chapter 5, Chang, 2012).

The linear regression analysis and model building was done using the MS Excel 2013 software. Data was arranged and regression was done using the "Data Analysis" feature provided in the software.

The two-band model was chosen to be used for TOC mapping since the two-band model helps reduce "noise" significantly. The study area is a coastal area so the reflectance from the land may interfere with the reflectance of water nearer to the shore. The two-band model helps cancel out this effect. Fig. A-1 shows the peak and valley of reflectance of CDOM for different coastal areas and estuaries of the East Coast. From the figure, we chose band 3 of Landsat-8 which corresponds to the peak reflectance of CDOM and band 4 which has the lowest reflectance. Fig. 2-6 shows the linear regression done to derive the two-band model.

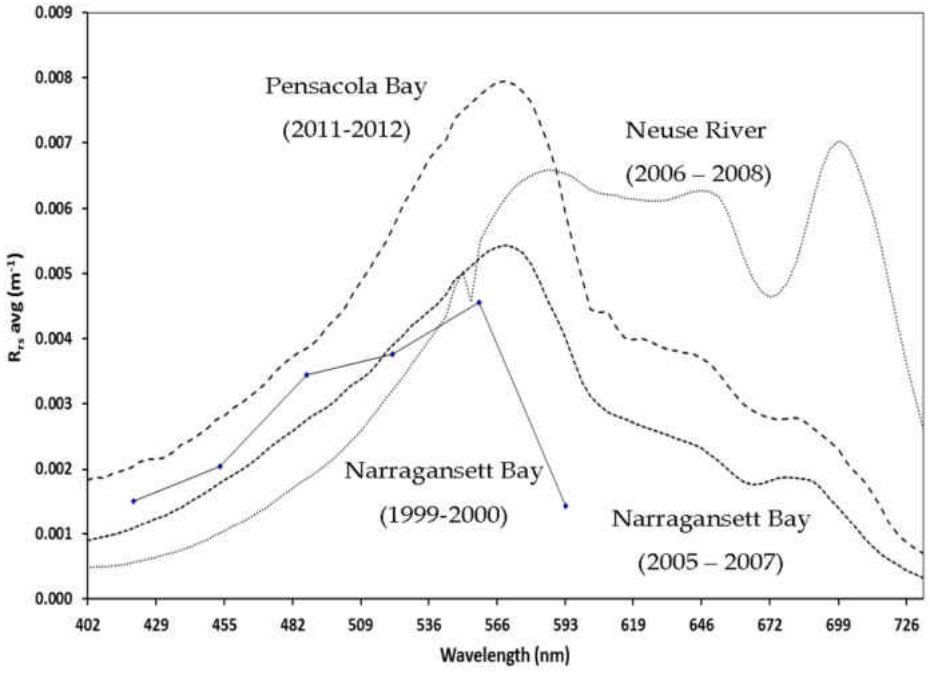

Figure 2-5: Average Remote Sensing Spectral Curves (Source: Keith et al., 2016)

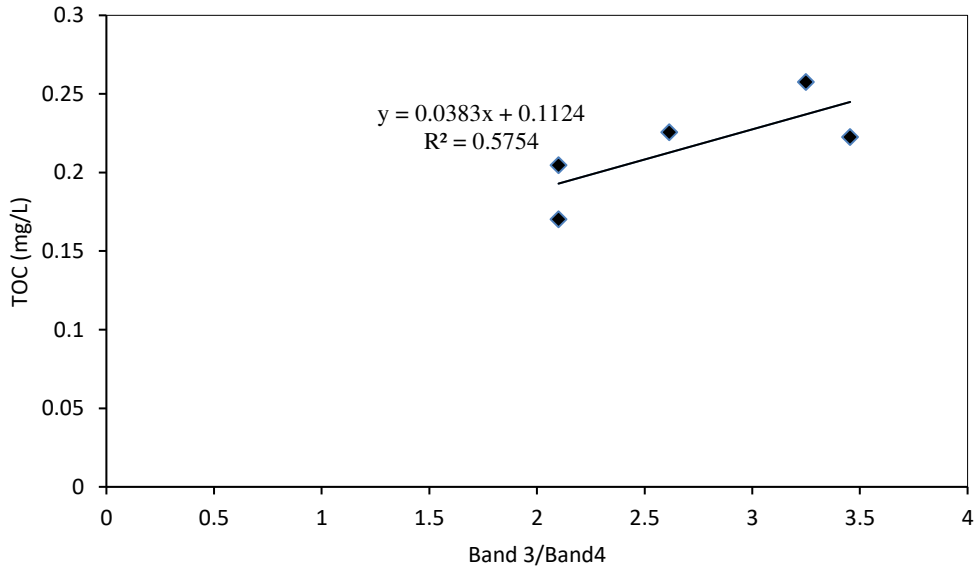

Figure 2-6: Linear Regression Analysis for Two-Band Model.

Based on the ground truth data, the equation developed for TOC mapping purposes in this study is:

The model used to derive the TOC maps is shown below in which Band 3 and Band 4 correspond to Landsat-8 bands:

$$TOC = 0.0383 \text{ x (Band 3/Band 4)} + 0.1124 \ (R^2 = 0.58) \ldots. \quad (2\text{-}3)$$

The equation above is for Landsat-8. When converted to Landsat-5 bands, the equation becomes

$$TOC = 0.0383 \text{ x (Band 2/Band 3)} + 0.1124 \ (R^2 = 0.58) \ldots. \quad (2\text{-}4)$$

For salinity mapping, a model derived by Keith et al. (2016) shows the correlation between CDOM and salinity (Fig. A3). This regression model is used for CDOM mapping where the basis is CDOM absorption. First, using Band 3 and Band 1 of Landsat-5, the CDOM absorption is calculated. Then, salinity is calculated based on the CDOM absorption as below:

$$a_{CDOM}412 = 1.3499 \times \text{(Band 3/Band 1)} - 0.1124 \ldots. \quad (2\text{-}5)$$

Salinity = 33.686 × exp (−0.374 × $a_{CDOM}412$) … (2-6)

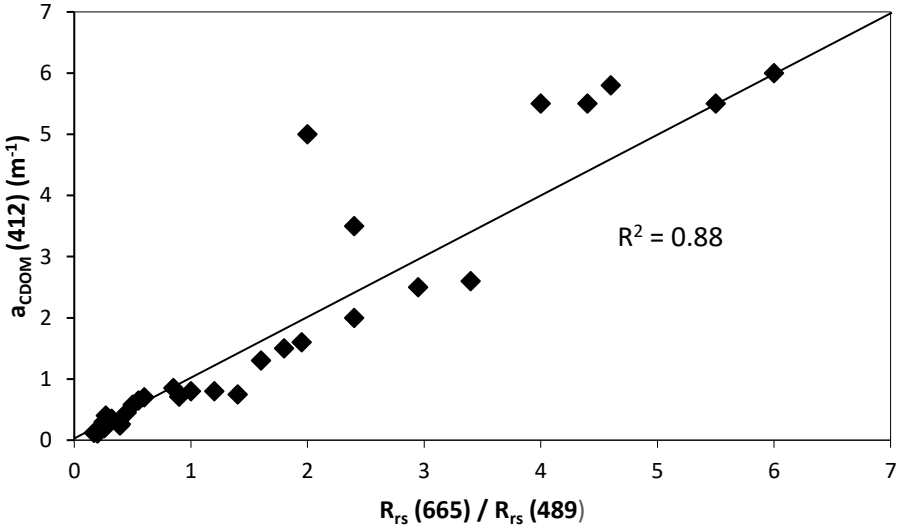

Figure 2-7: Relationship between CDOM and Salinity. (Adapted from Keith et al., 2016)

2.4.5 TOC & SSS Mapping

The content-based mapping effort was carried out finally to perform the environmental reconstruction and sea-land interactions that the hurricane had caused at that time. The concentration maps were generated using the "Raster Calculator" tool of ArcGIS software. In addition, the data extraction task was carried out by statistically calculating the average of the parameters to effectively delineate the global variation of the water quality parameters in a time series. The time series charts are also helpful in explaining the effect that Hurricane Bob had on the parameters. Additionally, the variations can be linked to different earth systems process such as temperature and precipitation to show the effects of the processes on the parameters with respect to sea-land interactions.

2.4.6 NDVI Mapping

Generally, healthy vegetation will retain a large portion of the visible light that falls on it, and reflects an enormous segment of the near infrared light. Inadequate or unhealthy vegetation reflects more portion of the visible light and less of the near infrared light. Uncovered soils then again reflect decently in both the red and infrared segment of the electromagnetic spectrum (Holme et al., 1987). The behavior of the green vegetation is known across the electromagnetic spectrum. The NDVI data can be determined by concentrating on the satellite bands that are most delicate to the vegetation data (red and near-infrared). The greater the distinction along these lines between the near-infrared and red reflectance, the vegetation there must be.

The NDVI algorithm is calculated by subtracting the red reflectance values from the near-infrared and dividing it by the sum of near-infrared and red reflectance values. The formula for NDVI can be written as;

$$NDVI = \frac{R_{NIR} - R_{Red}}{R_{NIR} + R_{Red}} \tag{2-7}$$

The NDVI mapping effort is also carried out using the "Image Analysis" tool of ArcGIS software. The algorithm is used as input in the tool and the NDVI maps are generated as output.

The algorithm used can be modified according to the NIR and red bands of Landsat-5. The NIR corresponds to band 4 and the red band corresponds to band 3 of Landsat-5 respectively. So for calculating NDVI, equation 4 becomes:

$$NDVI = \frac{Band\ 4 - Band\ 3}{Band\ 4 + band3} \tag{2-8}$$

This equation is used to generate the NDVI mappings. NDVI maps will be generated for the dates corresponding to the TOC concentration maps. The procedures for NDVI mapping are summarized in the form of a flowchart depicted in Fig. 2-8.

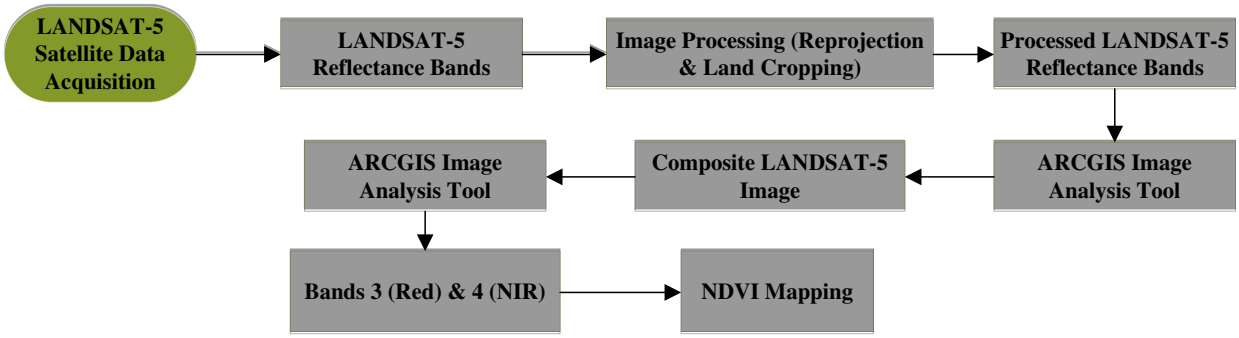

Figure 2-8: Methodological flowchart for NDVI mapping

In the second phase of the study, after the calibration of the TOC and SSS maps are complete and based on limited field data of TOC and SSS, the reconstruction of the TOC and SSS maps five months before and six months after Hurricane Bob that made landfall in New England on August 19, 1991 can be retrieved. This gives a yearlong observation time series depicting clearly the before and after hurricane landfall. The NDVI mapping is done after the TOC and SSS maps generated to connect the variation of important water quality parameters with that of variations of NDVI. Only one map snapshot for each month will be utilized to observe the time series variations of both water quality constitutes as Landsat images are available roughly twice a month for a location subject to the images remaining cloud-free.

2.5 Results & Discussion

2.5.1 TOC Mapping

Results of the environmental reconstruction of TOC concentration maps using calibrated regression equation are detailed in Fig. 2-9. The maps show the monthly variation of TOC concentration over a period of one year beginning from March 1991 and ending in February 1992. In addition to the mapping efforts carried out by the ArcGIS software, statistical analysis was done as well to calculate the monthly mean TOC concentrations. The mean TOC value for March 1991

was 0.165 mg/L. It gradually drops to the lowest value of 0.143 mg/L and climbs steadily to the value of 0.15 mg/L until the month of June (Fig. 2-9n). This steady rise can be attributed to the fact that the average rainfall gradually increases from 3.68 cm to 5.71 cm. So the average discharge of the Mattapoisett river increases, bringing with it organic material and in turn TOC which is dispersed over the bay area as time passes. The months of April and May have seen subsequent drops in rainfall. The average rainfall was 10.59 cm in April and drops to 6.53 cm in May (Table 4). Due to this low rainfall, the level of TOC can be seen to be lower in the month of May at the mouth of the harbor (Fig. 2-9c). The overall average TOC concentration was also low to the tune of 0.143 mg/L (Table 2-4). The average TOC concentration starts to pick up again from the month of June even though there was low rainfall. This can be attributed to the fact that high average temperatures contribute to the growth of flora and fauna in the coastal area and the watershed surrounding the Mattapoisett River. Appendix A lists the variations of temperatures. The concentration of TOC is higher even when they are washed down with low rainfall. The TOC map for the month of August depicts mainly the effect of Hurricane Bob as the TOC concentration is the situation one week after hurricane made landfall (Fig. 2-9f). The average concentration drops to 0.144 mg/L from 0.150 mg/L that is seen in the previous month. There is a drastic drop in concentration when hurricane landed as the high amount of rainfall and the tidal waves associated with high wind speed tends to upend the normal concentration gradient that prevails in the bay area. The month of September witnesses a sharp increase in rainfall. The monthly average was 20.70 cm (Table 2-4). While the rainfall decreases for the following month, it again increases in November, with monthly average of 17.60 cm. this contributed to a steady increase in TOC value with the average values being, 0.149 mg/L, 0.152 mg/L and 0.155 mg/L for the months of October, November and December respectively. During the months of December and January, the spatial

distribution of TOC can be seen to be uniform in nature (Fig. 2-9j and 2-9k). This can be attributed to the near freezing temperatures that prevail during this time of the months. However, the spatial pattern begins to change and form gradient as thawing occurs and temperatures begin to rise.

In addition to the spatial distribution maps, the yearlong monthly variation can also be depicted in time series charts (Fig. 2-9m and n). The impact of Hurricane Bob can also be seen in a localized form (Fig. 2-9n). The charts clearly show the lowering of the TOC concentrations during the month of hurricane impact (Fig. 2-9n) caused due to dilution effects of the discharge from the river and excessive rainfall over the bay area. The concentration values steadily recover in the following months as the average rainfall steadily increases. Even though there is a decline in rainfall for the month of October, the TOC value continues to rise steadily due to the effects of the sharp increase in rainfall in the previous month (Fig. 2-9m)

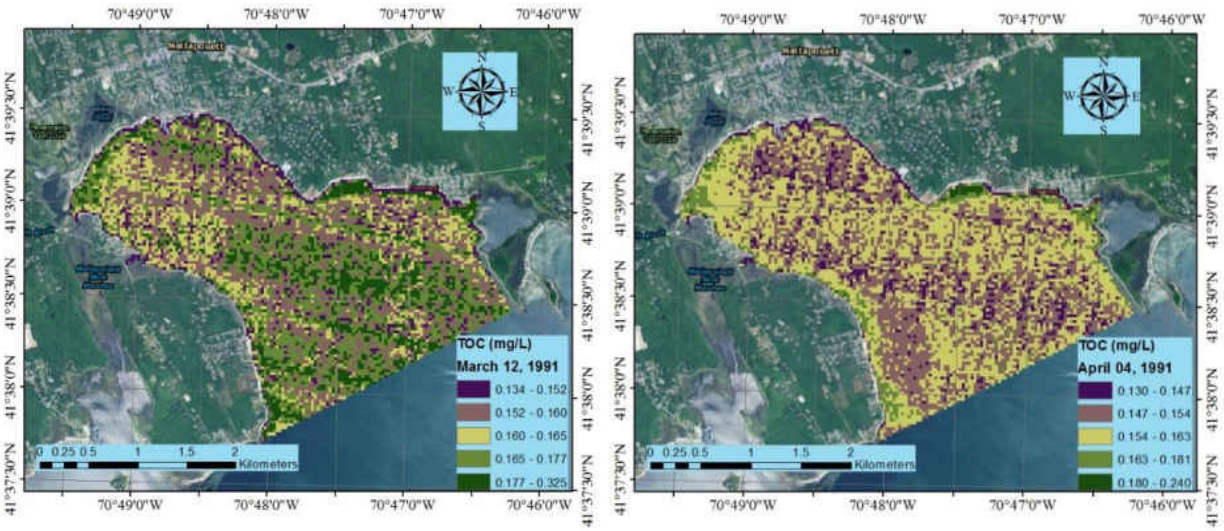

a) March 12, 1991 b) April 04, 1991

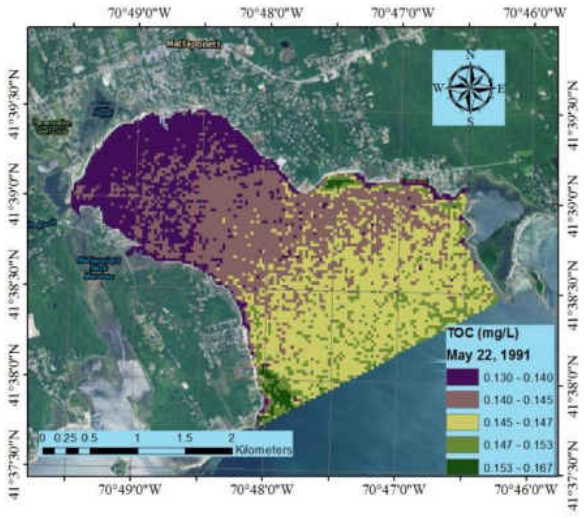

c) May 22, 1991

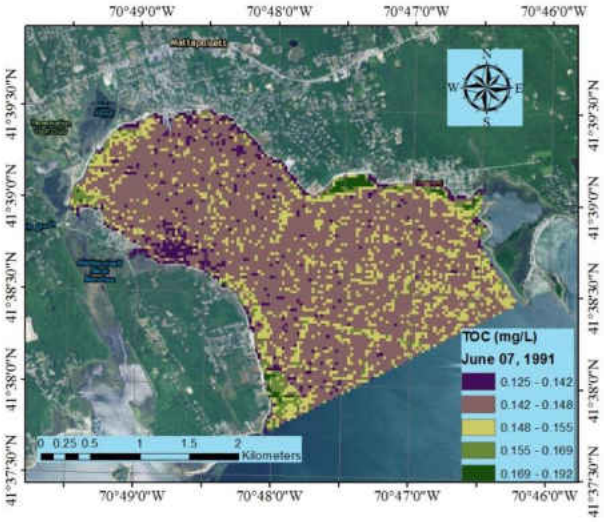

d) June 07, 1991

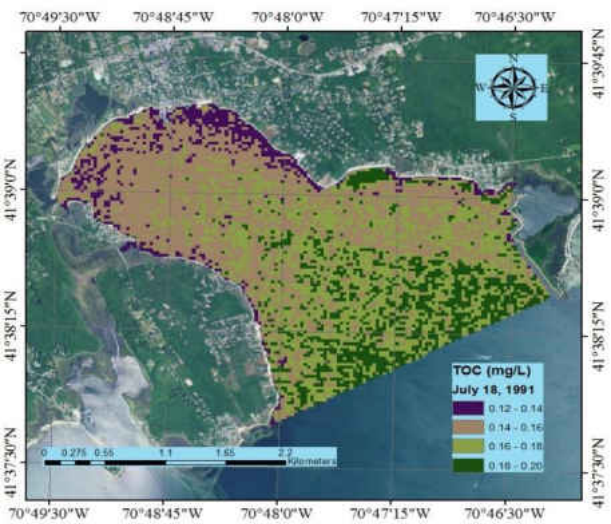

e) July 18, 1991

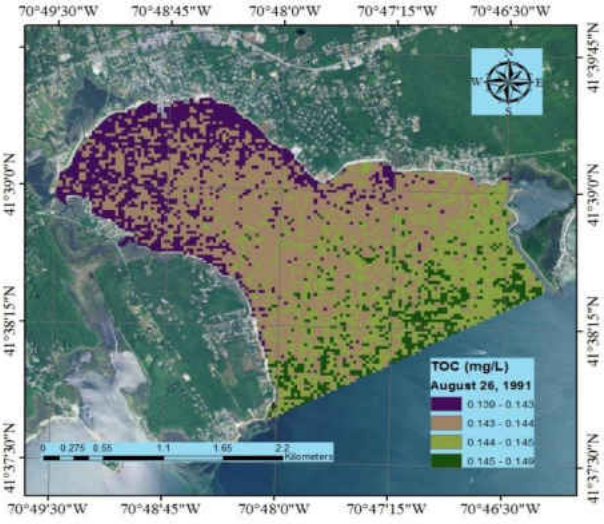

f) August 26, 1991

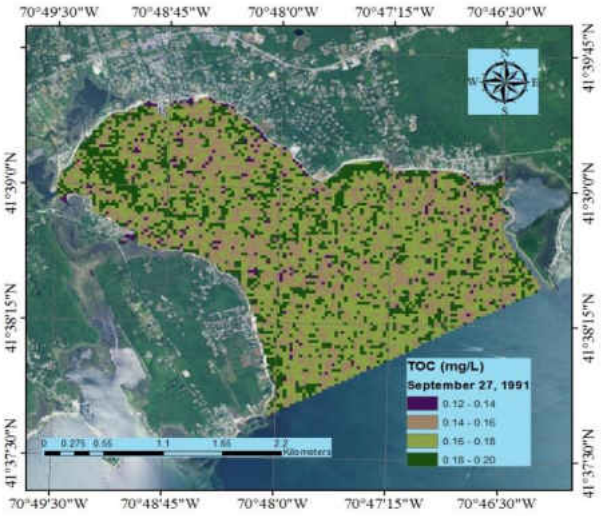

g) September 27, 1991

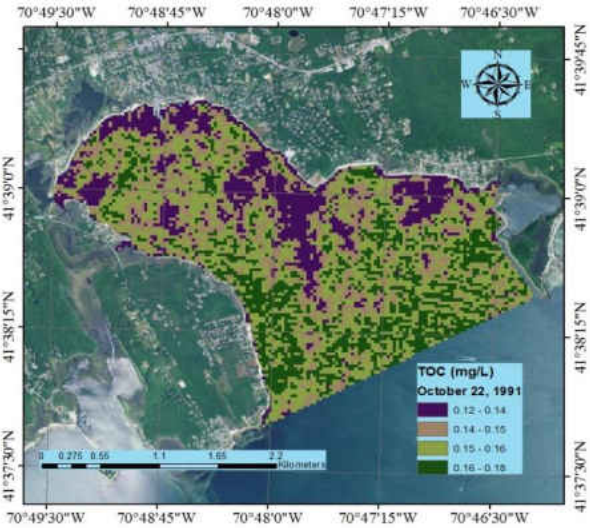

h) October 22, 1991

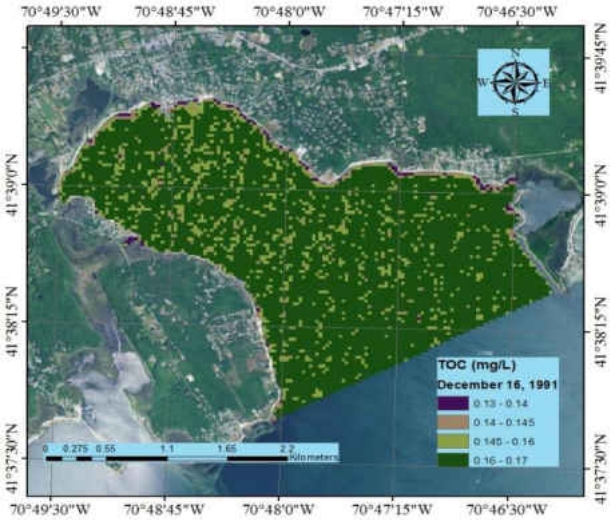

i) November 14, 1991

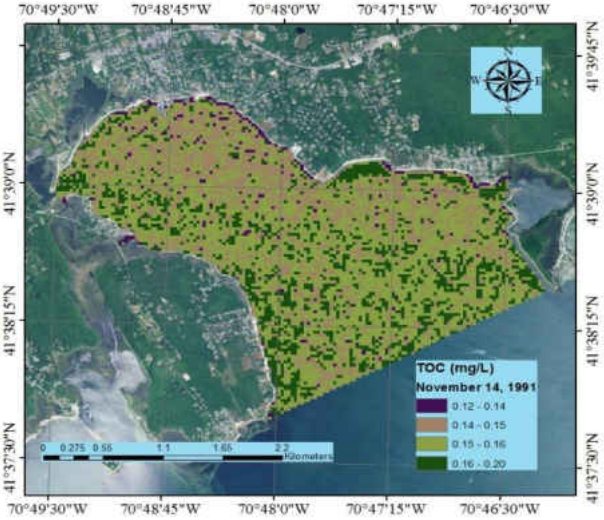

j) December 16, 1991

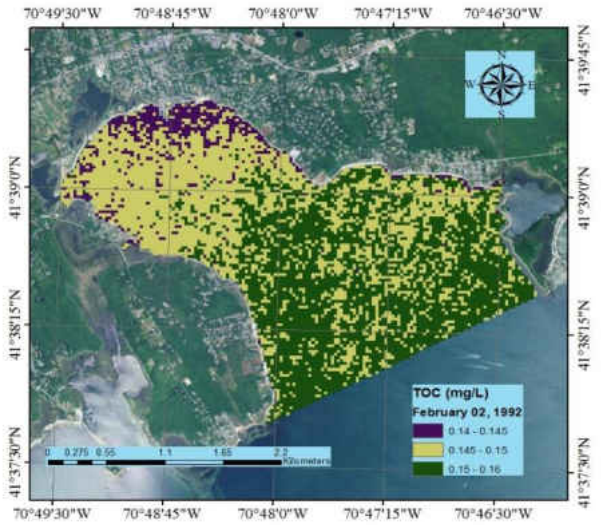

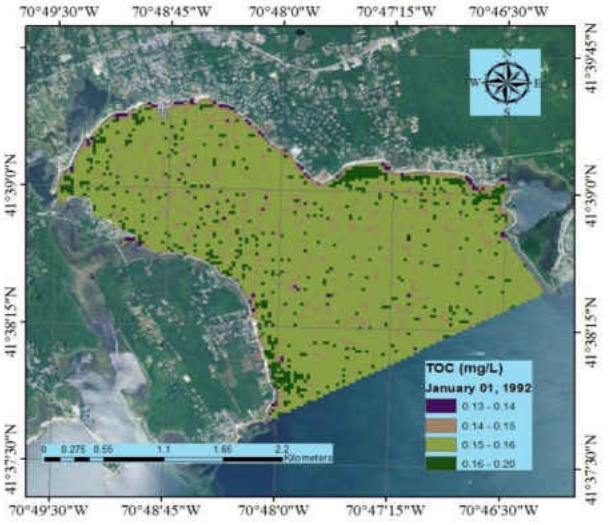

k) January 01, 1991

l) February 02, 1991

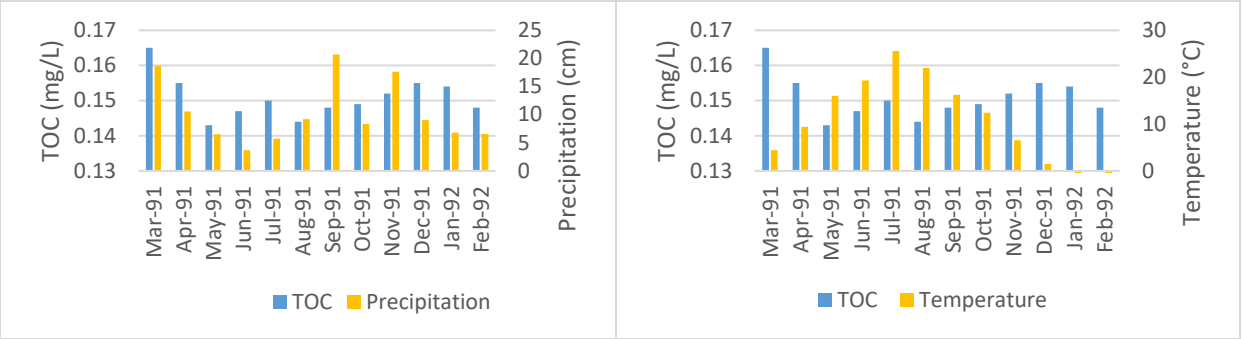

(m)

(n)

Figure 2-9: Spatial variability (a)-(l) in TOC concentration for Mattapoisett Harbor area. Temporal variability of TOC (m) in the form of monthly anomalies compared with precipitation anomalies over a year and temporal variability of TOC (n) in the form of monthly anomalies compared with temperature anomalies.

2.5.2 SSS Mapping

The details of spatial and temporal variation of SSS concentration spanning over a period of one- year are represented in Fig. 2-10. Monthly variations begin from March 1991 to February 1992. This yearlong variation concentration images are helpful in assessing the environmental situation that prevailed during that period and especially the situation before and after the impact of Hurricane Bob that made landfall. The average monthly concentrations for SSS shows somewhat similar pattern to TOC for the same yearly period (Fig. 2-10a). The concentration was highest during the month of March 1991 with a value of 25.249 psu and plummets to a low of 22.798 psu during the month of May 1991 (Table 2-4). However, during July, the concentration shoots up to 25.612 psu. This can be attributed to the fact that consistent lower levels of precipitation helped accumulate salinity in the bay area. When the hurricane landed, the salinity level plummets signifying that higher levels of precipitation have had a dilution effect on the salinity concentration. After the impact of hurricane, the salinity levels begin to recover in the

following months with a steady increase. However, the concentration levels varied with the varying levels of precipitation. Similar to the pattern of variation of TOC, SSS concentration shows a steady spatial distribution for the months of December and January. This steady distribution can be attributed to the freezing temperatures that prevail in the area during these two months. From February, the average temperature begins to increase and thawing occurs, water from melting of snow is discharged through the river into the bay. This causes the dilution effect on SSS concertation where the average value was 21.575 psu (Table 2-4).

The impact of Hurricane Bob is clearly visible in the spatial distribution of the month of August (Fig. 2-10f). The average SSS concentration before the month of hurricane impact i.e. for July was 25.612 psu. The value decreases to 22.013 psu for the month of August (Table 2-4). This can be attributed to the heavy rains and the tidal effects caused by high wind speed. The heavy rains have a dilution effect on the concentration. The tidal waves also affected the concentration by disturbing the gradient. The concentration gradient slowly begins to recover and return to normal gradient patterns over the course of the months following the hurricane landing. The spatial pattern for the month of October is somewhat similar to the pattern of TOC for the same month. There are patches of lower concentration on the mouth of the bay and eastern part of the bay where the bay begins to widen out to the sea. This phenomenon happens due to residual effects of high average rainfall for the month of September, which was 20.70 cm. The dilution effect carried on to the month October and can be visible (Fig. 2-10h). The spatial pattern shows a near constant distribution for the months of November, December and January (Fig. 2-10i, j and k). The freezing average temperatures contribute to this phenomenon. However, from February, when the average temperature starts to rise, the spatial patterns begin to change and show gradient as thawing effects take over. In addition, due to discharge of snowmelt from the watershed, the concentration of SSS

goes down, even if the average precipitation for the month of February was low. Apart from spatial distribution maps, the impacts of the hurricane and yearlong monthly variation can also be depicted in time series charts (Fig. 2-10 m and 2-10 n). The temporal pattern is consistent with the variation of spatial patterns and shows lowering of concentration during the hurricane impact. In the following months after the hurricane, the average monthly concentration begins to recover and return to normal conditions.

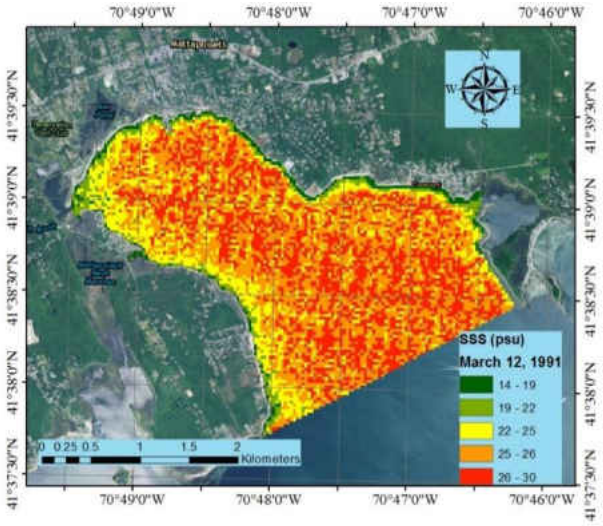

a) March 12, 1991

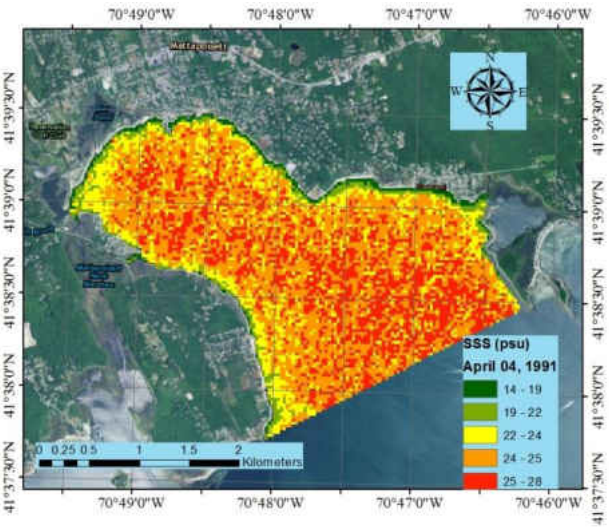

b) April 04, 1991

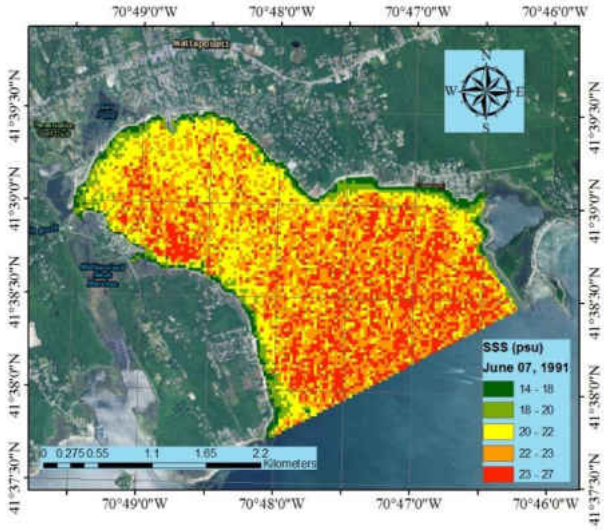

c) May 22, 1991

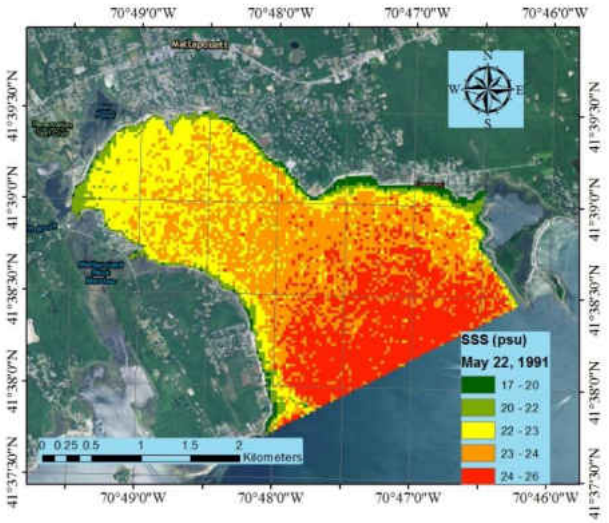

d) June 07, 1991

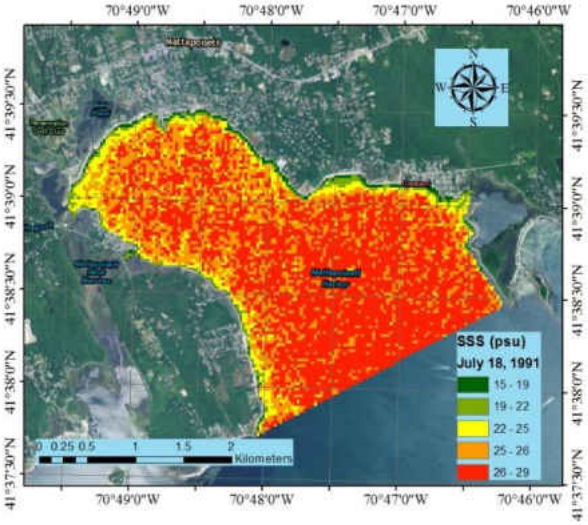

e) July 18, 1991

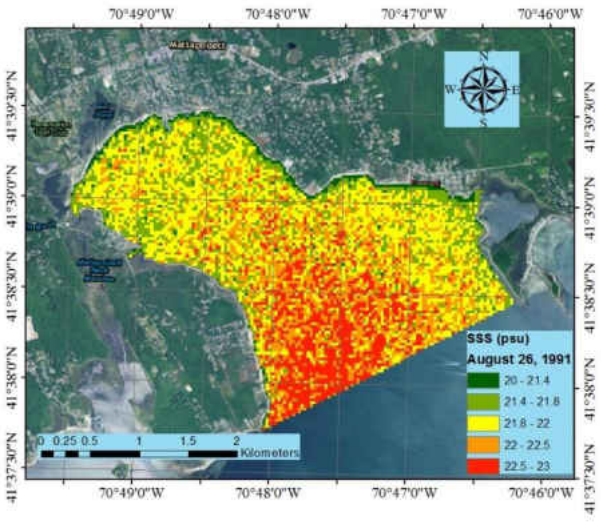

f) August 26, 1991

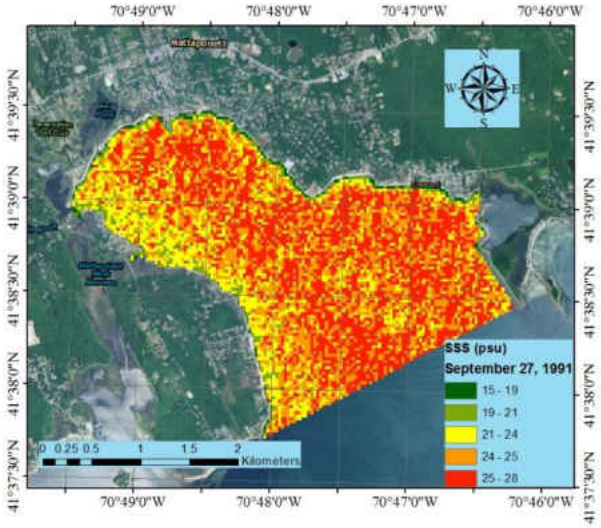

g) September 27, 1991

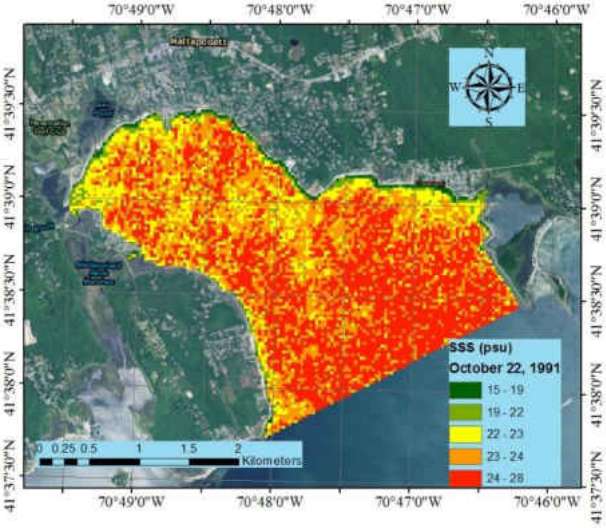

h) October 22, 1991

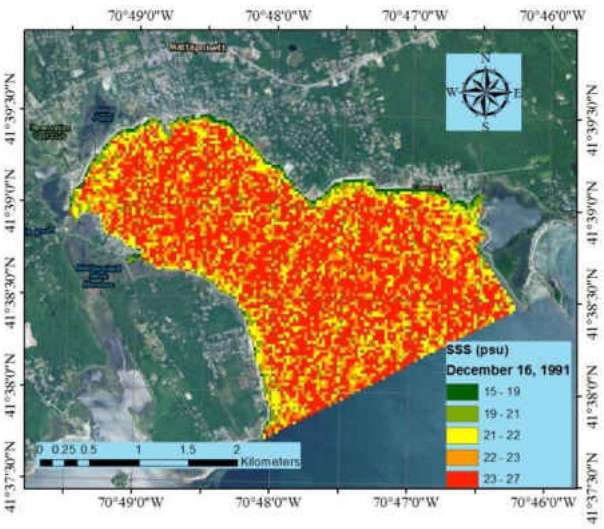

i) November 14, 1991

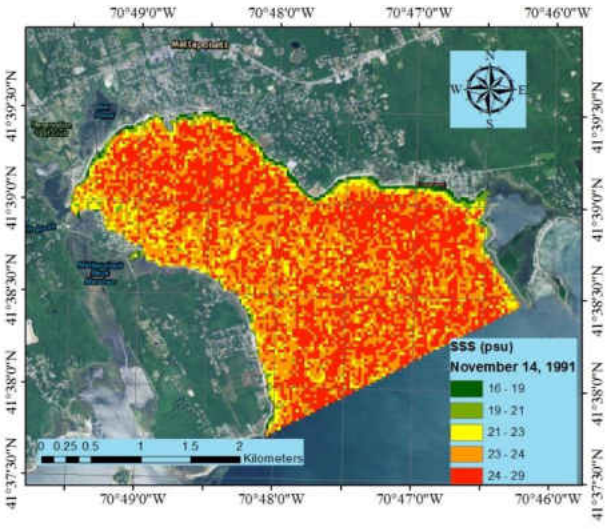

j) December 16, 1991

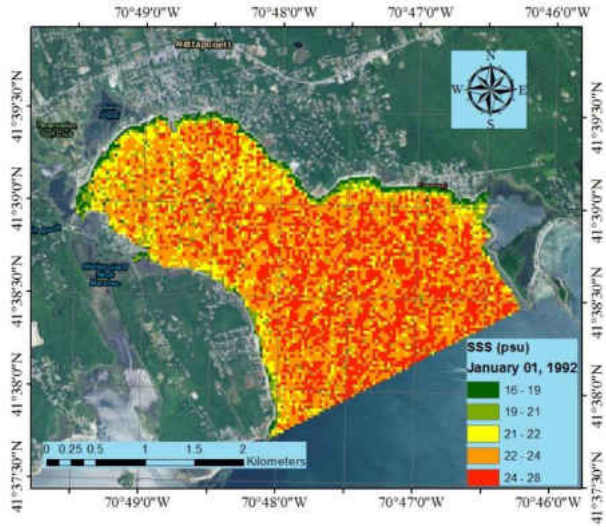

k) January 01, 1991

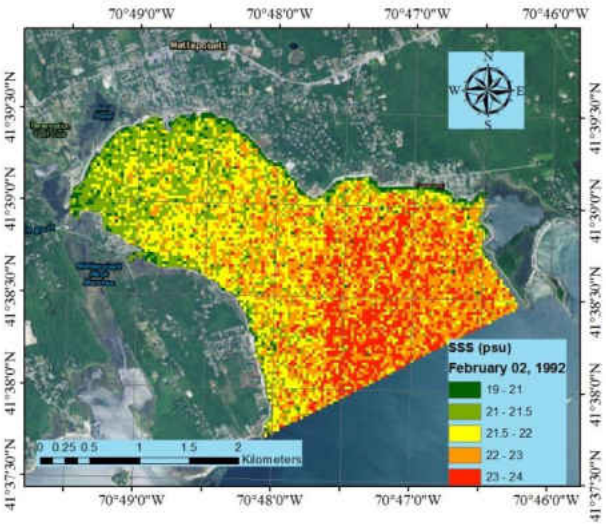

l) February 02, 1991

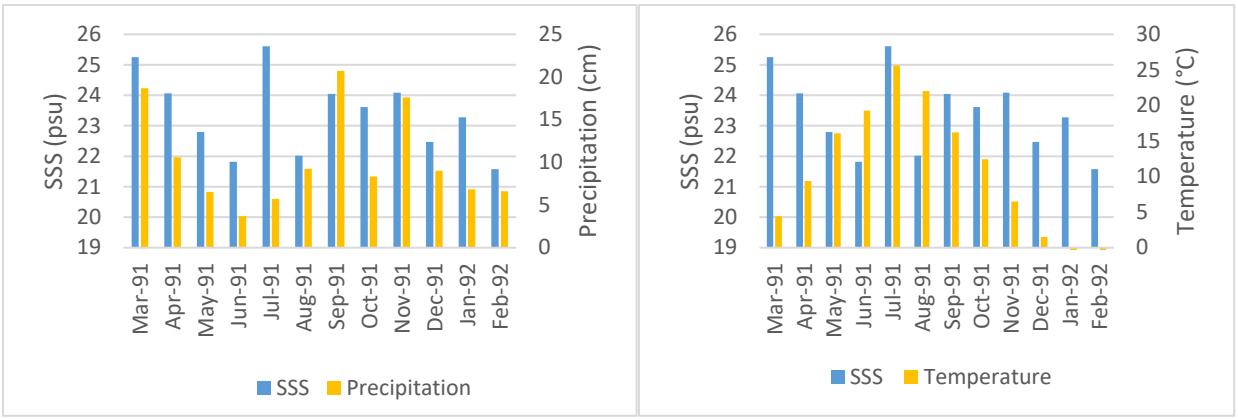

(m) (n)

Figure 2-10: Spatial variability (a)-(l) in SSS concentration for Mattapoisett Harbor area. Temporal variability of SSS (m) in the form of monthly anomalies compared with precipitation anomalies and temporal variability of SSS (n) in the form of monthly anomalies compared with temperature anomalies.

2.5.3 NDVI Mapping

The NDVI mapping effort was carried out simultaneously to depict and assess the spatial and temporal variation of the vegetation cover over a period of one year beginning from the month of March 1991 and continuing up to February 1992. The images lucidly project the variation occurring on a monthly basis and the impact of the hurricane on the vegetation cover of the watershed. The NDVI or vegetation cover of an area can be tied to temperature and precipitation of that area as higher temperature is associated with longer exposure of sunlight. Sunlight is needed for the photosynthesis process of the plants and rainfall is associated with the amount of water available to the plants to complete the photosynthesis process and create glucose, the primary source of energy for plants for growth and other processes.

As can be seen in the monthly NDVI maps for the Mattapoisett river watershed, the months of March and April has lower vegetation cover (Fig 2-11a and b). The index is also quite lower to the tune of 0.474 and 0.479, respectively (Table 2-4). As the temperature and average precipitation

increases over the flowing months, the vegetative cover begins to see a steady increase with indices of 0.633, 0.787, and 0.750 for the months of May, June and July respectively. The highest average NDVI is found for the month of June 1991 with a value of 0.787 (Table 2-4). This is because it is the peak summer time, temperatures are high and so sunlight is in abundance. This accelerates the photosynthesis process of the plants, which creates a dense vegetation cover over the watershed. The lowest NDVI value is found for the month of February 1991 with a value of 0.114 (Table 2-4). This can be attributed to the long-term effect of freezing temperatures that prevails in the area from December to February. The freezing conditions are not conducive to plant growth and so the NDVI steadily decreases from the month of December with a value of 0.359, January with a value of 0.351 and February with a value of 0.114 (Table 2-4). The values again see a steady increase as average temperature increases in the following months.

The impact of Hurricane bob can be clearly seen in the map of August 1991 (Fig. 2-11f). The NDVI value is 0.560 for the month of August, which are the effects of the hurricane. The spatial distribution for August shows that in the near middle of the watershed, the vegetation cover is lower than the upper and lower portions. This indicated the affected portion of the watershed. The hurricane impact is also depicted in the time series charts (Fig. 2-11m and n).The charts show normal patterns of NDVI values associated with temperature and precipitation except for the month of hurricane impact in August 1991.

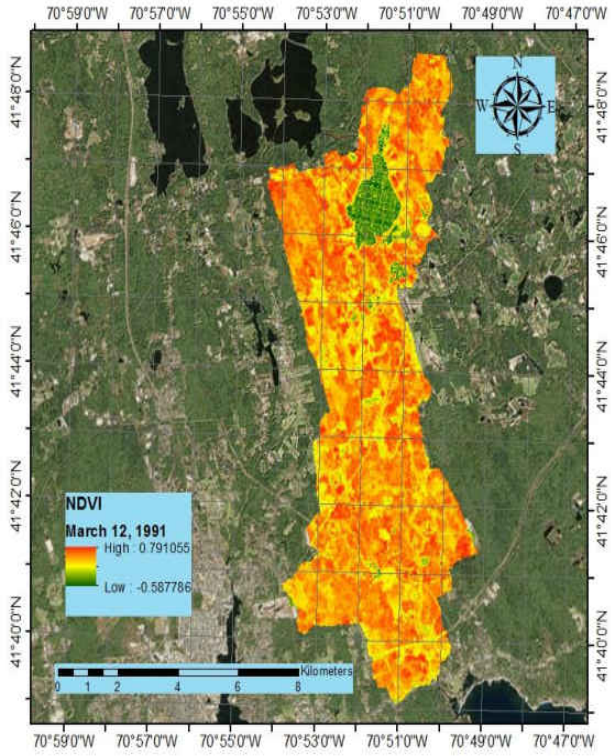

a) NDVI mapping for March 12, 1991

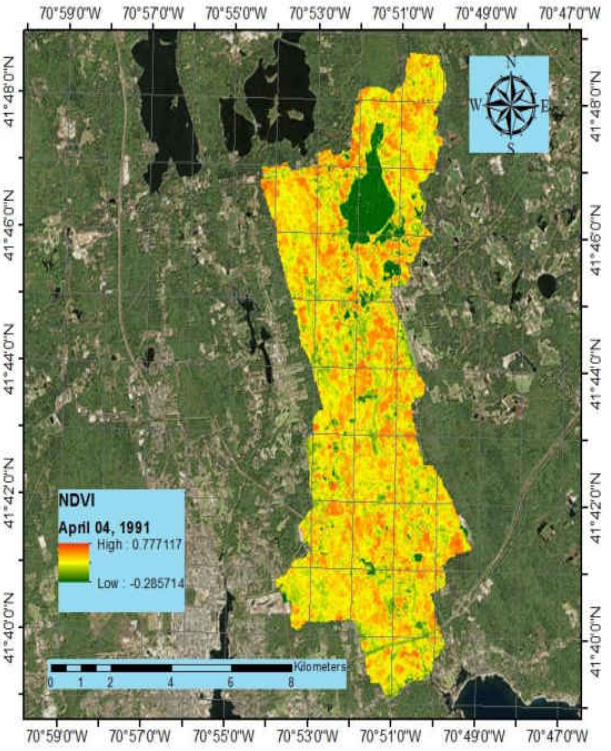

b) NDVI mapping April 04, 1991

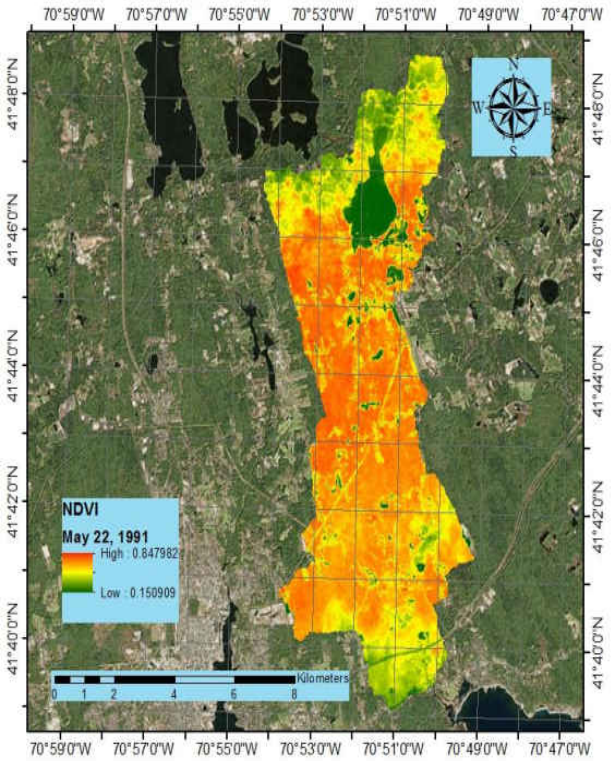

c) NDVI mapping for May 22, 1991

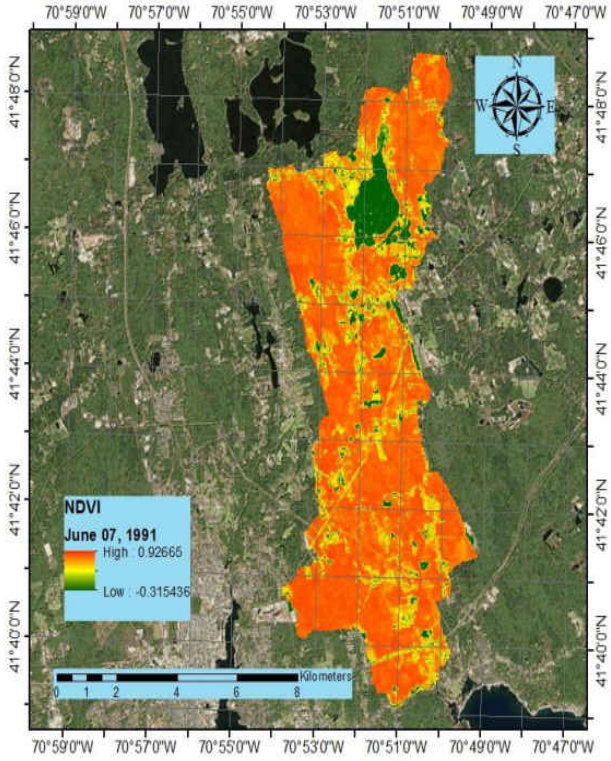

d) NDVI mapping June 07, 1991

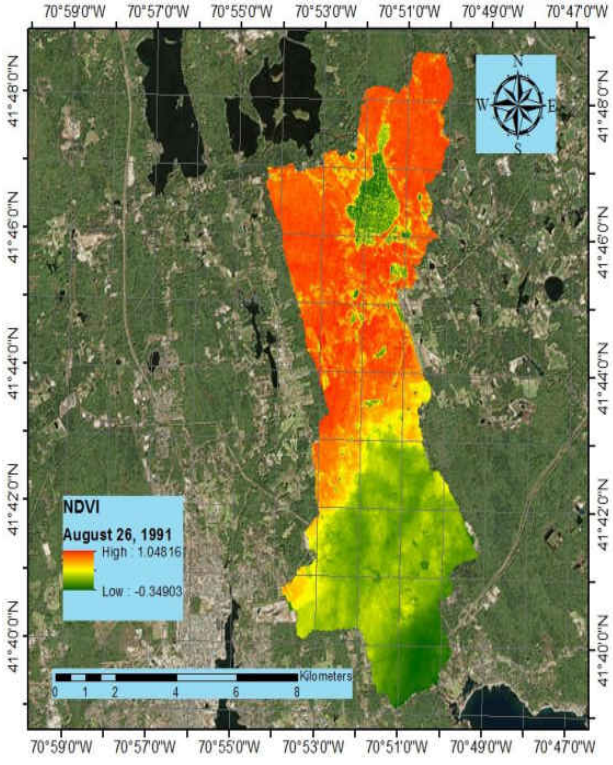

e) NDVI mapping for July 18, 1991

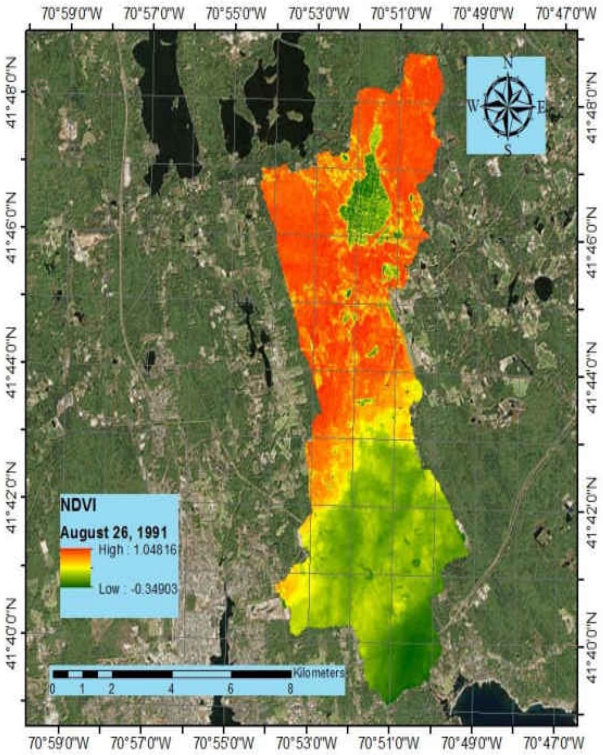

f) NDVI mapping August 26, 1991

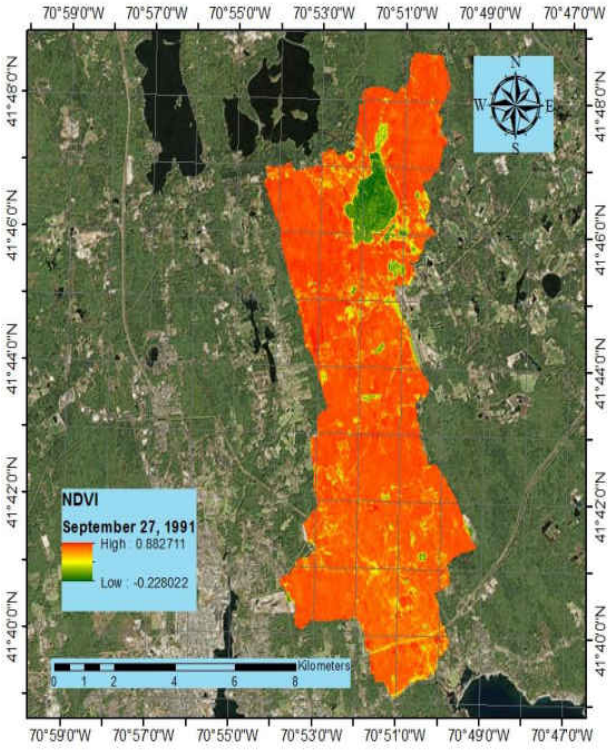

g) NDVI mapping for September 27, 1991

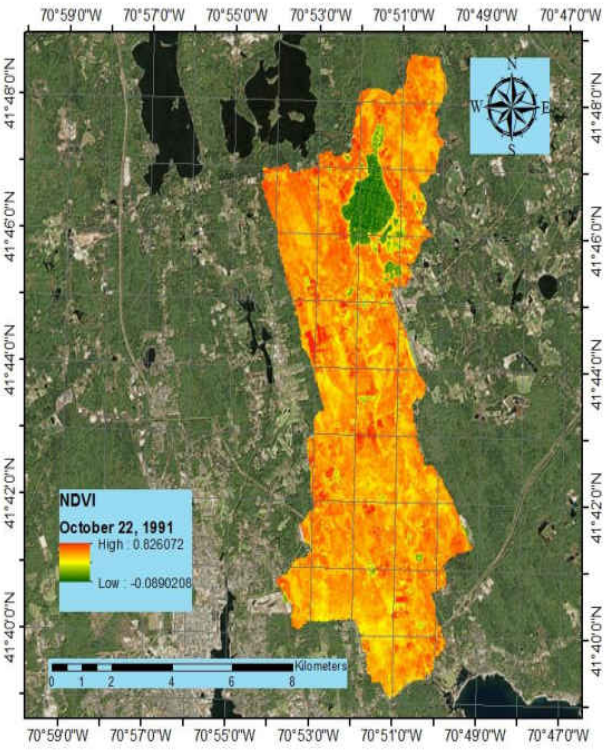

h) NDVI mapping October 22, 1991

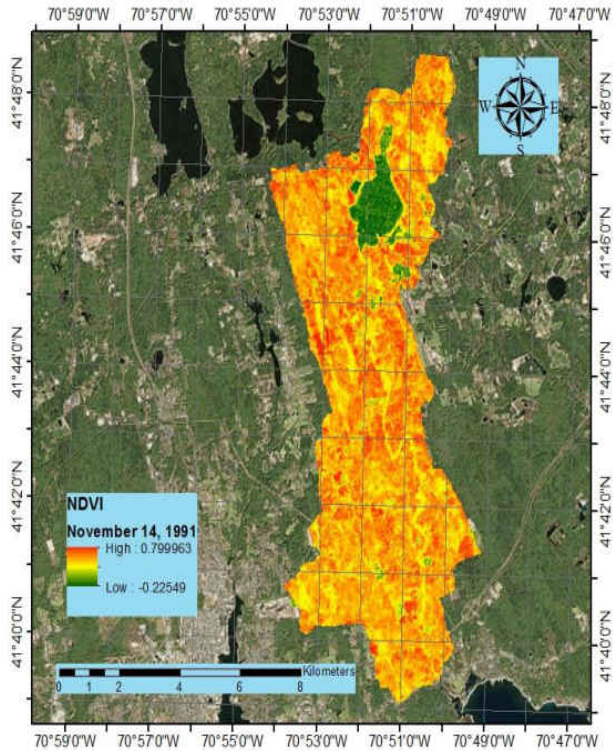

i) NDVI mapping for November 14, 1991

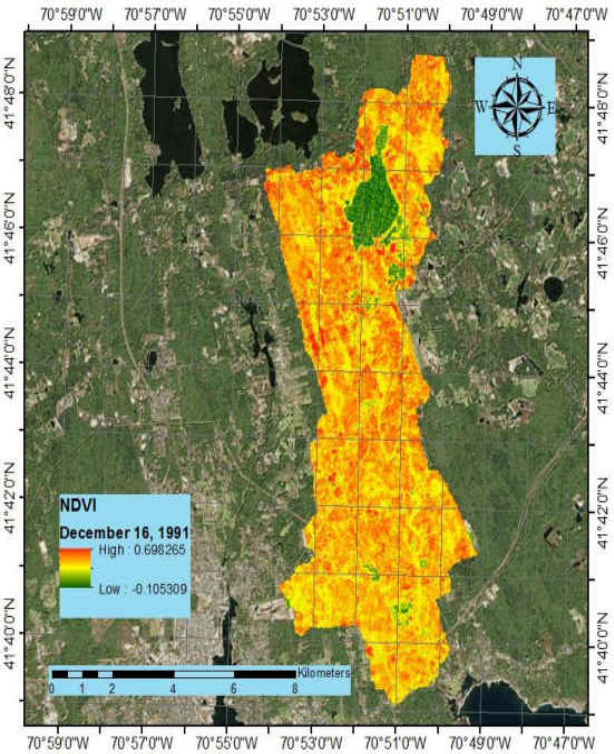

j) NDVI mapping December 16, 1991

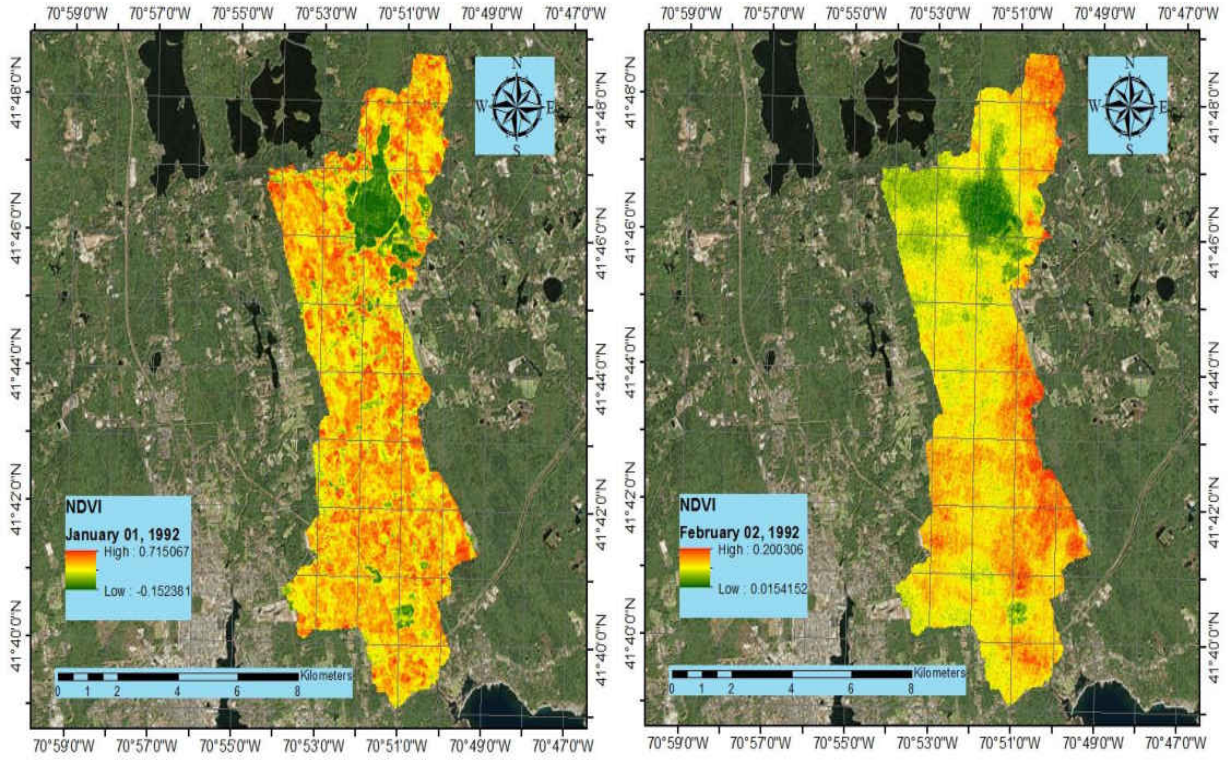

k) NDVI mapping for January 01, 1992

l) NDVI mapping February 02, 1991

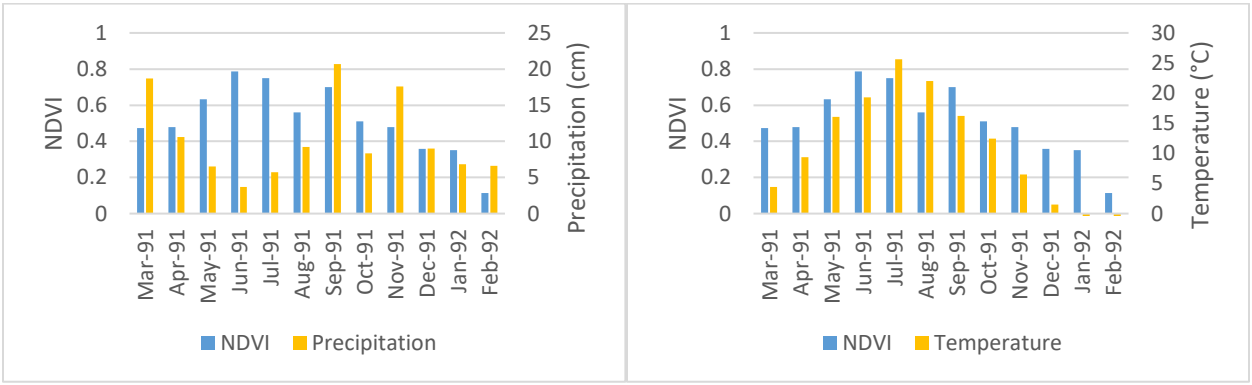

(m)

(n)

Figure 2-11: Spatial variability (a)-(l) in NDVI concentration for Mattapoisett River watershed. Temporal variability of NDVI (m) in the form of monthly anomalies compared with precipitation anomalies over a year and temporal variability of NDVI (n) in the form of monthly anomalies compared with temperature anomalies.

Table 2-4: Mean values of the parameters.

Months	Parameters				
	TOC (mg/L)	SSS (psu)	NDVI	Precipitation (cm)	Temperature (degree C)
March '91	0.165	25.249	0.474	18.69	4.44
April '91	0.155	24.063	0.479	10.59	9.39
May '91	0.143	22.798	0.633	6.53	16.06
June '91	0.147	21.822	0.787	3.68	19.28
July '91	0.150	25.612	0.750	5.72	25.60
August '91	0.144	22.013	0.560	9.22	22.00
September '91	0.148	24.046	0.700	20.70	16.22
October '91	0.149	23.613	0.510	8.33	12.44
November '91	0.152	24.087	0.479	17.60	6.50
December '91	0.155	22.467	0.359	9.02	1.50
January '92	0.154	23.281	0.351	6.83	-1.56
February '92	0.148	21.575	0.114	6.60	-0.72

2.5.4 Sea-Land Interaction within the Earth Systems Process

TOC trends (Fig. 2-6m) seem to follow SSS trends (Fig. 2-10m) for the period of March 1991 until May 1991 possibly due to increased inflow of freshwater from snowmelt in inland areas as temperatures increase. TOC has less variation around the mean (Fig. 2-6m) compared to SSS (Fig. 7 m) after May 1991. The greater variation in SSS can possibly be attributed to seasonal changes. From the period of April 1991 until June 1991 (Fig. 2-10 m and 2-10n), SSS decreases with increasing temperature. This could possibly indicate that snowmelt (from winter periods) in inland areas begin draining to the harbor, subsequently diluting the salinity concentration in the harbor. The period of July 1991 represents the impact of temperature changes on salinity changes in the harbor such that substantial increases in salinity concentration, compared to average (Fig. 2-10m), correspond to substantial increases in temperature, which can be associated with increased evaporation of water.

Hurricane Bob in August 1991 had impacts on TOC, SSS and NDVI in differing ways. TOC impacts after the Hurricane Bob seem to be long lasting rather than immediate. SSS and NDVI parameters were impacted immediately showing noticeably lower than average values in August 1991 compared to July and September. As evident in Fig. 2-10 m, SSS shows a dramatic decrease in August 1991 compared to that in July 1991 and rebounds above average in September 1991. Similarly, the impact of Hurricane Bob may have been the cause of the dramatic decrease in NDVI for the month of August compared to other summer months such as June and July (Fig. 2-11m); however, NDVI begins to make a rebound during the month of September after the hurricane landfall. To further illustrate, let us consider the months of July, August and September 1991, where July is the month before the hurricane landfall, August is the month when the hurricane made landfall, and September is the month after the hurricane. The NDVI image of July 1991 (Fig. 2-11e) shows considerable levels of vegetation cover. At the same time, the TOC image

(Fig. 2-6e) shows the normal gradient in the harbor area, i.e. the concentration is higher at the mouth of the river whereas the concentration is lower as it moves out of the sea. This shows normal discharge levels of the river and so, the sea-land interaction is normal. However, the NDVI image of August 1991 (Fig. 2-11f) shows the damage caused to the watershed vegetation cover to the southeast of the watershed. The high-sustained winds along with the heavy rainfall contributed to the damage sustained. Also, the TOC image (Fig. 2-6f) shows patches of lower concentration in the coastal area of the harbor that signifies the discharge and overland flow that eventually made way to the bay.

2.5.5 Impact of TOC and SSS gradient on Drinking Water

The Mattapoisett river watershed is an important source of drinking water supply for various municipalities situated around the area. The river basin has eight public water supply wells and numerous private wells that supply the water needs to the communities. Almost all of the wells are situated in the Mattapoisett River watershed area except for one that is near Fairhaven. The positions of the wells are clearly depicted in the figure below.

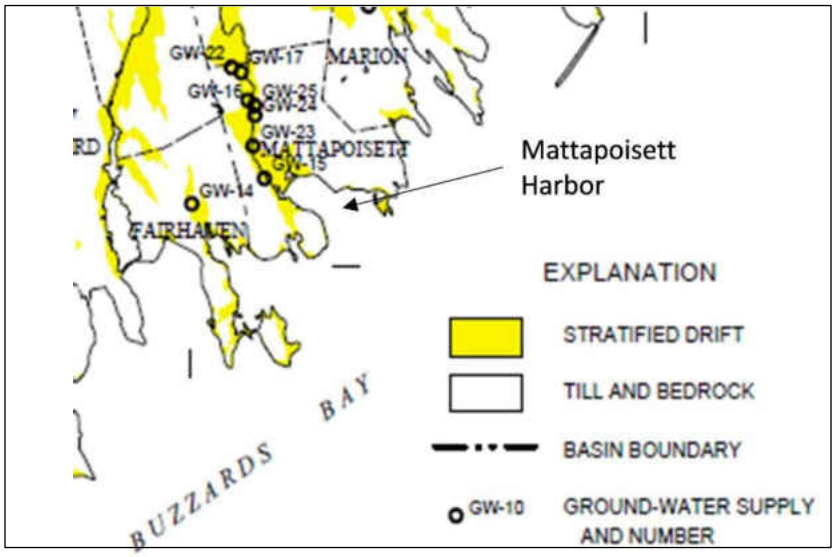

Figure 2-12: Map of positions of drinking water supply wells for Mattapoisett River watershed area (Adapted from Olimpio et al., 1984).

Since the watershed has considerable vegetation cover, there are concerns about the effect of TOC on the quality of groundwater that has been the major tap water source in the local communities. TOC, especially the dissolved part of TOC, which is known as Dissolved Organic Carbon (DOC). A fraction of DOC is biodegradable which in turn can cause bacterial growth in water (Vaan der Kooji et al., 1982). Other effects of DOC are that during disinfection process, it may produce disinfection by-products such as trihalomethanes and haloacetic acids (Fleck et al., 2004; Nguyen et al., 2005) and these are known carcinogenic compounds. These are strictly regulated by USEPA. DOC can also affect the pH of water (Butler et al., 2009), disrupt the chlorination (Nguyen et al 2005) and ozonation processes (Volk et al., 1993) of drinking water treatment systems. That is why it is necessary to monitor the TOC of estuary where river water is discharged. The monitoring of TOC to know its spatial and temporal distribution considerations may gain some understanding concerning possible impact on groundwater quality (Goni et al., 2003).

2.6 Conclusion

Using remote sensing technologies for data collection, is has been possible to gather satellite images for determining key water quality parameters for areas of concern not only temporally but also spatially. From remote sensing, sea-land interactions of water quality parameters such as SSS can be assessed on a larger scale. Results of this study show that SSS is primarily affected by sea-land interactions via both seasonal and meteorological changes, both directly and indirectly. SSS near coastal estuaries can be affected by influx of freshwater near inland outlet points such as rivers or streams. This influx can be exacerbated during winter months, for northern latitude regions, such that snowmelt in inland areas can affect directly connected coastal waterbodies. Hurricane impact can also affect SSS since its movement can be impacted by tides and waves, which can be highly variable during hurricane landfall. Results also indicate that TOC and NDVI can be impacted by hurricane impact as well; however, the pathways of such impacts are less complex compared to SSS and are more direct for NDVI. In addition, the spatial and seasonal monitoring of TOC and SSS reveals that the groundwater supply system is not harmed due to hurricane landfall.

2.7 References

Anderson, G. L., Hanson, J. D., & Haas, R. H. (1993). Evaluating Landsat Thematic Mapper derived vegetation indices for estimating above-ground biomass on semiarid rangelands. *Remote sensing of Environment*, *45*(2), 165-175.

Baban, S. M. (1997). Environmental monitoring of estuaries; estimating and mapping various environmental indicators in Breydon Water Estuary, UK, using Landsat TM imagery. *Estuarine, coastal and shelf science*, *44*(5), 589-598.

Brando, V. E., & Dekker, A. G. (2003). Satellite hyperspectral remote sensing for estimating estuarine and coastal water quality. *IEEE transactions on geoscience and remote sensing*, *41*(6), 1378-1387.

Butler, B. A. (2009). Effect of pH, ionic strength, dissolved organic carbon, time, and particle size on metals release from mine drainage impacted streambed sediments. *Water research*, *43*(5), 1392-1402.

Carlson, T. N., & Ripley, D. A. (1997). On the relation between NDVI, fractional vegetation cover, and leaf area index. *Remote sensing of Environment*, *62*(3), 241-252.

Chandrasekar, K., Sesha Sai, M. V. R., Roy, P. S., & Dwevedi, R. S. (2010). Land Surface Water Index (LSWI) response to rainfall and NDVI using the MODIS Vegetation Index product. *International Journal of Remote Sensing*, *31*(15), 3987-4005.

Chang, N. B., Vannah, B. W., Yang, Y. J., & Elovitz, M. (2014). Integrated data fusion and mining techniques for monitoring total organic carbon concentrations in a lake. *International Journal of Remote Sensing*, *35*(3), 1064-1093.

Chang, N. B. (2012). *Environmental Remote Sensing and Systems Analysis*. CRC Press, Boca Raton, Florida.

Chen, C., Tang, S., Pan, Z., Zhan, H., Larson, M., & Jönsson, L. (2007). Remotely sensed assessment of water quality levels in the Pearl River Estuary, China. *Marine Pollution Bulletin*, *54*(8), 1267-1272.

Delcroix, T., Henin, C., Porte, V., & Arkin, P. (1996). Precipitation and sea-surface salinity in the tropical Pacific Ocean. *Deep Sea Research Part I: Oceanographic Research Papers*, *43*(7), 1123-1141.

Doxaran, D., Froidefond, J. M., Lavender, S., & Castaing, P. (2002). Spectral signature of highly turbid waters: Application with SPOT data to quantify suspended particulate matter concentrations. *Remote sensing of Environment*, *81*(1), 149-161.

Environmental Protection Agency. (1998). *Your Coastal Watershed* (EPA Publication No. 842-F-98-006). Office of Water, (4504F): U.S. Environmental Protection Agency

Evans, C. D., Monteith, D. T., & Cooper, D. M. (2005). Long-term increases in surface water dissolved organic carbon: observations, possible causes and environmental impacts. *Environmental pollution*, *137*(1), 55-71.

Felisa, G., Ciriello, V., & Di Federico, V. (2013). Saltwater Intrusion in Coastal Aquifers: A Primary Case Study along the Adriatic Coast Investigated within a Probabilistic Framework. *Water*, *5*(4), 1830-1847.

Fleck, J. A., Bossio, D. A., & Fujii, R. (2004). Dissolved organic carbon and disinfection by-product precursor release from managed peat soils. *Journal of environmental quality*, *33*(2), 465-475.

Goñi, M. A., & Gardner, I. R. (2003). Seasonal dynamics in dissolved organic carbon concentrations in a coastal water-table aquifer at the forest-marsh interface. *Aquatic Geochemistry*, *9*(3), 209-232.

Hansell, D. A., & Carlson, C. A. (2001). Biogeochemistry of total organic carbon and nitrogen in the Sargasso Sea: control by convective overturn. *Deep Sea Research Part II: Topical Studies in Oceanography*, *48*(8), 1649-1667.

Hellweger, F. L., Schlosser, P., Lall, U., & Weissel, J. K. (2004). Use of satellite imagery for water quality studies in New York Harbor. *Estuarine, Coastal and Shelf Science*, *61*(3), 437-448.

Holm, A. M., Burnside, D. G., & Mitchell, A. A. (1987). The development of a system for monitoring trend in range condition in the arid shrublands of Western Australia. *The Rangeland Journal*, *9*(1), 14-20.

Hu, C., Chen, Z., Clayton, T. D., Swarzenski, P., Brock, J. C., & Muller–Karger, F. E. (2004). Assessment of estuarine water-quality indicators using MODIS medium-resolution bands: Initial results from Tampa Bay, FL. *Remote Sensing of Environment*, *93*(3), 423-441.

Hurcom, S. J., & Harrison, A. R. (1998). The NDVI and spectral decomposition for semi-arid vegetation abundance estimation. *International Journal of Remote Sensing*, *19*(16), 3109-3125.

Keith, D. J., Lunetta, R. S., & Schaeffer, B. A. (2016). Optical Models for Remote Sensing of Colored Dissolved Organic Matter Absorption and Salinity in New England, Middle Atlantic and Gulf Coast Estuaries USA. *Remote Sensing*, *8*(4), 283.

KHORRAM, S. (1985). Remote sensing of water quality in the Neuse River Estuary, North Carolina. *Photogrammetric Engineering and Remote Sensing*, *51*(3), 329-341.

Khorram, S., Cheshire, H., Geraci, A. L., & ROSA, G. L. (1991). Water quality mapping of Augusta Bay, Italy from Landsat-TM data. *International Journal of Remote Sensing*, *12*(4), 803-808.

Kreitler, C. W. (1993). *Geochemical techniques for identifying sources of ground-water salinization*. CRC press.

Lukina, E. V., Stone, M. L., & Raun, W. R. (1999). Estimating vegetation coverage in wheat using digital images. *Journal of Plant Nutrition*, *22*(2), 341-350.

Meyer, J. L., & Tate, C. M. (1983). The effects of watershed disturbance on dissolved organic carbon dynamics of a stream. *Ecology*, *64*(1), 33-44.

Mkhabela, M. S., Bullock, P., Raj, S., Wang, S., & Yang, Y. (2011). Crop yield forecasting on the Canadian Prairies using MODIS NDVI data. *Agricultural and Forest Meteorology*, *151*(3), 385-393.

Nguyen, M. L., Westerhoff, P., Baker, L., Hu, Q., Esparza-Soto, M., & Sommerfeld, M. (2005). Characteristics and reactivity of algae-produced dissolved organic carbon. *Journal of Environmental Engineering*, *131*(11), 1574-1582.

Nuttle, W. K., Fourqurean, J. W., Cosby, B. J., Zieman, J. C., & Robblee, M. B. (2000). Influence of net freshwater supply on salinity in Florida Bay. *Water Resources Research*, *36*(7), 1805-1822.

Pettorelli, N., Vik, J. O., Mysterud, A., Gaillard, J. M., Tucker, C. J., & Stenseth, N. C. (2005). Using the satellite-derived NDVI to assess ecological responses to environmental change. *Trends in ecology & evolution*, *20*(9), 503-510.

VALLEY, M. R. By Julio C. Olimpio and Virginia de Lima.

Van der Kooij, D., Visser, A., & Hijnen, W. (1982). Determining the concentration of easily assimilable organic carbon in drinking water. *Journal (American Water Works Association), 74*(10), 540-545. Retrieved from http://www.jstor.org/stable/41271382

Prasad, A. K., Chai, L., Singh, R. P., & Kafatos, M. (2006). Crop yield estimation model for Iowa using remote sensing and surface parameters. *International Journal of Applied Earth Observation and Geoinformation*, *8*(1), 26-33.

Quarmby, N. A., Milnes, M., Hindle, T. L., & Silleos, N. (1993). The use of multi-temporal NDVI measurements from AVHRR data for crop yield estimation and prediction. *International Journal of Remote Sensing*, *14*(2), 199-210.

R. Sempe´re´ , C. Panagiotopoulos, R. Lafont, B. Marroni, F. Van Wambeke (2001) Total organic carbon dynamics in the Aegean Sea, Journal of Marine Systems 33–34 (2002) 355–364

Ritchie, J. C., Zimba, P. V., & Everitt, J. H. (2003). Remote sensing techniques to assess water quality. *Photogrammetric Engineering & Remote Sensing*, *69*(6), 695-704.

Rouse Jr, J., Haas, R. H., Schell, J. A., & Deering, D. W. (1974). Monitoring vegetation systems in the Great Plains with ERTS.

Ruhl, C. A., Schoellhamer, D. H., Stumpf, R. P., & Lindsay, C. L. (2001). Combined use of remote sensing and continuous monitoring to analyse the variability of suspended-sediment concentrations in San Francisco Bay, California. *Estuarine, Coastal and Shelf Science*, *53*(6), 801-812.

Scanlon, T. M., Albertson, J. D., Caylor, K. K., & Williams, C. A. (2002). Determining land surface fractional cover from NDVI and rainfall time series for a savanna ecosystem. *Remote Sensing of Environment*, *82*(2), 376-388.

Schumacher, B. A. (2002). Methods for the determination of total organic carbon (TOC) in soils and sediments. *Ecological Risk Assessment Support Center*, *2002*, 1-23.

Swift, C. T., & Mcintosh, R. E. (1983). Considerations for microwave remote sensing of ocean-surface salinity. *IEEE Transactions on Geoscience and Remote Sensing*, (4), 480-491.

Valiela, I., Peckol, P., D'avanzo, C., Kremer, J., Hersh, D., Foreman, K., & Crawford, R. (1998). Ecological effects of major storms on coastal watersheds and coastal waters: Hurricane Bob on Cape Cod. *Journal of Coastal Research*, 218-238.

Volk, C., Renner, C., Roche, P., Paillard, H., & Joret, J. C. (1993). Effects of ozone on the production of biodegradable dissolved organic carbon (BDOC) during water treatment. *Ozone: science & engineering*, *15*(5), 389-404.

Wang, Q., Adiku, S., Tenhunen, J., & Granier, A. (2005). On the relationship of NDVI with leaf area index in a deciduous forest site. *Remote sensing of environment*, *94*(2), 244-255

Woodruff, D. L., Stumpf, R. P., Scope, J. A., & Paerl, H. W. (1999). Remote estimation of water clarity in optically complex estuarine waters. *Remote Sensing of Environment*, *68*(1), 41-52.

Yengoh, G. T., Dent, D., Olsson, L., Tengberg, A. E., & Tucker, C. J. (2014). The use of the normalized difference vegetation index (NDVI) to assess land degradation at multiple scales: A review of the current status, future trends, and practical considerations. *Lund University Center for Sustainability Studies (LUCSUS), and the Scientific and Technical Advisory Panel of the Global Environment Facility (STAP/GEF)*.

CHAPTER 3: COMPARISON OF SOIL MOISTURE, VEGETATION COVER AND CANOPY CONDITION IN COASTAL WATERSHEDS DURING TWO DIFFERENT HURRICANE LANDFALLS

3.1 Introduction

Hurricane Bob was the first hurricane of the 1991 Atlantic hurricane season and was one of the most devastating hurricanes in New England's history. The total cost of the damage caused by the hurricane landfall was $ 1.5 billion of 1991 USD equivalent to $2.64 billion 2017 USD (NCDC, 2017). The resulting winds and high tidal waves devastated the Buzzards Bay and Cape Cod areas. High amount of rainfall, which was almost 20 cm, also contributed to the damage (Valeila et al., 1998). On-site inspections in the areas of direct impact in Buzzards Bay and Cape Cod have shown the impact of hurricane landfall on vegetative cover ending up trunk snapping, breakage of limbs, and defoliation of trees and death of herbaceous vegetation (Valeila et al., 1998).

Hurricane Irma is categorized as the strongest hurricane observed in the Atlantic after Hurricane Wilma in 2005. This was the second major hurricane for 2017 Atlantic hurricane season. The storm developed into category 5 hurricane before making landfall in Cuba on September 6 2017 and by the time it made landfall in Florida through Marco Island, the hurricane weakened to a category 3 hurricane and it went on through the mainland of USA until it dissipated off the coast of New England on September 16, 2017. The damage sustained on the mainland USA due to hurricane Irma landfall is estimated to be upwards of $50 billion.

The tasseled cap transformation (TCT) was first developed by Kauth and Thomas in 1976 to describe the growth of wheat cover in an agricultural field. They have linked the patterns found in Landsat data from the croplands as a function of the life cycle of the crops. The TCT involves the conversion of original satellite band data into composite band readings, which has arisen out

of empirical observations (Watkins, 2005). In other words, it is the weighted sum of separate channel readings over a set of satellite images. This method enhances the spectral information content of Landsat TM data. Typically, there are six TCTs. Of them, only three are generally used. They are brightness (measure of soil), greenness (measure of vegetation) and wetnesss (interrelationship of soil and canopy moisture). This transformation optimizes data viewing that helps in the studies of dynamics of vegetative cover of an area during an event. TCTs have become a global vegetative index that particularly separates the amount of soil brightness, vegetation, and moisture content in individual pixels.

The TCTs can be correlated to Normalized Difference Vegetative Index (NDVI) since NDVI also deals with the issue of vegetation cover of an area (Rouse et al., 1974). The NDVI is a numerical index, which uses the visible and infrared bands of the electromagnetic spectrum. In general, healthy vegetation retains a significant portion of visible light and reflects a large amount of near infrared light (Holme et al., 1987). The NDVI is determined using the red and infrared bands. These two bands are delicate to vegetation data. The more difference along the lines of these two bands, the denser the vegetation cover will be on the target site. It is used to monitor the live green vegetation of an area of interest. NDVI is applicable in a broad range of vegetation studies for the assessment of crop yields (Quarmby et al., 1993; Mkhabela 2011; Prasad et al., 2006), rangelands conveyance capacities (Yengoh et al., 2014) etc. It is often directly identified with other ground parameters such as ground cover percentage (Lukina et al., 1999; Scanlon et al., 2002), photosynthetic movement of the plant (Penuelas et al., 1995; Pettorelli et al., 2005), surface water (Fu et al., 2015; Chandrasekar et al., 2010), leaf territory record which is also known as leaf area index (Carlson et al., 1997; Wang et al., 2005), and the measure of biomass (Anderson et al., 1993).

The damage of vegetative cover in the Buzzards Bay and Cape Cod in the New England area during the Hurricane Bob event in 1991 had been extensive as assessed by physical inspection (Valeila et al. 1996; Valeila et al. 1998). On the other hand, the damage of vegetation cover of Big Cypress Swamp and flooding impact on the whole watershed during the Hurricane Irma event in 2017 had been devastating in southwest Florida. The dispersion phenomenon associated with TCTs before and after different types of hurricane landfall at the two entirely different landscapes has not yet been fully understood in the literature. With the availability of synchronous satellite imagery before and after the landfall and essential remote sensing image processing techniques, it is now possible to examine and explore more inherent surface earth processes with respect to TCTs and NDVI simultaneously in a timely manner without having ground truth data (site visits). Comparative statistical assessment, including box plots, dispersion coefficients, and coefficient of variations, may be grouped together to provide a holistic viewpoint with numerical scales to indicate the level of hurricane impact.

The damage of vegetative cover in the Buzzards Bay and Cape Cod in the New England area during the Hurricane Bob event in 1991 had been extensive as assessed by physical inspection (Valeila et al. 1996; Valeila et al. 1998). On the other hand, the damage of vegetation cover of Big Cypress Swamp and flooding impact on the whole watershed during the Hurricane Irma event in 2017 had been devastating in southwest Florida. The dispersion phenomenon associated with TCTs before and after different types of hurricane landfall at the two entirely different landscapes has not yet been fully understood in the literature. With the availability of synchronous satellite imagery before and after the landfall and essential remote sensing image processing techniques, it is now possible to examine and explore more inherent surface earth processes with respect to TCTs and NDVI simultaneously in a timely manner without having ground truth data (site visits).

Comparative statistical assessment, including box plots, dispersion coefficients, and coefficient of variations, may be grouped together to provide a holistic viewpoint with numerical scales to indicate the level of hurricane impact.

3.2 Study Areas and Natural Hazard Events

Hurricane Bob was the first hurricane of the 1991 Atlantic hurricane season and was one of the most devastating hurricanes in New England's history and the landfall date was August 19, 1991. The resulting winds and high tidal waves devastated the Buzzards Bay and Cape Cod areas. High amount of rainfall, which was almost 20 cm, also contributed to the damage (Valeila et al. 1998). It made landfall in the Mattapoisett River watershed creating a big impact on its landscape. The total cost of the damage caused by the hurricane landfall was $ 1.5 billion of 1991 USD equivalent to $2.64 billion 2017 USD (NCDC, 2017). On-site inspections in the areas of direct impact in Buzzards Bay and Cape Cod have shown the impact of hurricane landfall on vegetative cover ending up trunk snapping, breakage of limbs, defoliation of trees and death of herbaceous vegetation (Valeila et al. 1998).

Hurricane Irma is categorized as the strongest hurricane observed in the Atlantic after Hurricane Wilma in 2005. This was the second major hurricane in 2017 Atlantic hurricane season. The storm developed into category 5 hurricane before making landfall in Cuba on September 6 2017 and by the time it made landfall in Florida through Marco Island, the hurricane weakened to a category 3 hurricane and it went on through the mainland of USA until it dissipated off the coast of New England on September 16, 2017. The damage sustained on the mainland USA due to hurricane Irma landfall is estimated to be upwards of $50 billion.

There are two study areas considered herein for comparison. The first study area is a coastal watershed surrounding the Mattapoisett River and the area is 66.85 square kilometers (Fig. 1). A

Digital Elevation Model (DEM) of the two watersheds is provided to gain a better understanding of the area of interest (Fig. 2). The DEM figure of the Mattapoisett River watershed indicates that the lowest elevation is at the mouth of the river just before it drains out to the bay, which is 6 m (Fig. 2a). The elevation increases as we move further inland to the north. The highest elevation is 39 m and is situated at the northwestern side of the watershed. The average elevation is 22.5 m.

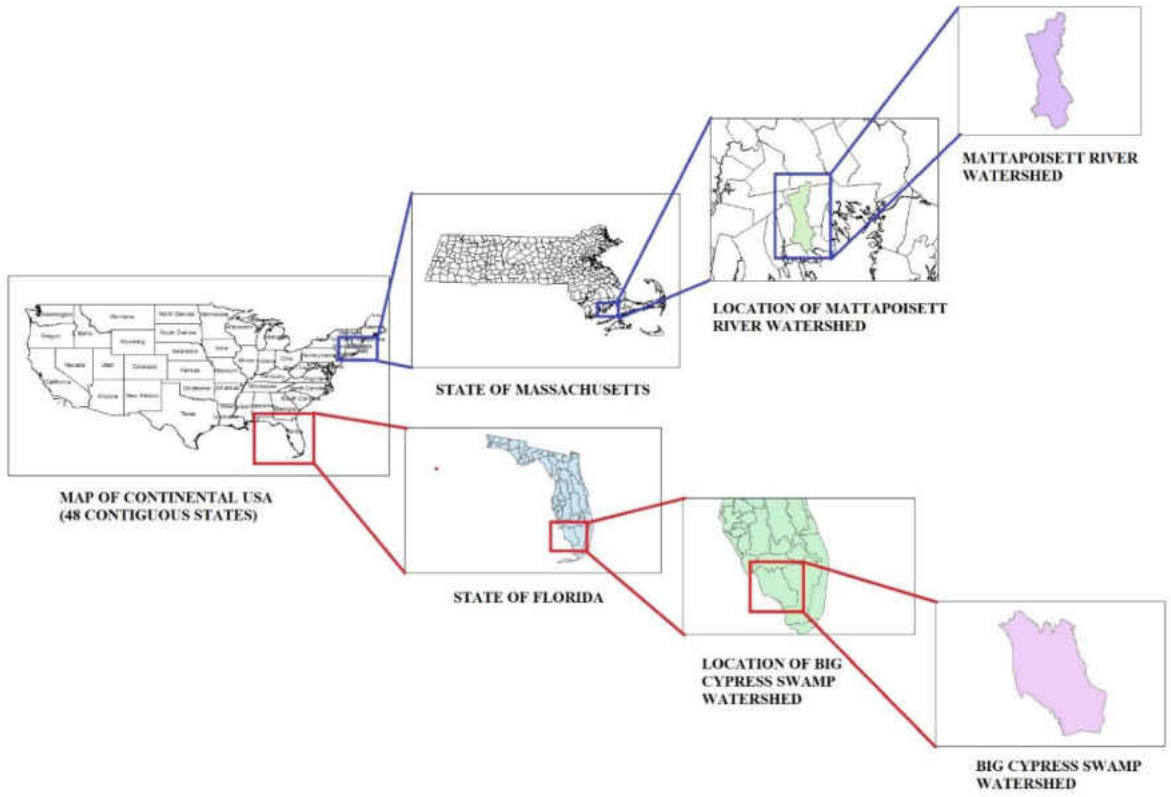

Figure 3-1: Geographical locations of Mattapoisett River watershed and Big Cypress Swamp watershed in the hurricane prone region, the United States.

The meteorological situation of the Mattapoisett area can be characterized by warm summers and relatively mild, wet winters. The summer season lasts from June to September, having an average temperature of 22°C (71°F). The winter season starts from December to March with an average temperature below 8°C (46°F). There is no significant seasonal variation in the

frequency of precipitation in Mattapoisett harbor area. The annual average rainfall is about 130 cm (51 inches) and is evenly distributed throughout the year (Olimpio et al. 1984).

There are two aspects of geological conditions that are important in the Mattapoisett river watershed. They are bedrock and surficial sediments of the Mattapoisett River. The bedrock of Mattapoisett river and adjacent valley mainly consist of granite and granite gneiss that is moderately weathered and fractured. The bedrock is relatively impermeable when compared with sand and gravel above the bedrock (Olimpio et al, 1984). In case of sediments, it can be said the river basin is comprised mostly of unconsolidated glacial sediments, consisting mostly of till and stratified drift (Olimpio et al. 1984).

The second study area is designated as the Big Cypress Swamp watershed situated in the southwestern part of Florida. The watershed is a part of Big Cypress National Preserve, which is one of the first preserves established in 1974 in the United States. It has an area of 2,900 square kilometers (728,000 ha) (History of Big Cypress, 1974). The preserve is mainly covered with cypress trees, consisting about one-third of all the trees and is host to diverse biological species. The DEM map provided for the watershed is a partial DEM for the watershed. The South Florida Water Management District provided this partial DEM. The elevation near the coastal area and out to the sea is an average of 2.84 meters and the elevation increases to a maximum of 37.02 meter at the northeast corner (Fig. 2b). The climate of Big Cypress Swamp watershed is that of tropical savannah. The wet months are May through October when it receives about 142 cm (56 inches) of rain annually. The dry months are November through April (Source: National Park Service). The hottest month is July with a high temperature of 32°C (89°F). The coldest month is January with a low of 12°C (54°F).

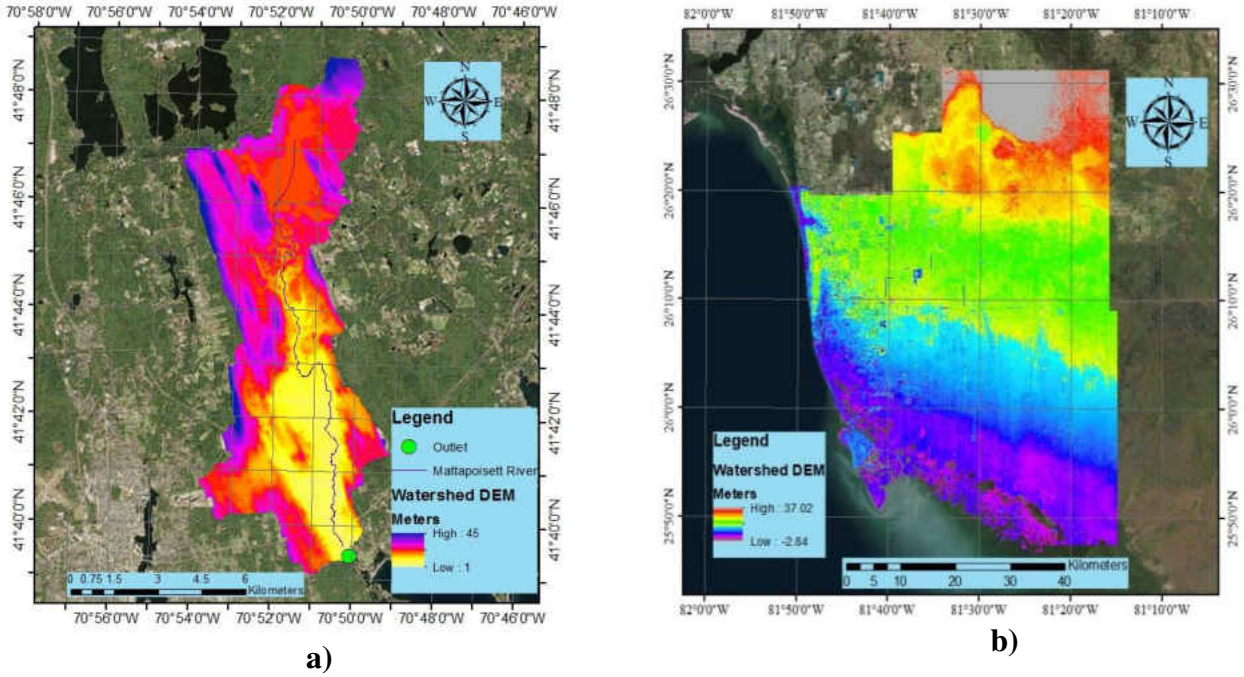

a) **b)**

Figure 3-2: DEM of a) Mattapoisett River watershed and b) partial Big Cypress Swamp watershed.

3.3 Methods and Data

A TCT is performed by taking linear combinations of the original spectral bands. This is similar to the concept of principal component analysis. Principal component analysis helps form new variables as weighted sums of different band readings. Equivalently, the first three transformations i.e. brightness, greenness, and wetness contain most of the information and so these are applied. The rest of the transformations are treated as noise and rarely used. The TCT coefficients used are derived statistically, which are specific to each sensor. The TCT coefficients in the current study are generated based on Landsat-5 TM and Landsat-8 OLI/TIRS images, which are depicted in Table 1 and Table 2. The tasseled cap components, when pixel values are plotted, give a better understanding of the landscape dynamics for which the transformation is being

implemented. The plots of tasseled cap components in Fig. 3 depict how the landscape looks when it is in an undisturbed state.

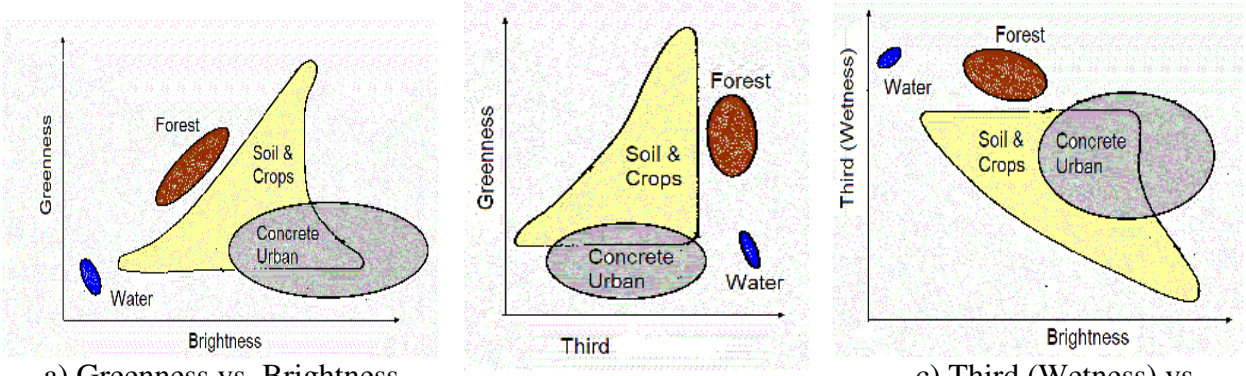

a) Greenness vs. Brightness

b) Greenness vs. Third (Wetness)

c) Third (Wetness) vs. Brightness

Figure 3-3: Tasseled cap transformation plots for landscape interpretation (Adapted from Kauth and Thomas, 1976; Crist et al., 1986).

Table 3-1: Tasseled cap coefficients for Landsat-5 TM (Crist, 1985)

Bands	**Landsat-5 TM**		
	Brightness	**Greenness**	**Wetness**
Band 1	0.2043	-0.1603	0.0315
Band 2	0.4158	-0.2819	0.2021
Band 3	0.5524	-0.4934	0.3102
Band 4	0.5741	0.7940	0.1594
Band 5	0.3124	-0.0002	-0.6806
Band 7	0.2303	-0.1446	-0.6109

Table 3-2: Tasseled cap coefficients for Landsat-8 OLI/TIRS (Baig et al., 2014)

Bands	Landsat-5 TM		
	Brightness	**Greenness**	**Wetness**
Band 2	0.3029	-0.2941	0.1511
Band 3	0.2786	-0.243	0.1973
Band 4	0.4733	-0.5424	0.3283
Band 5	0.5599	0.7276	0.3407
Band 6	0.508	0.0713	-0.7117
Band 7	0.1872	-0.1608	-0.4559

To carry out this study, the first step was to create a shapefile of the Mattapoisett River watershed area. This was done using the DEM map as the base. The shapefile was created in Ground Control System (GCS) coordinates. The actual shape of the image was obtained after projection of the shapefile from GCS to Universal Transverse Mercator (UTM) coordinate system. The shapefile for Big Cypress Swamp watershed was created in the same way. The collection of Landsat-5 TM imagery and Landsat-8 OLI/TIRS imagery from USGS data pool is the second step. The spatial resolution of both Landsat-5 TM and Landsat-8 OLI/TIRS imagery is 30 m and the temporal resolution is 16 days. The images were selected in such a way that one image for the months of July, August and September was collected for the years 1990, 1991, and 1992, respectively, to cover the scenarios before, during and after the event of the Hurricane Bob landfall, and the landfall date was August 19, 1991. Landsat-5 TM bands 1-5, 7 were selected for downloading. For Big Cypress Swamp, the images selected were for the dates of August 29, 2017 and September 14, 2017; representing before and after landfall images respectively. The Landsat-

5 surface reflectance products are radiometrically corrected at sensor level. The products are preprocessed using an algorithm named Second Simulation of a Satellite Signal in the Solar Spectrum (6S). This algorithm applies atmospheric, geometric and other necessary corrections before delivering the final product. For Landsat-8, the surface reflectance images are generated Landsat Surface Reflectance Code (LaSRC) algorithm. This algorithm applies atmospheric and radiometric corrections before delivering the final product. After download was complete, they were processed and reprojected to UTM coordinate system for the watershed using ArcGIS toolbox created specifically for this purpose. The final step was generating the TCT plots. The processed images were used to create composite images, comprising all the bands. Then the composite images were used in ENVI® software to create these TCT plots using the coefficients in Table 3-1. For Landsat-8, the tasseled cap transformations were performed in ArcGIS manually using "Raster Calculator" tool. The images were then fed into ENVI® software to generate the plots. Since most of the information (95-98%) are contained in the first three transformations (Vorovencii, 2007), i.e. brightness, greenness and wetness (third), only these three transformations were performed and presented herein. The whole process is summarized in a flowchart as shown in Fig. 4. It led to the development of TCT maps based on multi-sensor Landsat images and associated statistical analyses.

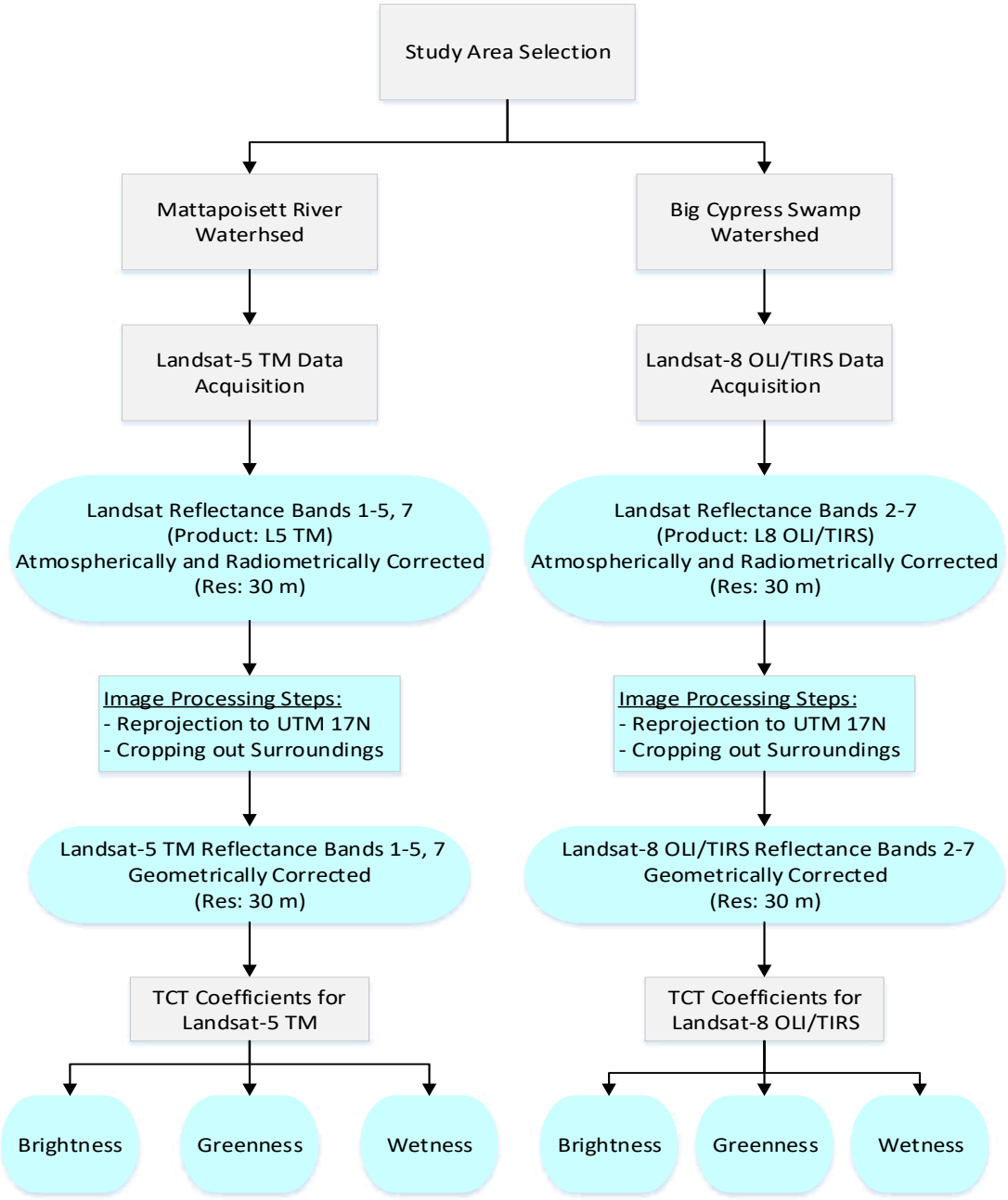

Figure 3-4: Flowchart depicting the GIS and Remote Sensing work conducted for TCT transformation

To clearly depict the critical areas of the tasseled cap transformation plots, the critical areas are marked by different color according to Fig. 3-3 and a name convention has been established so that the areas are distinguished across the various plots to ease our discussion later. As an example, let us consider the marking GBMA1. The first two letters indicate the name of the plot.

In this case, it is Greenness vs. Brightness plot (GB). Subsequently, GW stands for Greenness vs. Wetness plots and WB stands for Wetness vs. Brightness plots. The third letter stands for the study area. Here, M stands for Mattapoisett River Watershed area and B stands for Big Cypress Swamp watershed. The fourth letter stands for the month of hurricane event. Here, A stands for the month before hurricane made landfall, B stands for the month hurricane made landfall, and C stands for the month after hurricane made landfall. The fifth place is numerical. It indicates the type of land cover. For this study, 1 represents concrete cover, 2 is for turbid water, 3 is for clear water and 4 represents forest area. This name convention will be applied in our holistic assessment.

Finally, the NDVI algorithm was also calculated by subtracting the red reflectance values from the near-infrared and dividing it by the sum of near-infrared and red reflectance values. The formula for NDVI can be written as;

$$NDVI = \frac{R_{NIR} - R_{Red}}{R_{NIR} + R_{Red}} \quad (3\text{-}1)$$

The NDVI mapping effort was also carried out using the "Image Analysis" tool of ArcGIS software. The two bands in equation (3-1) were used as input in the tool and the NDVI maps were generated as output. The NIR corresponds to band 4 and the red band corresponds to band 3 of Landsat-5, respectively.

The TCT plots help us see the qualitative significance. However, it is important to back up the qualitative significance with quantitative analysis and prove the numerical significance. For this purpose, a series of statistical analysis was performed. The pixels values of the entire watershed were collected for brightness, greenness and wetness plots for before and after the landfall scenarios. For Hurricane Bob, the before-landfall date was chosen as July 18, 1991 and after-landfall date was August 26, 1991 i.e. five days after hurricane landfall. The same statistical

analysis was performed for the before- and after-landfall scenario of Hurricane Irma. The results of the statistical analysis are tabulated in Table 3-3.

The formulas for standard deviation, coefficient of variance and quartile coefficient of variation is listed below,

Standard Deviation:

$$s = \sqrt{\frac{1}{N-1}\sum_{i=1}^{N}(x_i - \overline{x})^2}, \tag{3-2}$$

where $\{x_1, x_2, ..., x_N\}$ is the sample and $\overline{x}$ is the mean of the sample. The denominator $N - 1$ is the number of degrees of freedom in the vector $(x_1 - \overline{x}, ..., x_N - \overline{x})$.

Coefficient of variation:

$$CV = \frac{s}{\bar{x}} \tag{3-3}$$

Where, s is the standard deviation and $\bar{x}$ is the mean of the sample.

Quartile coefficient of dispersion: $\frac{Q_3 - Q_1}{Q_3 + Q_1}$ (3-4

where, Q_1 is the first quartile of a dataset and Q_3 is the third quartile of the same dataset. Note that the first quartile, denoted by Q_1, is the median of the lower half of the data set.

Since the pixels close to one another, they are also checked for autocorrelation using a statistical index called Moran's I. Moran's I is the measure of spatial autocorrelation (Dormann et al., 2007). This index is defined as,

$$I = \frac{N}{W}\frac{\sum_i \sum_j w_{ij}(x_i - \bar{x})(x_j - \bar{x}))}{\sum_i (x_i - \bar{x})\text{^}2} \tag{3-5}$$

where N is the number of spatial units indexed by i and j; x is the variable of interest; $\bar{x}$ is the mean of x; w_{ij} is the matrix of spatial weights with zeroes in the diagonal.

Moran's I values are within +1 to -1. If the value is close to +1, it indicates the values of the data set are spatially clustered and if the value is close to -1, the values of the data set are dispersed. A value of zero or close to zero indicates random distribution. A literature search reveals that the Moran's I values are mainly used in ecology (Lichstein et al., 2002; Koenig et al., 1999; Dale et al., 2002; Fortin et al., 1990), species distribution (Dormann et al., 2007; Naimi et al., 2011), rangeland ecology (Augustine et al., 2012; Sankey et al., 2008) and host of other biological and ecological branches. The Moran's I values are used to determine if the species distribution in a given area have any effect from the neighboring area as the distribution of the species data are generally not considered random. This is why Moran's I is more useful in case of spatial analysis of ecological species.

For our study we took into consideration the TCT and NDVI indices to explore how a particular natural extreme event wreaked havoc on the vegetative cover of a given watershed area. This study does not take into account the distribution of neither plant species nor any other ecological species over the study area and so, the use of Moran's I indices for this study is not necessary.

3.4 Results and Discussion

3.4.1 Hurricane Bob

The TCT plots for the Mattapoisett River watershed is shown in the Fig. 3-4, 3-5 and 3-6.. The plots help us demonstrate the effect that hurricane landfall had on the watershed landscape. The plots also feature the landscape conditions one year before, during hurricane year and one year after the hurricane landfall. In the case of aftermath scenario, cloud-free Landsat images are not available for the month of July 1992. Thus, no plots are provided for this month.

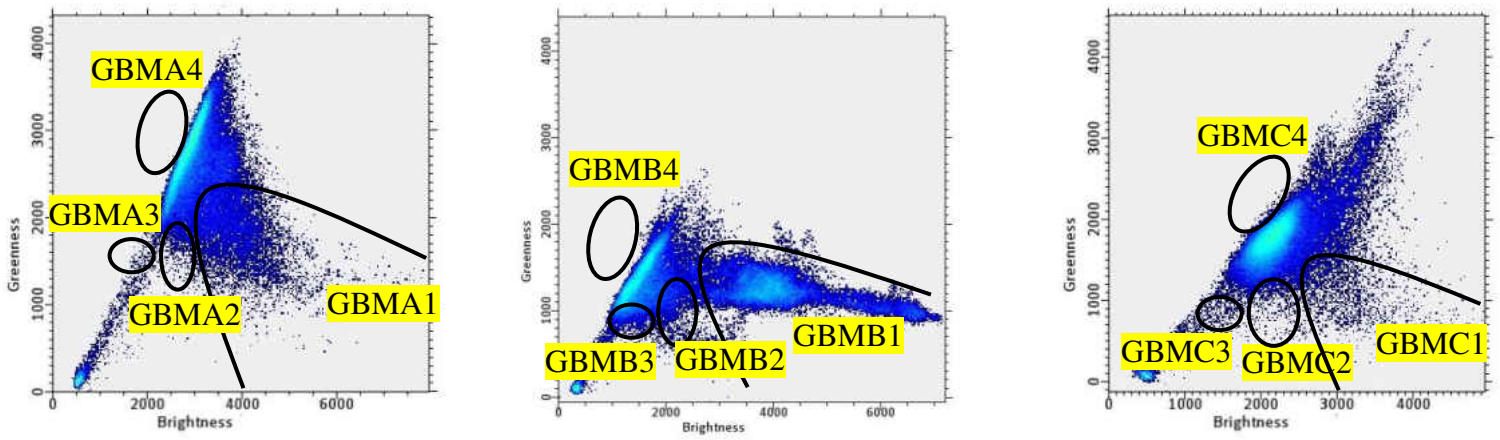

a) July 18, 1991

b) August 26, 1991

c) September 27, 1991

Figure 3-5: TCT comparison for Greenness vs. Brightness plots for Mattapoisett River watershed area. The light blue areas in the plots indicate the probability of higher density of pixel values. Fig. 5a depicts the plot for one month before landfall, Fig. 5b one week after landfall, and Fig. 5c the month after landfall..

It is now possible to interpret the landscape using the reference plot in Fig. 3-3a based on the greenness vs. brightness plots depicted in Fig. 3-5. One month before the hurricane landfall, i.e. for July 18, 1991 (Fig. 3-5a), the plot is marked with regions of interest according to Fig. 3-3-3a where region GBMA1 is concrete urban, GBMA2 is turbid water, GBMA3 is clear water and GBMA4 is forest region. The regions with higher pixel concentrations are the place where the pixels of soils and crops and in our case, small vegetation cover is situated. The plot for July 18, 1991 shows the typical and normal regional distribution. The change in landscape is clearly noticeable in the plot of August 26, 1991, which is one week after the hurricane landfall (Fig 3-5b). There is fragmentation in the regions of soil and vegetation pixels, clear water (GBMB3), and turbid water (GBMB2) pixels. This plot does not show any major fragmentation in the forest region (GBMB4). The concrete urban areas (GBMB1) also show significant disturbances via scattering of the pixels, depicting significant damage to the infrastructure and urban residential areas situated within the watershed. Due to emergency response and restoration efforts, the landscape appears to be reverting to its former conditions one month after the hurricane (Fig. 3-5c). One month after, the landscape returns to what it was before the hurricane landfall. The regions of clear water (GBMC3) and turbid water (GBMC2) have gone back to normal positions. The concrete urban regions (GBMC1) also reflect the signs of recovery. The forest regions (GBMC4), however, remain unchanged. However, the plots of greenness vs. wetness (third) and wetness (third) vs. brightness may yield more information about the changes in the landscape before and after the hurricane landfall.

.

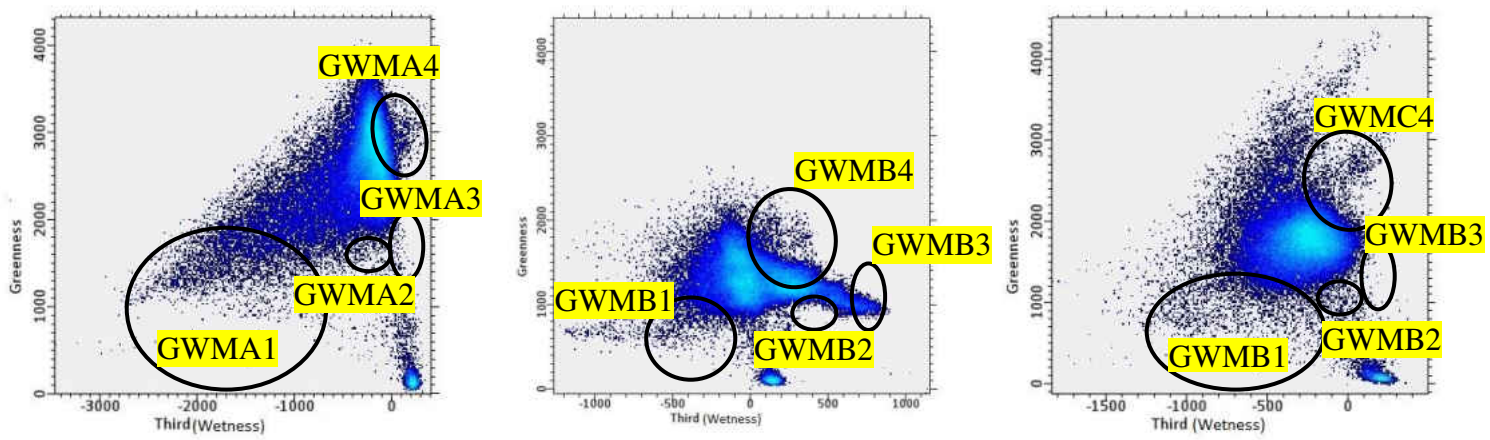

a) July 18, 1991 b) August 26, 1991 c) September 27, 1991

Figure 3-6: Tasseled cap transformation Greenness vs. Third (Wetness) plots for Mattapoisett River watershed area. The light blue areas in the plots indicate the probability of higher density of pixel values. Fig. 6a depict, the plot for one month before landfall, Fig. 6b one week after landfall, and Fig. 6c the month after landfall,

Let us now compare the greenness vs. wetness plots of the watershed (Fig. 6) with the aid of the plot in Fig. 3-3b. The plot for July 18, 1991 (Fig 3-6a) i.e. the month before hurricane landfall shows normal landscape conditions for clear water (GWMA2), turbid water (GWMA3), forest (GWMA4) and concrete urban (GWMA1) regions. However, one week after the hurricane landfall, significant changes in the landscape are evident as was the case for previous plot (Fig 3-6b). The soil and small vegetation pixels show significant distortion with a strong dispersion phenomenon, indicating damage to the vegetation cover. In addition, the pixels on the side of concrete urban (GWMB1) show significant scattering with a strong dispersion phenomenon too, indicating significant damage caused by wind and storm surges. The regions of clear water (GWMB2) and turbid water (GWMB3) pixels also show distortions. There are significant changes in the forest regions as well (GWMB4). One month after the hurricane i.e. for the plot of September 27, 1991 (Fig. 3-6c), we can see that recovery is in progress in the concrete urban (GWMC1) and small vegetation sections. The clear water (GWMC2) and turbid water (GWMC3) areas also show return to normalization. However, the pixels in the forest regions (GWMC4) show scattering still present, although with less intensity. This indicates that recovery is slow in the forest regions.

.

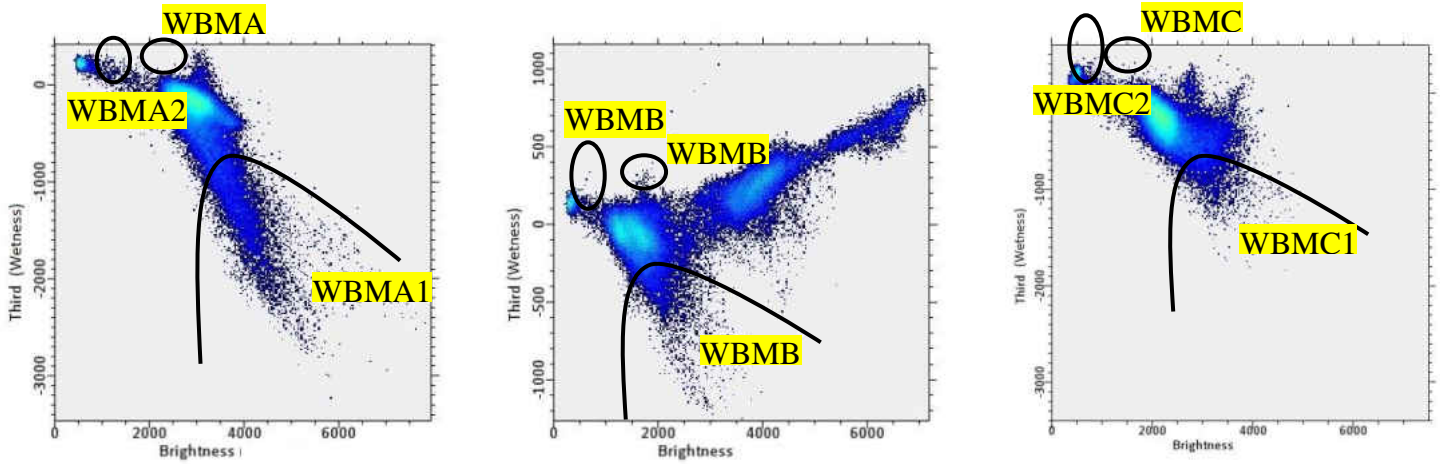

d) July 18, 1991 e) August 26, 1991 f) September 27, 1991

Figure 3-7: Tasseled cap transformation Third (Wetness) vs. Brightness plots for Mattapoisett River watershed area. The light blue areas in the plots indicate the probability of higher density of pixel values. Fig. 7a depicts the plot for one month before landfall, Fig. 7b one week after landfall, and Fig. 7c the month after landfall.

Similarly, the wetness vs. brightness plot also yield evidence of hurricane impact when compared to the typical plot of Fig. 3-3c. In this case, the interactions and changes of the soil and small vegetation cover are more evident (Fig. 3-7). In essence, the plots of third (wetness) vs. brightness provide more information about soil moisture condition and urban concrete cover than vegetative cover. This can be seen in the plots for the Mattapoisett River watershed landscape. One month before the hurricane landfall, the landscape shows consistent patterns concerning clear water (WBMA2), turbid water (WBMA3) and concrete urban cover (WBMA1). The light blue area of the plot, where the bulk of the pixel values reside, represents crops and small vegetation regions (Fig. 3-7a). One week after the hurricane landfall, the effect is clearly visible on these parameters (Fig. 3-7b). The significant distortions as shown by the dispersion phenomena are in the pixel areas soil and small vegetation region and concrete cover (WBMB1). The clear water (WBMB2) and turbid water (WBMB3) regions. The disappearance of dry soil pixels indicates flooding due to rain and storm surges and the disappearance of concrete cover pixels indicate the damage to urban areas situated within the boundary of the watershed. However, one month after the hurricane landfall, the dry soil pixels and the concrete cover (WBMC1) pixels show a slow return, indicating the emergency response efforts and the gradual return of the landscape to its normal conditions, indicating the recovery efforts (Fig. 3-7c). The clear water (WBMC2) and turbid water (WBMC3) pixels are also showing signs of return to previous values.

3.4.2 Hurricane Irma

Let us now look at the TCT plots for Big Cypress Swamp watershed and analyze how hurricane Irma landfall affected the landscape of the watershed. The TCT plots in Fig. 8 represent the conditions of landscape of Big Cypress Swamp watershed of Florida, which is where Hurricane Irma made landfall as a Category 3 hurricane. This watershed was directly in the path of the

hurricane when it made landfall, resulting in the damages in the landscape of the area. This watershed area is comprised of dense vegetation and swamps, which is an unfavorable condition for obtaining ground samples for laboratory testing and on-the-spot surveying. That is why, the best method to assess and observe this watershed is to use remote sensing. The significant changes in the tasseled cap transformation plots in the before and after scenario are an attestation to that. The plots are so arranged so that the difference in the before and after scenarios are clearly visible and easily interpretable

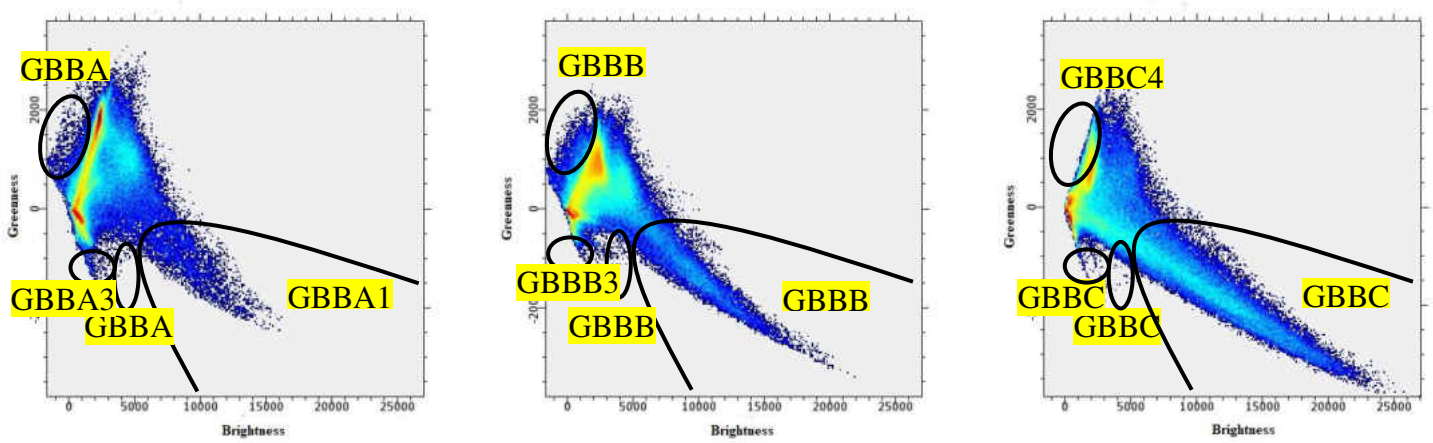

a) August 29, 2017 b) September 14, 2017 c) October 16, 2017

Figure 3-8: Tasseled cap plots Greenness vs, Brightness (ENVI 5.3 software output) derived for Big Cypress Swamp watershed area. The yellow and red areas in the plots, which becomes light blue as it moves out, indicate the probability of higher density of the pixel values. Fig. 8a depicts the plot for month before landfall, Fig. 8b four days after landfall, and Fig. 8c the month after landfall.

Let us look at the Greenness vs Brightness plots for the before and after scenarios (Fig. 3-8). For, the plot is comparable to the standard plot depicted in Fig. 3-3a. The plot for before landfall shows the condition of clear water (GBBA3), turbid water (GBBA2), concrete urban (GBBA1), forest (GBBA4) and vegetation conditions (Fig. 3-8a). After hurricane made landfall, significant changes are noticed in the after-landfall scenarios. The changes are noticeable in the soil and small vegetation area. The yellow and red, which becomes light blue as it moves out areas in all three plots, represent soil and small vegetation regions. Distortion in the pixel values are seen after the landfall (Fig. 3-8b). Huge waves made inland when the hurricane hit, along with heavy rainfall, which contributed to the changes in the urban section (GBBB1). The clear water (GBBB2) and turbid water (GBBB3) sections also show changes. The more significant change is noticed in the forest region (GBBB4), as there is distortion in the values relative to the before condition. One month after landfall i.e. for the plot of October 16, 2017 (Fig 3-8c), we can see that the forest (GBBC4), clear water (GBBC2) and turbid water regions (GBBC3) have returned to previous conditions.

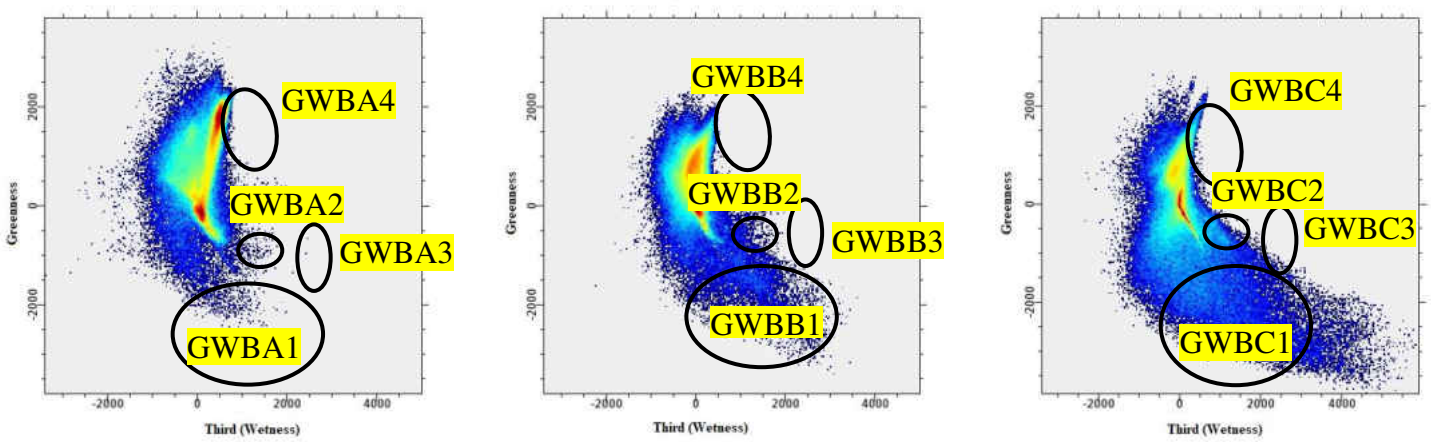

a) August 13, 2017 b) September 14, 2017 c) October 16, 2017

Figure 3-9: Tasseled cap plots Greenness vs Wetness (ENVI 5.3 software output) derived for Big Cypress Swamp watershed area. The yellow and red areas in the plots, which become light blue as it moves out, indicate the probability of higher density of the pixel values. Fig. 9a depicts the plot for month before landfall, Fig. 9b four days after landfall, and Fig. 9c the month after landfall,.

Similarly, in the greenness vs. wetness plots for the before-landfall scenario (Fig. 3-9a), shape of the plots has small resemblance to the standard plot depicted in Fig. 3-3b. The clear water (GWBA2), turbid water (GWBA3), forest covers (GWBA4) and urban regions (GWBA1) can be seen in Fig. 3-9a. Although the plots before and after conditions are also quite similar, there is significant distortion in the after-landfall scenario in the sections of clear water (GWBB2) and turbid water (GWBB3) (Fig. 3-9b). This can be attributed to the heavy rains that poured down and coupled with storm surges, created a flooding situation in the watershed area. The pixels in the concrete urban area also show significant distortion, which reveals the impact of flooding in the urban areas. The concrete cover (GWBB1) also underwent significant change. However, one month after hurricane i.e. on October 16, 2017, the clear water (GWBC2), turbid water (GWBC3) and forest cover (GWBC4) sections are going back to previous conditions. The concrete cover (GWBC1) pixels that show distortions have not subsided, indicating that the concrete cover of the watershed has not yet recovered.

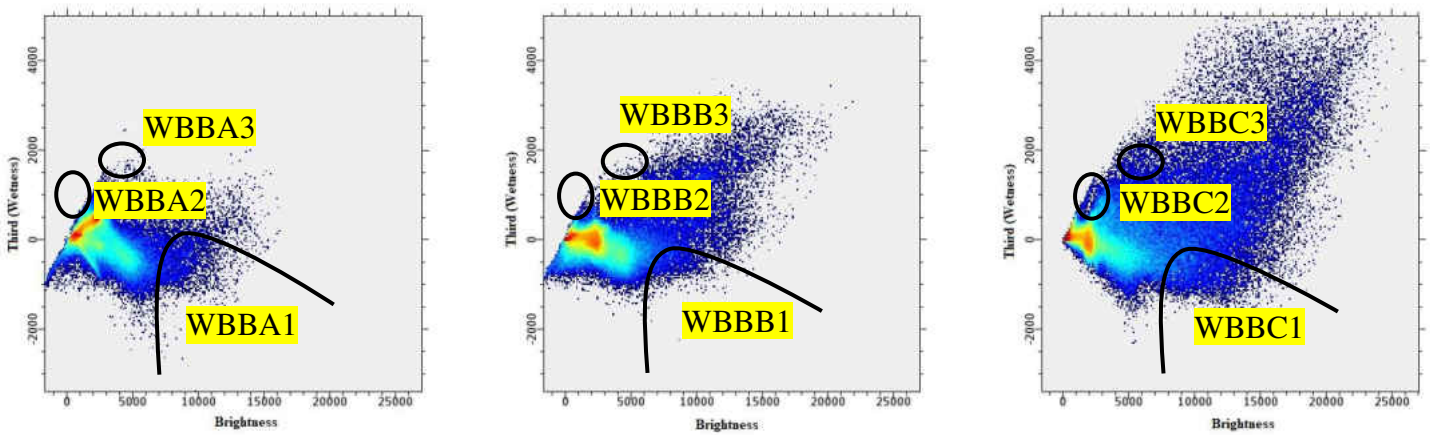

a) August 29, 2017 b) September 14, 2017 c) October 16, 2017

. Figure 3-10: Tasseled cap plots Wetness vs. Brightness (ENVI 5.3 software output) derived for Big Cypress Swamp watershed area. The yellow and red areas in the plots, which becomes light blue as it moves out, indicate the probability of higher density of the pixel values Fig. 10a depicts the plot for month before landfall, Fig. 10b four days after landfall, and Fig. 10c the month after landfall

For the last and final plot of wetness vs brightness plots (Fig. 3-10), it can be seen that there are noticeable changes in the clear water and turbid water sections when compared to the standard plot depicted in Fig 3-3c. In Fig. 3-10a, the before landfall conditions of clear water (WBBA2), turbid water (WBBA3) and concrete cover (WBBA1) are shown. The scattering and increase in pixels in the clear water (WBBB2) and turbid water (WBBB3) sections show that there is an increase in water over the watershed. The pixels representing the wet soils also show an increase, which is an indication of increase of water content over the watershed. One month after landfall i.e. for October 16, 2017 (Fig. 3-10c), the clear water (WBBC2), turbid water (WBBC3) and concrete regions (WBBC1) do not show signs of recovery. That is because the watershed area is a swamp area. The water dumped due to heavy rains do not drain out easily and they become stagnant. This is evident in the image one month after landfall.

Overall, the changes in the TCTs can be correlated to the NDVI change caused by the hurricane impact. The average NDVI for the corresponding dates is presented in Table 3-3. The mean NDVI values for July, August, and September for the year 1990 show that the vegetation cover is almost the same and there are no changes. This unchanged condition is also reflected in the tasseled cap plots where it is indicated that there is no change in the vegetation cover. For the year of hurricane landfall, the NDVI value for July 1991 shows the same value as the previous year. However, there is a drop in the NDVI value for the month of August 1991, i.e., marked in bold red, as this month had hurricane landfall. This indicates the big loss of vegetative cover of the watershed due to the impact of hurricane landfall. This phenomenon is also reflected in the tasseled cap plots for August 1991. In the following month, i.e. on September 1991, we can see the recovery of the vegetative cover as indicated in the NDVI value returning to almost the normal levels. In the year after the hurricane landfall, we have only the NDVI value of August 1992 with

no cloud contamination in Landsat TM images. The value indicates a full recovery of the vegetative cover. The NDVI and tasseled cap plot are not available for July 1992 as no cloud free images were available. Also, the low value of NDVI for the month of September 1992 can be attributed to the partial cloud cover that existed for that day. For the case of hurricane Irma landfall in Big Cypress watershed, the NDVI value before landfall was 0.469 and after landfall the value is 0.311. This indicates a significant reduction in the amount of vegetation cover over the area caused by wind and flood.

Table 3-3: Mean NDVI values for before, during and after hurricane landfall years in Hurricane Bob event.

Year	Months		
	July	August	September
1990	0.756	0.796	0.787
1991	0.750	0.560	0.700
1992	N/A	0.778	0.451

Table 3-4: Mean NDVI values for before, during and after hurricane landfall years in Hurricane Irma event.

Year	Months		
	August	September	October
2016	0.624	0.478	0.428
2017	0.469	0.311	0.499

3.4.3 Pattern Analysis of Land Cover Change

Box and whisker plots are used to graphically represent groups of numerical data through their quartiles. The vertically extending lines called whiskers indicate variability outside the upper and lower quartiles. These plots display variation in data samples with any assumptions of statistical distribution being absent. In addition, these plots are useful in comparing two or more datasets. The ends of the plotted box are upper and lower quartiles, so the box represents the interquartile range. A line inside the box marks the median. The box and whisker plots shown in Fig. 3-11 and Fig. 3-12 are also a testament to correlation between NDVI and TCTs that confirm the consistent trends with respect to brightness, wetness, and greenness holistically and this will help in observing the land cover change pattern distribution in the event of a hurricane landfall.

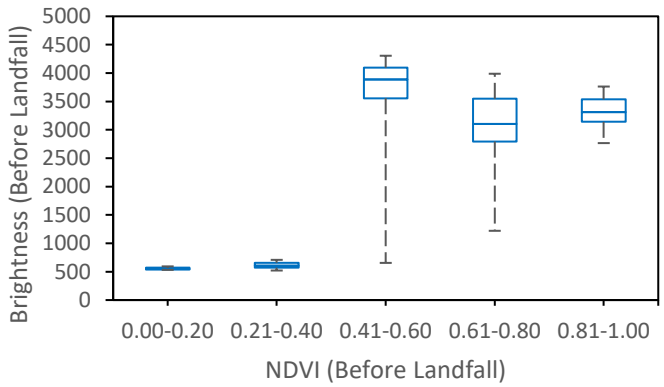

a) Brightness Pattern (Before Landfall)

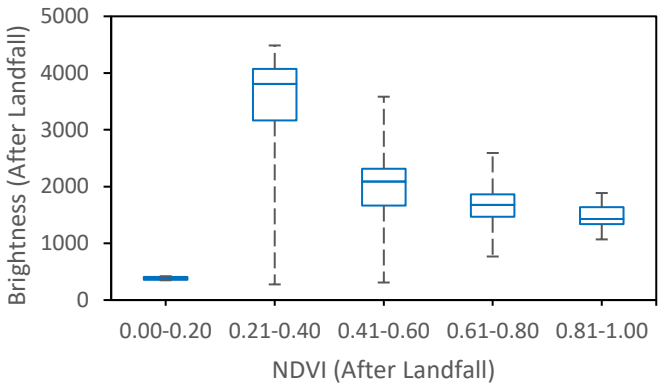

b) Brightness Pattern (After Landfall)

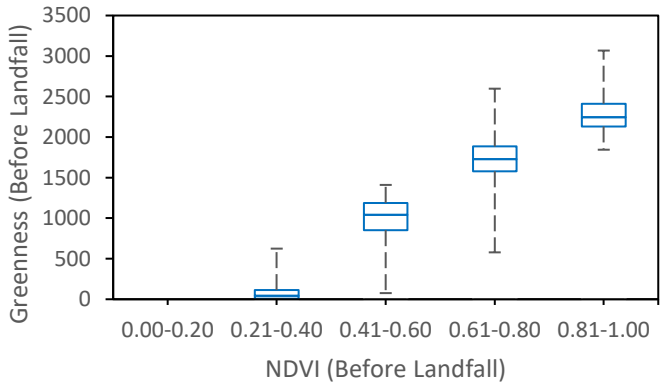

c) Greenness Pattern (Before Landfall)

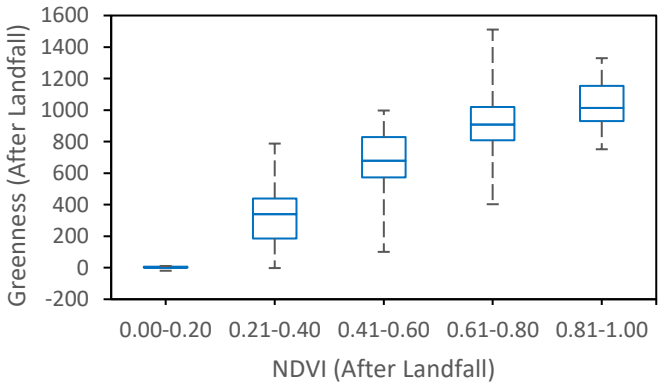

d) Greenness Pattern (After Landfall)

Figure 3-11: Box and whisker plots depicting the correlation between NDVI and Tasseled Cap Transformations before and after Hurricane Bob landfall on the Mattapoisett river watershed.

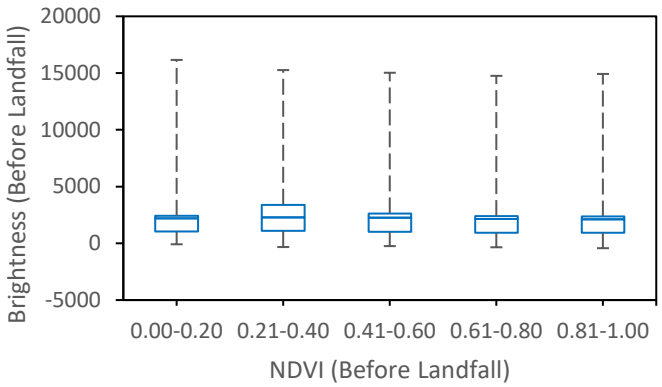

a) Brightness Pattern (Before Landfall)

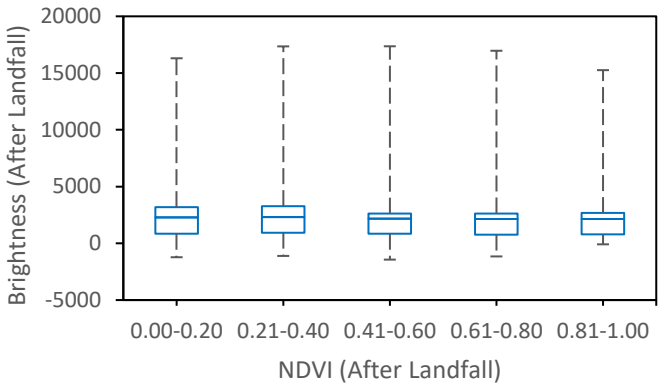

b) Brightness Pattern (After Landfall)

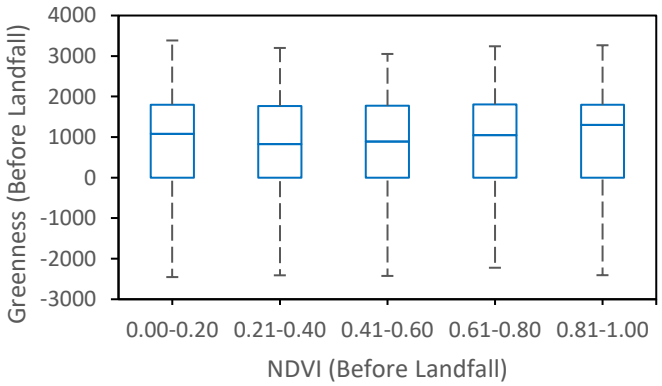

c) Greenness Pattern (Before Landfall)

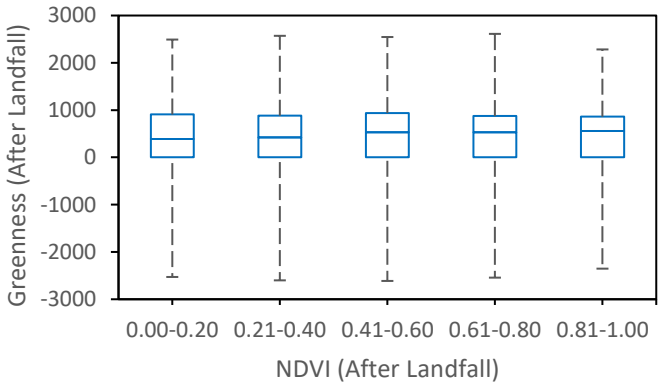

d) Greenness Pattern (After Landfall)

Figure 3-12: Box and whisker plots depicting the correlation between NDVI and Tasseled Cap Transformations before and after Hurricane Irma landfall on the Big Cypress Swamp watershed.

The box and whisker plots depicted show the land cover pattern for scenarios of before and after hurricane landfall for both watersheds. For the brightness vs. NDVI box plots, there is significant difference in the values of brightness within the NDVI range of 0.21-0.40. The interquartile range of brightness in this NDVI range has a dramatic increase in case of after-landfall situation than in case of before-landfall situation (Fig. 3-11a, 3-11b). The increased size of the box plot for after-landfall in 0.21-0.40 range suggests that the pixel values at this range has undergone significant dispersion. The median value is also quite high after hurricane landfall. Although for the NDVI ranges 0.41-0.60, 0.61-0.80 and 0.81-1.00 the interquartile ranges and the median values are lower for scenarios of after-landfall than before-landfall. In case of Big Cypress Swamp watershed, there are changes in the plots for all the NDVI ranges (Fig. 3-12a, 3-12b) especially in the NDVI range of 0.00-0.20. For greenness in relation to NDVI, the overall situation for the Mattapoisett river watershed is that there is a decrease in the interquartile ranges as well as the median values (Fig. 3-11c, 3-11d). The pattern in both scenarios are the same although the box plots in the after-landfall scenario are much shorter than those in before-landfall scenario. This indicates that the values are more clustered in after-landfall scenario than those in before-landfall scenario in the sense that larger NDVI area was devastated severely during the landfall. The same decreasing trend of NDVI can be seen in case of Big Cypress Swamp watershed (Fig. 3-12c, 3-12d). However, the insignia difference in values in between before- and after-landfall scenarios associated with hurricane Irma explains the smaller distortion in the plots and indicates the larger resistance or resilience embedded in such swamp landscape. This also signifies noticeable change in the wetness of the same area in such swamp landscape due to hurricane Irma landfall. In any circumstance, all these changes conform to the dispersion phenomenon noticed in the tasseled cap plots depicted before.

3.4.4 Statistical Assessment of the Dispersion Phenomenon

The TCT plots help us see the qualitative significance. However, it is important to back up the qualitative significance with quantitative analysis and prove the numerical significance. For this purpose, relevant statistical analysis was performed for the two watersheds. The results of the analysis are tabulated in Table 4, 5 and 6 for Mattapoisett river watershed and Table 7, 8 and 9Big Cypress watershed respectively.

Table 3-5: Statistical calculations for dataset pairs of before and after landfall scenario for brightness (Mattapoisett river watershed).

Statistical parameters	**Brightness**	
	July 18, 1991	**August 26, 1991**
Mean	3312.89	2689.64
Standard Deviation	759.59	1404.18
Coefficient of variation	22.93%	52.21%
Quartile coefficient of dispersion	0.08	0.40
Pearson correlation	0.35	

Table 3-6: Statistical calculations for dataset pairs of before and after landfall scenario for greenness (Mattapoisett river watershed).

Statistical parameters	Greenness	
	July18, 1991	**August26, 1991**
Mean	1920.80	758.19
Standard Deviation	626.58	414.77
Coefficient of variation	32.62%	54.71%
Quartile coefficient of dispersion	0.15	0.37
Pearson correlation	0.37	

Table 3-7: Statistical calculations for dataset pairs of before and after landfall scenario for wetness (Mattapoisett river watershed).

Statistical parameters	Wetness	
	July 18, 1991	**August 26, 1991**
Mean	135.77	199.10
Standard Deviation	77.65	152.63
Coefficient of variation	57.19%	79.17%
Quartile coefficient of dispersion	0.40	0.55
Pearson correlation	0.43	

Table 3-8: Statistical calculations for dataset pairs of before and after landfall scenario for brightness (Big Cypress watershed).

Statistical parameters	Brightness	
	August 29, 2017	**September 14, 2017**
Mean	1869.37	1968.22
Standard Deviation	1382.15	2028.43
Coefficient of variation	73.94%	99.06%
Quartile coefficient of dispersion	0.46	0.63
Pearson correlation	0.424	

Table 3-9: Statistical calculations for dataset pairs of before and after landfall scenario for greenness (Big Cypress watershed).

Statistical parameters	Greenness	
	August 29, 2017	**September 14, 2017**
Mean	1289.84	706.67
Standard Deviation	634.31	381.15
Coefficient of variation	49.18%	53.94%
Quartile coefficient of dispersion	0.41	0.42
Pearson correlation	0.63	

Table 3-10: Statistical calculations for dataset pairs of before and after landfall scenario for wetness (Big Cypress watershed).

Statistical parameters	Wetness	
	August 29, 2017	**September 14, 2017**
Mean	345.25	155.23
Standard Deviation	193.01	278.63
Coefficient of variation	55.91%	179.50%
Quartile coefficient of dispersion	0.55	0.61
Pearson correlation	0.147	

The statistical calculations indicate that there is an 18.81% change in mean pixel values for brightness; 60.53% change for greenness, and 46.64% difference in wetness when compared to pixel values before the hurricane landfall scenario for Mattapoisett harbor watershed. The changes are 5.28%, 45.21% and 55.04% for brightness, greenness and wetness respectively for Big Cypress watershed. These significant differences in values conform to the tasseled cap plots that after hurricane landfall, there was significant change in the landscape which contributed to the dispersion of pixels i.e. change in the value of pixels. The Pearson correlation coefficients for the three transformations are also quite low, indicating a significant difference in the data pairs for both cases. Especially for Big Cypress watershed, the Pearson coefficient is very low for wetness. This indicates a widespread dispersion of the values, which can be attributed to flooding caused by heavy rainfall and storm surge in the watershed.

The standard deviation and coefficient of variation are effective statistical tools to compare between two datasets. For brightness, the standard deviation is 759.59 for before landfall and

1404.18 for after landfall for Mattapoisett river watershed. The standard deviation is higher in case of after landfall than the before landfall scenario. This indicates that the difference between the pixel values in relation to their mean is higher for after landfall scenario than before landfall scenario. The same can be said of Big Cypress watershed where the standard deviation is greater for brightness and wetness for after landfall than before landfall scenario. The coefficient of variation is used to measure the spread or dispersion of data. The higher the value, the greater the dispersion is. In case of brightness, coefficient of variation is 22.93% for before landfall scenario and 52.21% for after landfall scenario. For greenness and wetness the values are 37.62% and 57.19% for before landfall whereas the values are 54.17% and 79.17%. This indicates that the pixel values for after landfall scenario are more dispersed than the before landfall scenario. This conforms to the dispersion phenomenon shown in the tasseled cap plots. The values for Big Cypress watershed show a similar trend for coefficient of variation values. Especially there is significant difference for the wetness value. Before landfall the value was 55.91% and after landfall the value became 179.50%. This high difference indicates the change in the wetness in the watershed primarily caused by flooding. The flooding was caused by heavy rain and storm surge that was associated with Hurricane Irma landfall.

The quartile coefficient of dispersion was used to measure level of dispersion quantitatively and to make comparison within and between datasets. In other words, it is a measure of spread of dataset. The quartile coefficient of dispersion of data associated with brightness, greenness and wetness for after landfall scenario is 5.00, 2.47 and 1.38 times greater than that of data for before landfall scenario. This means that the dispersion of pixel values for after landfall is 5.00 times greater than the dispersion of pixel values for before landfall condition. Subsequently, the dispersion of greenness is 2.47 times greater than before landfall condition. In the case of wetness,

the value is 1.38 time greater than before landfall values. All of these prove that there was significant dispersion of data in all three transformation cases as evident in the plots driven by the hurricane landfall. The values are low for Big Cypress watershed compared to Mattapoisett river watershed. The quartile coefficient of dispersion of data associated with brightness, greenness and wetness for after landfall scenario is 1.37, 1.02 and 1.11 times greater than that of data for before landfall scenario. Although low, the values are greater than 1; indicating the dispersion i=for after landfall scenario.

The Moran's I for all three cases is positive and closer to +1. Moran's I is an inferential statistics and as such, the z-score and p-values play a part in the interpretations. In all cases the z-scores are positive and p-values are less than 0.05. This indicates that the there is less than 1% chance that the values are the result of random spatial clustering. The values in the table indicate that the Moran's I values for before landfall are less than the values for after landfall. This indicates that the pixel values of after landfall are more clustered than the pixel values of before landfall.

3.4.5 Comparison between Hurricane Bob and Hurricane Irma

Hurricane Bob and Hurricane Irma both had devastating effects on the watersheds where they made landfall. The TCT plots of both events shows how the landscape pattern changed when compared to before-landfall conditions. The statistical calculations also prove the effect these hurricanes had on the landscapes. The most prominent statistical calculation to capture the dispersion effect was the coefficient of variation. The values are depicted in Table 7

Table 3-11: Comparison between Hurricane Bob and Hurricane Irma in regards to coefficient of variation

TCT	Hurricane Bob		Hurricane Irma	
	Coefficient of variation (%)		Coefficient of variation (%)	
	Before Landfall	After Landfall	Before Landfall	After Landfall
Brightness	22.93	52.21	73.94	99.06
Greenness	32.62	54.71	49.18	53.94
Wetness	57.19	79.17	55.91	179.50

Let us look at the brightness first for both the hurricane events. For hurricane Bob, the coefficient of variation shows a steep increase in the after-landfall date. This is also the case for hurricane Irma. This steep change in the values also explain the dramatic difference in the plots of after-landfall dates. This also explains the dispersion phenomenon shown in the plot for after-landfall scenario. Another explanation is that due to hurricane landfall, the heavy rains, tidal surges inundated the coastal watershed, and this increased the moisture content of the soil, which is depicted in the plots before. For greenness, the values for hurricane Bob show that there is a steady increase in the after-landfall scenario. The increase is also steady in case for hurricane Irma. However, the wetness values are the ones that show significant changes. For hurricane Bob, the value increases from 57.19% to 79.17%. This increase signifies the increase in moisture content in the Mattapoisett River watershed area. For hurricane Irma, the value increases from 55.19% to 179.50%. This dramatic increase also signifies the increase of moisture content of both soil and canopy cover brought about by heavy rainfall and tidal surges.

3.4.6 NDVI Difference Maps

As stated earlier, vegetation cover of a watershed undergoes change when hurricane landfall occurs. This change can be visualized by looking at the difference maps. These difference maps are created by using the before and after NDVI maps. These difference maps will show where the largest difference in values have occurred, which, in turn will help to see where the vegetation cover change was most impacted by hurricane landfall.

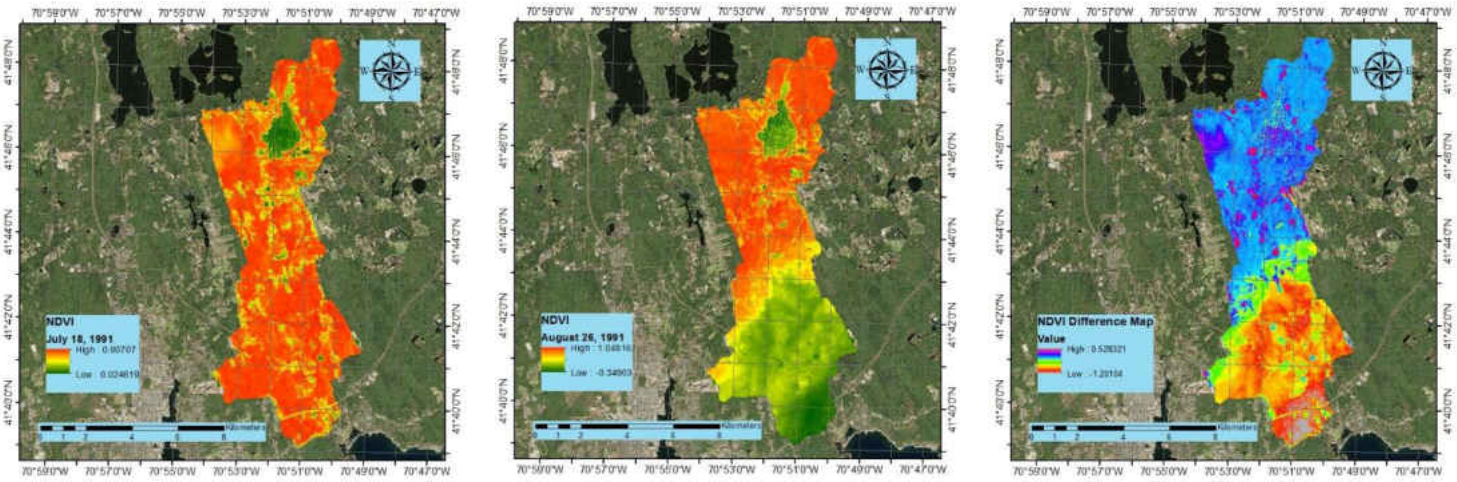

a) Before Landfall b) After Landfall c) NDVI Difference

Figure 3-13: NDVI maps for Mattapoisett River Watershed area. Fig. 14a is the map for before landfall. Fig. 14b is the map after landfall and Fig. 14c is the NDVI difference map.

The NDVI maps and the difference maps shown in Fig. 3-13 depict the vegetation covers for Mattapoisett River watershed for before and after landfall. Before landfall, the NDVI map shows the even distribution of vegetation cover over the watershed area (Fig. 3-13a). However, after landfall, there is significant change in the southeastern part of the watershed where the hurricane traced over the vegetation cover as it made landfall (Fig. 3-13b). This is also evident in the NDVI difference map where the largest differences are seen in the southeast part of the watershed (Fig. 3-13c). In the difference map, the negative values imply more severe change. The difference map was created by subtracting the before-landfall raster from after-landfall raster. Therefore, in the after-landfall raster, if a particular pixel had positive value before and negative after landfall, the resulting difference will be negative as the negative value of NDVI indicates diminishing of vegetation cover. This NDVI change can also be attributed to the change in greenness pattern as seen in Fig. 3-11c and Fig. 3-11d.

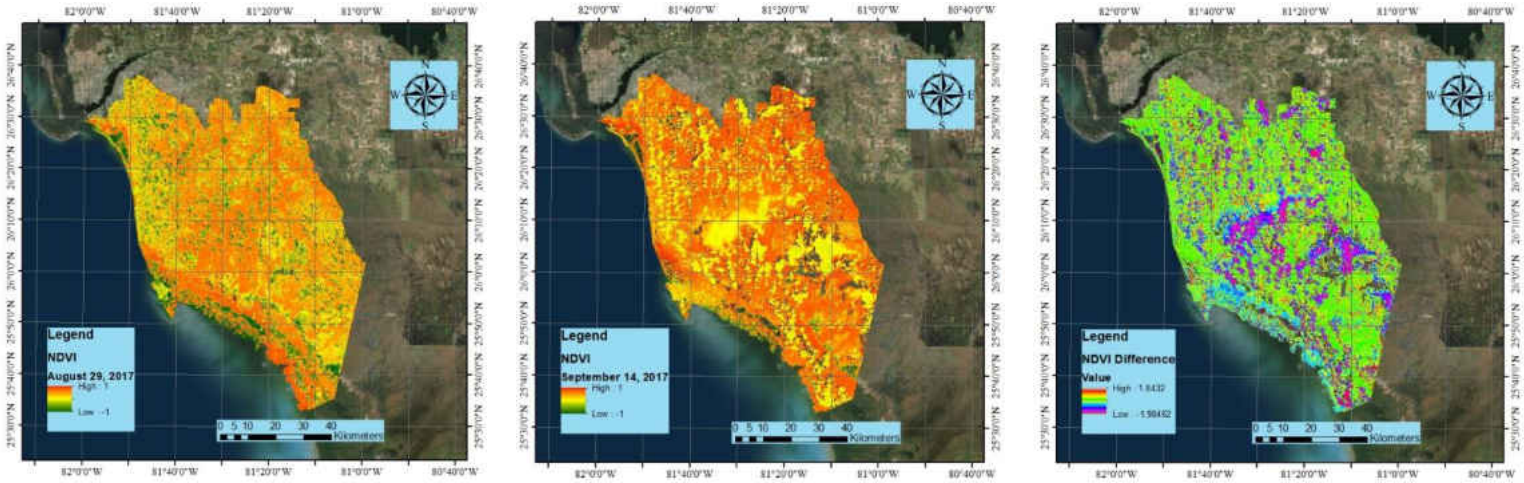

a) Before Landfall b) After Landfall c) NDVI Difference

Figure 3-14: **NDVI maps for Big Cypress Swamp Watershed area. Fig. 14a is the map for before landfall. Fig. 14b is the map after landfall and Fig. 14c is the NDVI difference map**

The NDVI images for before and after landfall for Big Cypress Swamp watershed as well as the difference map are depicted in Fig. 3-14. Before landfall, we can see that there is healthy vegetation cover in almost all the parts of the watershed (Fig. 3-14a). After hurricane landfall, there are changes in the vegetation cover in the watershed especially in the central part of the watershed (Fig. 3-14b). This change is also depicted in the difference map where it can be observed that the change is quite low in the central region (Fig. 14c). However, there is change in the vegetation cover over whole of the watershed area as shown in difference map. The change is not as severe as the Mattapoisett River watershed. The Mattapoisett river watershed has the Mattapoisett River flowing through the watershed; which acts as a drainage canal that transports discharge to the bay. However, the Big Cypress Swamp watershed is a swamp as the name suggests. The water remains stagnant in the event of heavy rainfall and due to saturation of soil; the percolation through soil is a very steady event. This is the reason why the wetness shows such high dispersion. The negative values in the difference map explain the places where the most change in vegetative cover has occurred. The difference is small compared to Mattapoisett river watershed due to the nature of the landscape of the swamp. This small but overall change in vegetation cover is reflected in the change of greenness pattern as seen in Fig. 3-13c and Fig. 3-13d. The density of the vegetation coupled with saturated marshy lands creates a unique land cover that is resistant to hurricane damage. From this observation, we can feel the importance of vegetation cover to minimize hurricane damage. It is imperative that afforestation drives are undertaken regularly in the coastal watersheds to ensure that natural preventive measures are bolstered against extreme natural events especially hurricanes.

3.5 Conclusion

TCT plots derived from remote sensing images can be a useful tool to glean vicarious land cover information in a cost-effective and time saving manner for environmental monitoring. Especially, from our study, we can convincingly say that the TCT can be employed to monitor and assess the rapid change conditions of a landscape after a major natural disaster event. The dispersion phenomenon in TCTs that is quantified by the quartile coefficient of dispersion in this study reflects the interactions among biosphere, atmosphere, and lithosphere with sustainability implication in a disaster-prone region. The subsequent NDVI analysis also testifies to the findings of the tasseled cap plots. There is a strong linkage between TCTs and NDVI echoes the trend analyses in terms of the brightness, greenness, and wetness reflecting the hurricane landfall impact. The joint NDVI-TCT box plots also testify to the findings of the tasseled cap plots via both major hurricane events. This helps in swift decision making and implementation of rescue efforts for the people concerned that may be crucial for life-saving purposes in the affected areas.

3.6 References

Anderson, G. L., Hanson, J. D., & Haas, R. H. (1993). Evaluating Landsat Thematic Mapper derived vegetation indices for estimating above-ground biomass on semiarid rangelands. *Remote Sensing of Environment*, *45*(2), 165-175.

Augustine, D. J., Booth, D. T., Cox, S. E., & Derner, J. D. (2012). Grazing intensity and spatial heterogeneity in bare soil in a grazing-resistant grassland. *Rangeland Ecology & Management*, *65*(1), 39-46.

Baig, M. H. A., Zhang, L., Shuai, T., & Tong, Q. (2014). Derivation of a tasselled cap transformation based on Landsat 8 at-satellite reflectance. *Remote Sensing Letters*, *5*(5), 423-431.

Carlson, T. N., & Ripley, D. A. (1997). On the relation between NDVI, fractional vegetation cover, and leaf area index. *Remote sensing of Environment*, *62*(3), 241-252.

Chandrasekar, K., Sesha Sai, M. V. R., Roy, P. S., & Dwevedi, R. S. (2010). Land Surface Water Index (LSWI) response to rainfall and NDVI using the MODIS Vegetation Index product. *International Journal of Remote Sensing*, *31*(15), 3987-4005.

Crist, E. P., & Cicone, R. C. (1984). Application of the tasseled cap concept to simulated thematic mapper data. *Ann Arbor*, *1001*, 48107.

Crist, E. P. (1985). A TM tasseled cap equivalent transformation for reflectance factor data. *Remote Sensing of Environment*, *17*(3), 301-306.

Crist, E. P., Laurin, R., & Cicone, R. C. (1986, September). Vegetation and soils information contained in transformed Thematic Mapper data. In *Proceedings of IGARSS'86 Symposium* (pp. 1465-1470). Paris: European Space Agency Publications Division.

Dale, M. R., & Fortin, M. J. (2002). Spatial autocorrelation and statistical tests in ecology. *Ecoscience*, *9*(2), 162-167.

Dormann, C. F. (2007). Effects of incorporating spatial autocorrelation into the analysis of species distribution data. *Global Ecology and Biogeography*, *16*(2), 129-138.

F Dormann, C., M McPherson, J., B Araújo, M., Bivand, R., Bolliger, J., Carl, G., ... & Kühn, I. (2007). Methods to account for spatial autocorrelation in the analysis of species distributional data: a review. *Ecography*, *30*(5), 609-628.

Fortin, M. J., Drapeau, P., & Legendre, P. (1990). Spatial autocorrelation and sampling design in plant ecology. In *Progress In Theoretical Vegetation Science* (pp. 209-222). Springer Netherlands.

Fu, B., & Burgher, I. (2015). Riparian vegetation NDVI dynamics and its relationship with climate, surface water and groundwater. *Journal of Arid Environments*, *113*, 59-68.

History of Big Cypress. (n.d.). Retrieved October 09, 2017, from http://www.evergladesonline.com/history-big-cypress.htm

Holm, A. M., Burnside, D. G., & Mitchell, A. A. (1987). The development of a system for monitoring trend in range condition in the arid shrublands of Western Australia. *The Rangeland Journal*, *9*(1), 14-20.

Kauth, R. J., & Thomas, G. S. (1976, January). The tasselled cap--a graphic description of the spectral-temporal development of agricultural crops as seen by Landsat. In *LARS Symposia* (p. 159).

Koenig, W. D. (1999). Spatial autocorrelation of ecological phenomena. *Trends in Ecology & Evolution*, *14*(1), 22-26.

Lichstein, J. W., Simons, T. R., Shriner, S. A., & Franzreb, K. E. (2002). Spatial autocorrelation and autoregressive models in ecology. *Ecological monographs*, *72*(3), 445-463.

Lukina, E. V., Stone, M. L., & Raun, W. R. (1999). Estimating vegetation coverage in wheat using digital images. *Journal of Plant Nutrition*, *22*(2), 341-350.

Naimi, B., Skidmore, A. K., Groen, T. A., & Hamm, N. A. (2011). Spatial autocorrelation in predictors reduces the impact of positional uncertainty in occurrence data on species distribution modelling. *Journal of Biogeography*, *38*(8), 1497-1509.

National Climatic Data Center (2017). Billion-Dollar U.S. Weather/Climate Disasters 1980-2017. Asheville, NC: National Oceanic and Atmospheric Administration. http://www.ncdc.noaa.gov/billions/events.pdf.

Penuelas, J., Filella, I., & Gamon, J. A. (1995). Assessment of photosynthetic radiation-use efficiency with spectral reflectance. *New Phytologist*, *131*(3), 291-296.

Pettorelli, N., Vik, J. O., Mysterud, A., Gaillard, J. M., Tucker, C. J., & Stenseth, N. C. (2005). Using the satellite-derived NDVI to assess ecological responses to environmental change. *Trends in Ecology & Evolution*, *20*(9), 503-510.

Rouse Jr, J., Haas, R. H., Schell, J. A., & Deering, D. W. (1974). Monitoring vegetation systems in the Great Plains with ERTS.

Sankey, T. T., & Germino, M. J. (2008). Assessment of juniper encroachment with the use of satellite imagery and geospatial data. *Rangeland Ecology & Management*, *61*(4), 412-418.

Scanlon, T. M., Albertson, J. D., Caylor, K. K., & Williams, C. A. (2002). Determining land surface fractional cover from NDVI and rainfall time series for a savanna ecosystem. *Remote Sensing of Environment*, *82*(2), 376-388.

Valiela, I., Peckol, P., D'Avanzo, C., Lajtha, K., Kremer, J., Geyer, W. R., ... & Crawford, R. (1996). Hurricance Bob on Cape Cod. *American Scientist*, *84*(2), 154-165.

Valiela, I., Peckol, P., C. D'Avanzo, Kremer, J., D. Hersh, K. Foreman, . . . Crawford, R. (1998). Ecological Effects of Major Storms on Coastal Watersheds and Coastal Waters: Hurricane Bob on Cape Cod. *Journal of Coastal Research, 14*(1), 218-238. Retrieved from http://www.jstor.org/stable/4298771

VALLEY, M. R. By Julio C. Olimpio and Virginia de Lima.

Vorovencii, I. (2007). Use of the “Tasseled Cap” transformation for the interpretation of satellite images. *Cadastre J. RevCAD*, *7*, 75-82.

Wang, Q., Adiku, S., Tenhunen, J., & Granier, A. (2005). On the relationship of NDVI with leaf area index in a deciduous forest site. *Remote Sensing of Environment*, *94*(2), 244-255.

Watkins, T. (2005). The Tasseled Cap transformation in remote sensing. *Available online ataccessed*, *14*.

Weng, Q., Fu, P., & Gao, F. (2014). Generating daily land surface temperature at Landsat resolution by fusing Landsat and MODIS data. *Remote Sensing of Environment*, *145*, 55-67.

Yengoh, G. T., Dent, D., Olsson, L., Tengberg, A. E., & Tucker, C. J. (2014). The use of the normalized difference vegetation index (NDVI) to assess land degradation at multiple scales: A review of the current status, future trends, and practical considerations. *Lund University Center for Sustainability Studies (LUCSUS), and the Scientific and Technical Advisory Panel of the Global Environment Facility (STAP/GEF)*.

Zhang, B., Zhang, L., Xie, D., Yin, X., Liu, C., & Liu, G. (2015). Application of synthetic NDVI time series blended from Landsat and MODIS data for grassland biomass estimation. *Remote Sensing*, *8*(1), 10.

CHAPTER 4: ENVIRONMENTAL RECONSTRUCTION OF TERRESTRIAL WATERSHED VEGETATION COVER OF HACKENSACK AND PASCACK WATERSHED FOR HURRICANE SANDY EVENT

4.1 Introduction

Land cover maps are an important tool to detect the influence of human activities and environmental changes (Ran et al., 2009). They are also important in the interpretation of climate change studies as well as understanding the complexities surrounding human activities and changes on a global scale (Jia et al., 2014). Remote sensing and associated technologies have been effective tools to this end. Remote sensing has the ability to collect information within a short time span on a large regional scale. Using data from remote sensing, especially Landsat images, land cover data were extracted on a global and regional scale (Friedl et al., 2002, Adam et al., 2014, Gong et al., 2013). However, Landsat satellite has an inherent disadvantage. It has a high spatial resolution (30 meters by 30 meters) but low temporal resolution. The revisit time of Landsat satellite is 16 days, which indicates low temporal resolution. MODIS on the other hand has a high temporal resolution with daily revisit times. However, it has low spatial resolution (250 meter/500 meter). Using the high spatial resolution of Landsat and high temporal of MODIS, it is now possible to create synthetic images using the Spatial and Temporal Adaptive Reflectance Fusion Model (STARFM) algorithm. (Gao et al., 2006). These synthetic images have the spatial resolution of Landsat images and can be used as a gap-fill technique for the missing days in between two Landsat revisits. This will help generate daily Landsat imagery albeit synthetic. These synthetic images derived from STARFM algorithm have been used in various studies of land use land cover changes such as generation of daily land surface temperature (LST) (Weng et al., 2014), monitoring of urban heat island (Huang et al ., 2013), forest cover classification using Normalized

Difference Vegetative Index (NDVI) (Jia et al., 2014; Rao et al ., 2015; Zhang et al., 2015) etc. Besides Landsat and MODIS, other sensors have also been used for data fusion purposes to study land use land cover changes. Some of them are listed in the table below.

Table 4-1: Fusion sensors for land use land cover purposes

Sensors	**Purpose**	**Reference**
ERS-1 & JERS-1	Land cover classification using fuzzy concept	Solaiman et al., 1999
SPOT-1 & NOAA-6 to NOAA-10 (Los Angeles) SPOT-2 & NOAA-12 and NOAA-14 (Paris)	Analysis of urban heat temperature and landcover	Dousset et al., 2003
Quickbird MS & RADARSAT SAR	Analysis of urban surface temperature	Ban et al ., 2010
PolSAR & PollnSAR	Land cover classification	Shimoni et al., 2009
Landsat ETM+ and MODIS Surface reflectance	Landscape changes in complex heterogeneous regions	Zhu et al., 2010
LiDAR & Landsat TM	Assessment of urban land cover	Singh et al., 2012
Landsat-7 ETM+ & MODIS (MOD21KM)	Land Surface Temperature for urban heat island monitoring	Huang et al ., 2013
Landsat-8 OLI & MODIS (MOD13Q1)	Land cover classification	Jia et al., 2014

Sensors	Purpose	Reference
Landsat TM & MODIS (MOD09GQ)	Assessment of land cover type of semi-arid rangeland	Olexa et al., 2014
Landsat TM & MODIS (MOD11A1 & MOD09GA)	Land surface temperature	Weng et al., 2014
Landsat TM, Landsat ETM+, MODIS, GOES 10 Imager & MSG SEVIRI	Land surface temperature	Wu et al., 2015
Landsat -7 ETM+, MODIS (MOD09A1/MYD09A1)	Forest Disturbance	Hilker et al., 2009
Landsat-7 ETM+, MODIS (MOD09GA)	Land cover classification	Chen et al., 2015
Landsat ETM+, MODIS	Forest cover classification	Jia eta al., 2014

Although the table above shows that data fusion is used in the study of land cover, there no indication of any study that was geared towards the study of the impact of hurricane on a land cover that was in direct path of the hurricane using data fusion at the core of the analysis. Therefore, in this study, we shall be investigating how data fusion can play a role in the analysis of hurricane impact on the Hackensack and Pascack watershed using NDVI and tasseled cap transformation imagery.

4.2 Study Area

The study area is comprised of two watersheds for comparison of NDVI and tasseled cap plot results. The two watersheds are 1) Hackensack and Pascack watershed situated in New Jersey State and 2) Mattapoisett River watershed situated in the Massachusetts state

4.2.1 Hackensack and Pascack Watershed

The New Jersey Department of Environmental Protection designates this watershed as Watershed Management area 5. The drainage area of this watershed is approximately 427 square kilometers (165 square miles). The watershed is comprised of three sub watersheds. They are Hackensack river watershed, Hudson River watershed and Pascack brook watershed. This is the most populated of all the watersheds in the state of New Jersey. About 50% of the land is undeveloped, with more than 30% residential development. The rest of the developed land is for commercial or industrial use. .

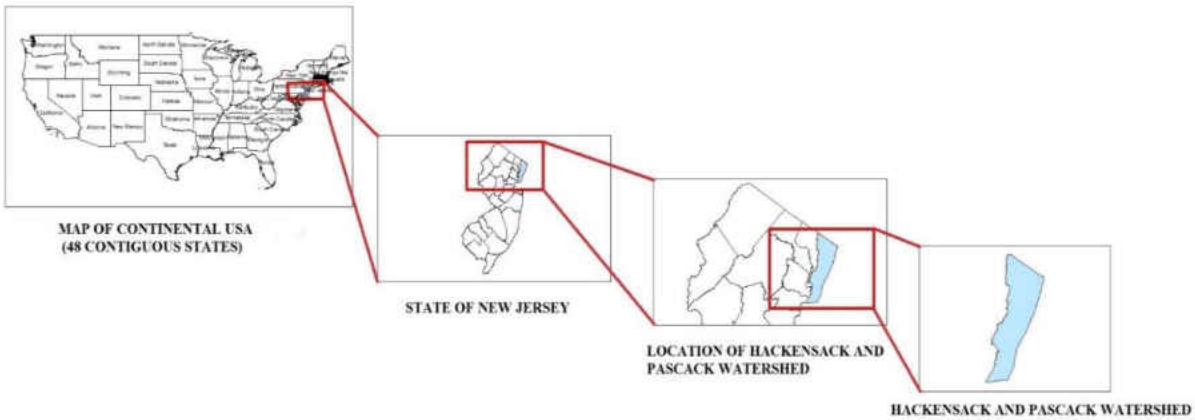

Figure 4-1: Geographical location of Hackensack and Pascack Watershed

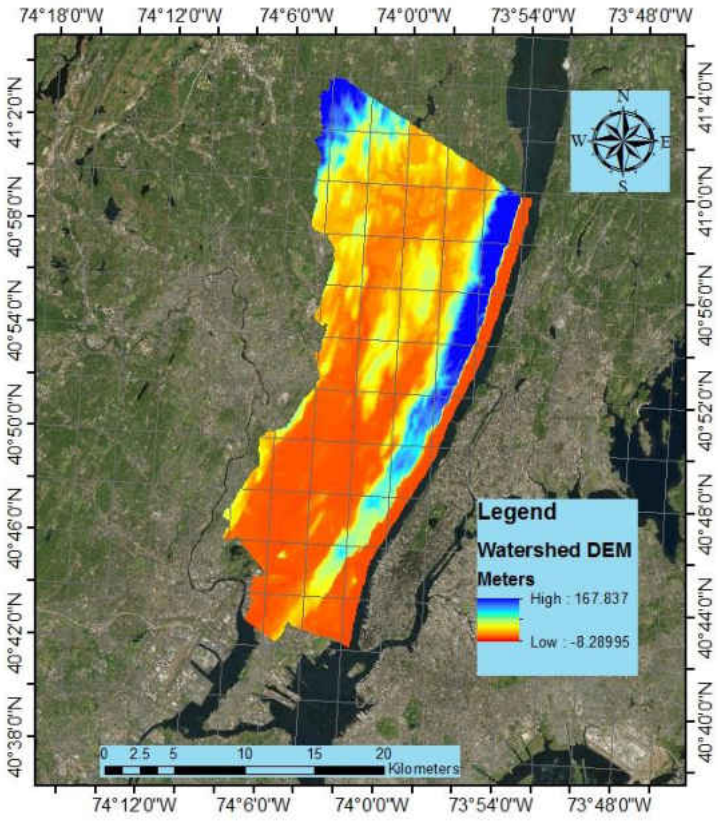

Figure 4-2: Digital Elevation Model (DEM) of Hackensack and Pascack watershed, New Jersey.

4.2.2 Mattapoisett River Watershed

The geographical location Mattapoisett river watershed is depicted in Fig. 4-3. This is a coastal watershed surrounding the Mattapoisett harbor. The Fig. 4-4 represents a digital elevation model (DEM) of the watershed. As seen in the figure, the lowest elevation is at the mouth of the river with 6m elevation. The elevation increases as the watershed moves inland. The highest elevation of the watershed is 39m. This highest elevation is situated to the northwestern side of the watershed. The average elevation of the watershed is 22.5m. The average area of the watershed is 66.85 square kilometers. The total perimeter of the watershed is 72 kilometers. The Mattapoisett River discharges at the harbor from the northwest. The river stretches approximately 10 miles from

its headwaters at the 710-acre Snipatuit Pond to the Mattapoisett harbor. The river basin has eight public water supply wells and many private wells that serve the needs of multiple municipalities.

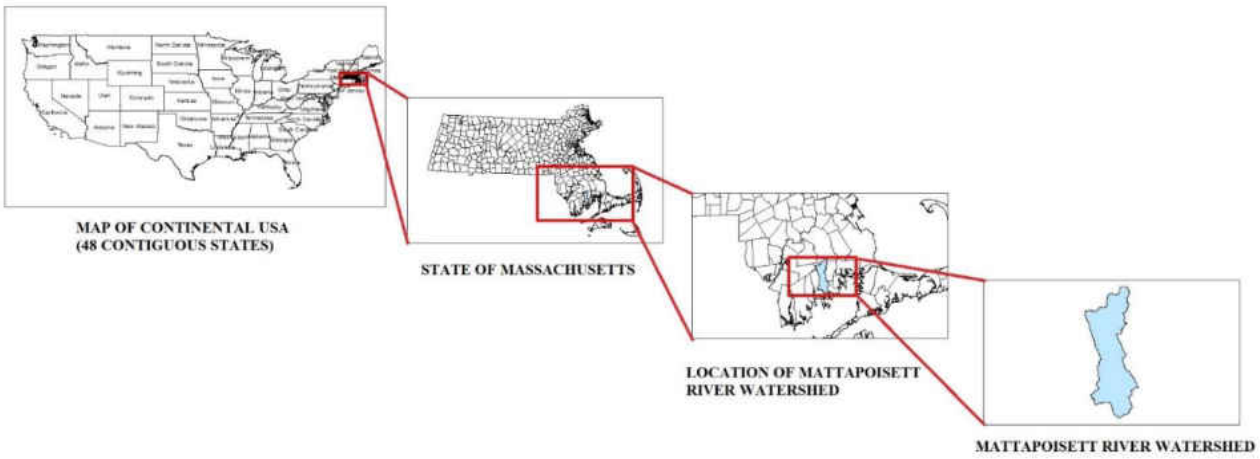

Figure 4-3: **Geographical location of Mattapoisett River Watershed**

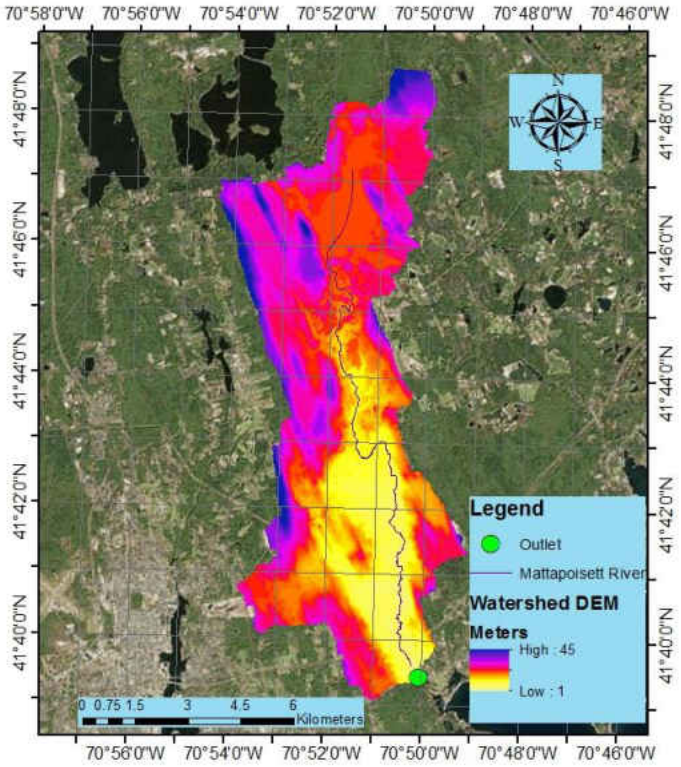

Figure 4-4: Digital Elevation Model (DEM) of Mattapoisett River watershed, Massachusetts.

4.3 Hurricane Sandy

Hurricane Sandy is regarded as the most lethal and the most destructive hurricane of the 2012 Atlantic hurricane season and the second costliest hurricane in US history. The hurricane is also referred to Superstorm Sandy in unofficial terms. This was a Category 3 storm and it made landfall in Cuba when it was at its maximum strength. It became a Category 2 storm as it approached United States. The hurricane caused damage to 24 stated in the US, including entire eastern seaboard from Florida to Maine. The damage was particularly severe in the states of New York and New Jersey. The total damage caused by the hurricane is estimated to be 75 billion USD (2012 USD) (Blake et al., 2013).

Hurricane Sandy had devastating effects of New Jersey and New York areas. The storm surge, in addition to the large and battering waves, devastated large portions of the coast of New York and New Jersey. The hardest hits were Monmouth and Ocean counties (Blake et al., 2013). The highest wave was 3.86 meters (12.65 ft.) and for New Jersey, it was 2.61 meters (8.57 ft.) (Blake et al., 2013). In New Jersey, these massive waves and tidal surges caused inundation of whole communities and a large number of houses were destroyed. A large number of residences lost power in the areas and power outages lasted for several weeks. Costs to businesses were estimated upward of about 8.3 billion USD. Gas and power lies cost about 1 billion USD and the repairing cost for wastewater and sewer services were about 3 billion USD.

Although the hurricane caused massive damages in New York and New Jersey area, the damage was relatively minimal in Massachusetts. Widespread power disruption occurred for days. Flooding of roadways and buildings were reported (WCVB). The sustained wind pressure in the Buzzards Bay and Cape Cod area was 83 mph. The tidal surges caused by heavy wind were as high as 0.61-1.22 meters 2-4 ft. in Massachusetts. (Blake et al., 2013). The total estimated damage

from Hurricane Sandy in Massachusetts is about 20.8 million USD (NCDC). The path of the hurricane is depicted in Fig. 4-5.

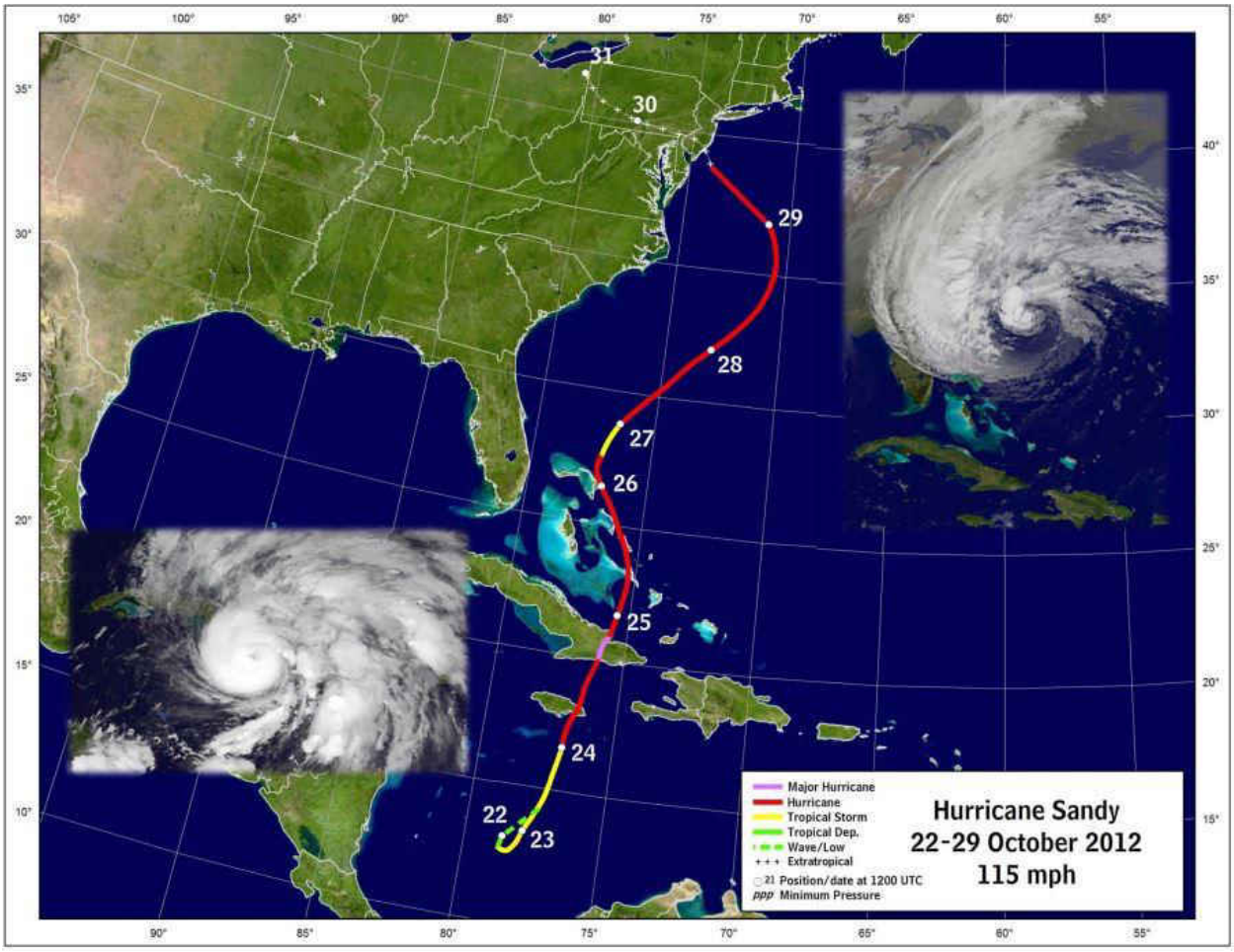

Figure 4-5: Trajectory of Hurricane Sandy, 2012. (Source: http://www.weather.gov)

4.4 Methodology

4.4.1 Data Fusion

Landsat-7 ETM+ satellite has a high spatial resolution (30m) but low temporal resolution (16 days). However, MODIS has high temporal resolution (daily) but low spatial resolution (250m/500m). In order to have both high spatial and temporal resolutions for the days where

Landsat-7 data is not available, a data fusion algorithm named STARFM is used. A pair or two pairs of Landsat and MODIS images are used as a base and with the MODIS image available for the day where Landsat is not available; the STARFM algorithm creates a predicted image with high spatial and temporal resolution for the given date. In order to create a fused image, the Landsat and MODIS images have to be free from any type of cloud cover.

The IDFM procedure undertaken in this study is comprised of three main steps. Step one involves the acquiring Landsat-7 and MODIS swath path images containing the watersheds. The swath path image acquisition was done exclusively for each watershed. The second step employs the procedures required to prepare the images for fusion. Step three is where data fusion is done using Spatial and Temporal Adaptive Fusion Model (STARFM).

The work process of the study can be divided into three major steps. 1) Data Fusion, 2) NDVI mapping and 3) Tasseled cap transformation plotting.

Data fusion is the necessary step needed to perform for the gap-filling process of Landsat images that are not available due to lengthy revisit times. Data fusion is comprised of three steps: a) Data acquisition b) Image processing and preparation and c) Data fusion algorithm utilization

a) Data Acquisition:

The basis of data fusion involving STARFM algorithm is the surface reflectance data. For our case, we collected surface reflectance data from landsat-7 ETM+ and Terra MODIS satellites. The images that were relatively cloud free were considered for download purposes for both the satellites. For Landsat-7 ETM+, bands 1-5,7 were downloaded from the designated website maintained by USGS. In addition, for MODIS Terra, bands 1-4, 6 and 7 were selected for download as GEOTIFF images from the online datapool managed by USGS. A comparison between these satellites is presented in Table 4-2.

Table 4-2: Satellite products utilized in this study.

Satellite Sensor	Product Selection	Spatial Resolution	Temporal Resolution	Bands Used
Terra MODIS Landsat 5 TM	Surface Reflectance	250/500 m	Daily	1–4,6,7
Landsat 7	Surface Reflectance	30 m	16 Days	1–5,7

Source: Chang et al., 2014

b) Image Processing and Preparation:

The MODIS images are at a level-2G basis. The MODIS data are radiometrically calibrated and atmospherically corrected to account for scattering and aerosols (Vermote et al., 2008). The data of Landsat-7 is radiometrically and atmospherically corrected and is on a level-1T basis. ArcGIS, a mapping and spatial analysis software, was used to process the images in preparation for the data fusion process. It was necessary to perform the following actions on the Landsat images: 1) Perform gap-filling operation Using ENVI classic software to account for data loss resulting from resulting from sensor failure; 2) Carry out reprojection to the Universal Transverse Mercator (UTM) zone 19 North fpr the Mattapoisett River watershed and zone 18 North for Hackensack and Pascack watershed; and 3) crop-out unnecessary land area. . Besides, the following steps were taken to process the MODIS images: 1) Perform reprojection to the UTM zone 19 North for Mattapoisett River watershedand 18 North for Hackensack and Pascack watershed; 2) Carry out resampling to a 30 m spatial resolution, and 3) crop-out unnecessary land data from both the watersheds.

c) Data Fusion Algorithm Utilization:

Fused images are the algorithmic fusion of the spectral, temporal, or spatial properties of two or more images into a composite or synthetic image possessing the characteristics of the input images (Van and Pohl 1994). The fusion of data streams into a single image has the potential to increase the reliability of the data, and displays more of an object's defining attributes at once (Pohl and Van 1998). There are a number of data fusion techniques available, and selecting an algorithm to apply depends upon the type of output data required for the application, the accuracy of the fused data, and the characteristics of the input data streams that the user would like to fuse. Data fusion techniques are classified into three groups according to the level at which the processing takes place (Pohl and Van 1998) including: 1) pixel level, 2) feature level, and 3) decision level. Pixel level image fusion refers to the fusion of the measured physical attributes of the data, prior to significant processing.

The algorithm selected for data fusion for this study is STARFM. This allow for creation of fused images of enhanced spatial, spectral and temporal properties. The spectral reflectance value for each pixel of the MODIS image is a conglomeration of the surface reflectance from each object in the 250 by 250 m area. Alternatively, spectral reflectance values provided by the Landsat image are an average of objects contained within a 30 by 30 m pixel. Thus, generating a regression model using the fused band data on a daily basis will be more accurate than using MODIS imagery alone, since the coarser MODIS data is integrated with the spectral reflectance values at Landsat's fine spatial resolution within their daily snapshots. With regard to the fusion process, the STAR-FM algorithm uses the original Landsat image as a base data set, and fuses the MODIS and Landsat images of the same date to produce the predicted image (Gao et al., 2006). One caution in the method is noted in fusing the data streams from Landsat and MODIS. Landsat band 1 does not have the same spectral range of MODIS band 1. Instead, band 1 of Landsat corresponds to Band

3 of MODIS and so on. Table 3 details the proper manner in which MODIS and Landsat bands must be compared.

Table 4-3: Landsat 7 ETM+ and Terra MODIS band comparisons

Landsat 7 ETM+ Band	Landsat Bandwidth (nm)	Terra MODIS Band	MODIS Bandwidth (nm)
1	450–520	3	459–479
2	520–600	4	545–565
3	630–690	1	620–670
4	760–900	2	841–876
5	1550–1750	6	1628–1652
7	2080–2350	7	2105–2155

Source: Chang et al., 2014

The whole process of data fusion is summarized in the flow chart shown in Fig. 4-6:

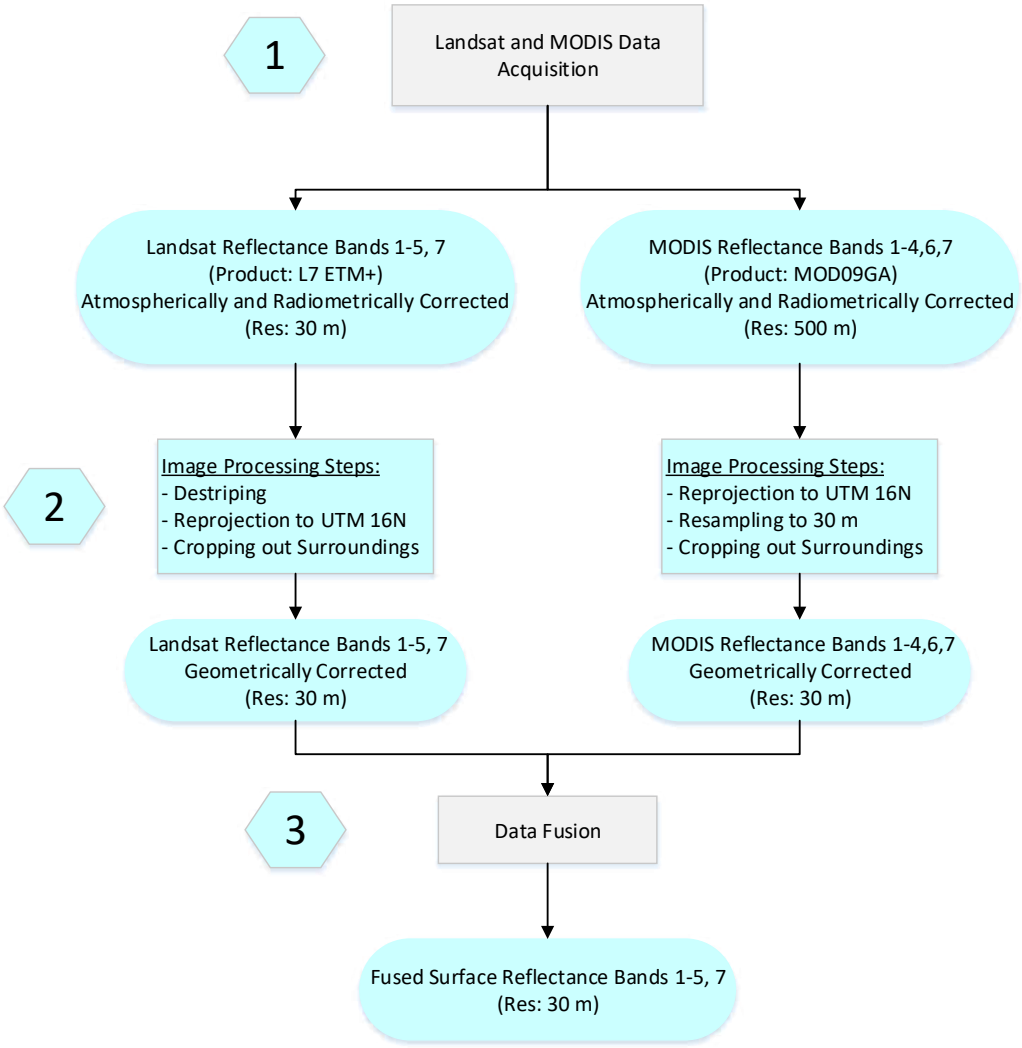

Figure 4-6: Flow chart of Data fusion work process.

As the STAR-FM program translates through the matrix of pixels in the Landsat and MODIS images, it may select a central pixel every few steps and reassign the pixel's value based upon candidate pixels that are both near the central pixel and spectrally similar. The candidate pixels are then filtered out if they exhibit more change over time than the central pixel, or if the spectral features of the candidate pixel are greater than the difference between the spectral features of the central pixel in the Landsat and MODIS images (Gao et al., 2006). Thus, the surface reflectance of the central pixel will be generated from the group of selected candidate pixels. However, the surface reflectance of the candidate pixels is not simply the average value of all

surface reflectance values involved. A weighted average is applied based upon how likely each of the selected candidate pixels could represent the central pixel. Higher weighting factors are assigned if the candidate pixel is spectrally and temporally similar to the central pixel, in addition to its geometric distance from the central pixel (Gao et al., 2006). Through this entire process, the synthetic Landsat image is generated based on the input candidate pixels in the MODIS image taken during the desired prediction date

For the Hackensack and Pascack watershed, data fusion works were carried out in two phases. The first phase was for before-landfall and the second phase was run for after-landfall scenario. For the first phase, cloud-free Landsat –7 images were available for September 19, 2012 and October 05, 2012. Images fused were the dates of 14,17,23 and 25 September 2012 as cloud-free MODIS images were available for these days only. For second phase, Landsat-7 Images were available for 21 October, 06 November and 22 November 2012. Due to conflict in the bofroe and after landfall dates, the image of 21 October 2012 was not utilized. The Landsat image of 06 November was used to predict the synthetic image of 04 November. The synthetic images of 09, 11 and 17 November were predicted using both 06 and 22 November Landsat images and lastly, the synthetic image for 26 November was predicted by using only Landsat image of 22 November.

4.4.2 NDVI Mapping

The NDVI is a numerical index that employs the visible and near-infrared bands of the electromagnetic spectrum and is used to analyze the remote sensing environment and to survey whether the area of interest contains live green vegetation or not. There is a wide range of applicability in vegetation estimation studies. It has been used in the assessment of crop yields (Quarmby et al., 1993; Mkhabela 2011; Prasad et al., 2006), rangelands conveyance capacities

(Yengoh et al., 2014) etc. It is often directly identified with other ground parameters such as ground cover percentage (Scanlon et al., 2002; Lukina et al., 1999), photosynthetic movement of the plant (Penuelas et al., 1995; Pettorelli et al., 2005), surface water (Fu et al., 2015; Chandrasekar et al., 2010), leaf territory record which is also known as leaf area index (Carlson et al., 1997; Wang et al., 2005) and the measure of biomass (Anderson et al., 1993). NDVI was initially utilized as a part of 1973 by (Rouse et al. 1974).

Generally, healthy vegetation will retain a large portion of the visible light that falls on it, and reflects back an enormous segment of the near infrared light. Inadequate or unhealthy vegetation reflects more portion of the visible light and lass of the near infrared light. Uncovered soils then again reflect decently in both the red and infrared segment of the electromagnetic spectrum (Holme et al., 1987). The behavior of the green vegetation is known across the electromagnetic spectrum. The NDVI data can be determined by concentrating on the satellite bands that are most delicate to the vegetation data (red and near-infrared). The greater the distinction along these lines between the near-infrared and red reflectance, the denser the vegetation there must be.

For our study, we shall be using synthetic images derived by fusion of Landsat and MODIS images by STARFM algorithm to monitor and assess the impact of Hurricane Sandy using NDVI images and tasseled cap transformation plots on the Hackensack and Pascack watershed of New Jersey; which was in the direct path of the hurricane. Our study will also extend to Mattapoisett River watershed as well to have a comparative scenario although it was not on the hurricane's direct path.

The NDVI algorithm is calculated by subtracting the red reflectance values from the near-infrared and dividing it by the sum of near-infrared and red reflectance values. The formula for NDVI can be written as;

$$NDVI = \frac{R_{NIR} - R_{Red}}{R_{NIR} + R_{Red}} \quad (4\text{-}1)$$

The NDVI mapping effort is also carried out using the "Image Analysis" tool of ArcGIS software. The algorithm is used as input in the tool and the NDVI maps are generated as output.

The algorithm used can be modified according to the NIR and red bands of Landsat-7 ETM+. The NIR corresponds to band 4 and the red band corresponds to band 3 of Landsat-7 ETM+ respectively. So for calculating NDVI, equation 4-1 becomes:

$$NDVI = \frac{Band\ 4 - Band\ 3}{Band\ 4 + band3} \quad (4\text{-}2)$$

4.4.3 Tasseled Cap Transformation Plots

The Tasseled Cap transformation involves the conversion of original band data into composite band readings (Watkins, 2005). In other words, it is the weighted sum of separate channel readings. This method enhances the spectral information content of Landsat TM data. It is a global vegetative index that separates the amount of soil brightness, vegetation, and moisture content in individual pixels. This transformation optimizes data viewing that helps in the studies of vegetative cover of an area. Typically, there are six tasseled cap transforms. Of them, only three are generally used. They are brightness (measure of soil), greenness (measure of vegetation) and wetness (interrelationship of soil and canopy moisture).

It is generally viewed that tasseled cap transformation has arisen out of empirical observations. The guide and inspiration for this method may have been the principal component analysis. Principal component analysis helps form new variables as weighted sums of different

band readings. The first three transformations i.e. brightness, greenness and wetness contain most of the information and so these are used. The rest of the transformations are treated as noise and rarely used.

The tasseled cap transformation was first shown by Kauth and Thomas in 1976 to describe the growth of wheat cover in an agricultural field. They have linked the patterns found in Landsat data from the croplands as a function of the life cycle of the crops. A tasseled cap transformation is performed by taking linear combinations of the original spectral bands. This is similar to the concept of principal component analysis. The coefficients used are derived statistically. The coefficients ae specific to each sensor. The plots of the tasseled cap for the two watersheds will be compared to the plots shown in Fig. 4-7 to compare the landscape changes that occurred after the hurricane made landfall on the east coast of US.

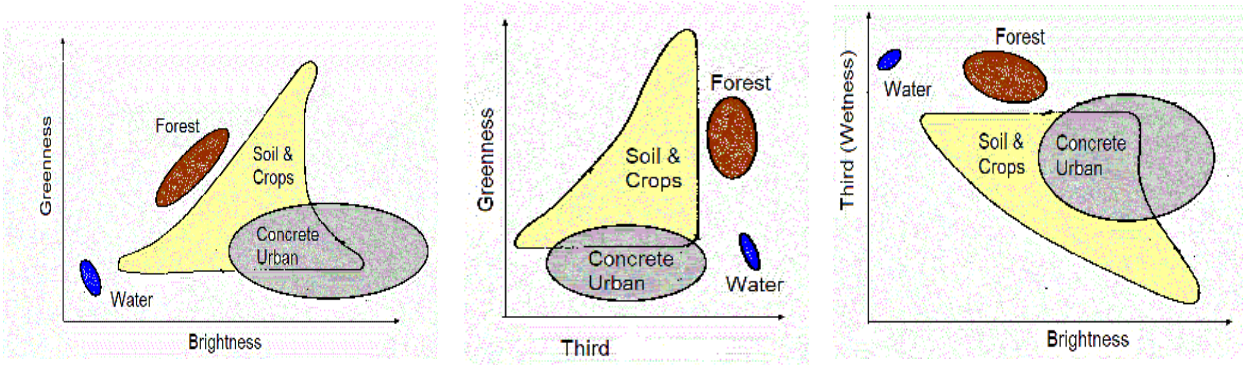

a) Greenness vs. Brightness

b) Greenness vs. Third (Wetness)

c) Third (Wetness) vs. Brightness

Figure 4-7: Tasseled cap transformation plots for landscape interpretation (Christ et al., 1986).

For this study, the tasseled cap transformation will be approached in two fronts. One front will create greenness, brightness and wetness (third) maps ArcGIS. The ArcGIS analysis will only be done for the Hackensack and Pascack watershed since this watershed was in the direct path of

Hurricane Sandy. The tool that will be used is the "Raster calculator." Since most of the information (95-98%) are contained in the first three transformations (Vorovencii, 2007), i.e. brightness and greenness, only these three transformations will be performed.

The equations to be used in the "Raster Calculator" tool are as follows,

Brightness = Float (((0.3561)*ETM+1) + ((0.3972)*ETM+2) + ((0.3904)*ETM+3) + ((0.6966)*ETM+4) + ((0.2286)*ETM+5) - ((0.1596)*ETM+7)) (4-3)

Greenness = Float (((-0.3344)*ETM+1) - ((0.3544)*ETM+2) - ((0.4556)*ETM+3) + ((0.6966)*ETM+4) - ((0.0242)*ETM+5) - ((0.2630)*ETM+7)) (4-4)

Wetness (Third) = Float (((0.2626)*ETM+1) - ((0.2141)*ETM+2) - ((0.0926)*ETM+3) + ((0.0656)*ETM+4) - ((0.7629)*ETM+5) - ((0.5388)*ETM+7)) (4-5)

The plots of tasseled cap transformation can help study in depth the effect of Hurricane Sandy on the Hackensack and Pascack watershed. With the help of data fusion, we shall plot the brightness, greenness and wetness maps for the watershed using fused images to have a daily time series mapping of the transformations.

4.5 Results and Discussion

4.5.1 NDVI Maps

Hurricane Sandy was first formed from a tropical wave in the western Caribbean sea on October 22, 2012 which quickly turned to a tropical storm a few hours later. The hurricane wreaked havoc on Cuba, Bahamas and the eastern seaboard of the US through October 29, 2012. This is also the date when it made landfall in New Jersey and New York, where the damage has been the most severe. The storm spread as far as the Buzzards bay and Cape Cod where heavy rains and storm surges caused damage to buildings and roadways. Trees were uprooted and power was cut

off. The extent of the damage on terrestrial vegetative cover of the coastal water shed adjacent to Mattapoisett harbor can be assessed on a day-to-day basis using the fused images created by STARFM. The NDVI maps for cloud free days for the month before Hurricane Sandy made landfall i.e. September is depicted in Fig. 4-8 below.

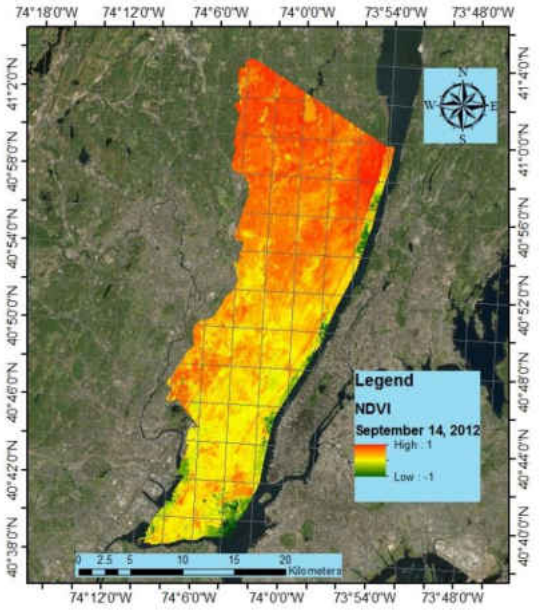

a) NDVI mapping for September 14, 2012

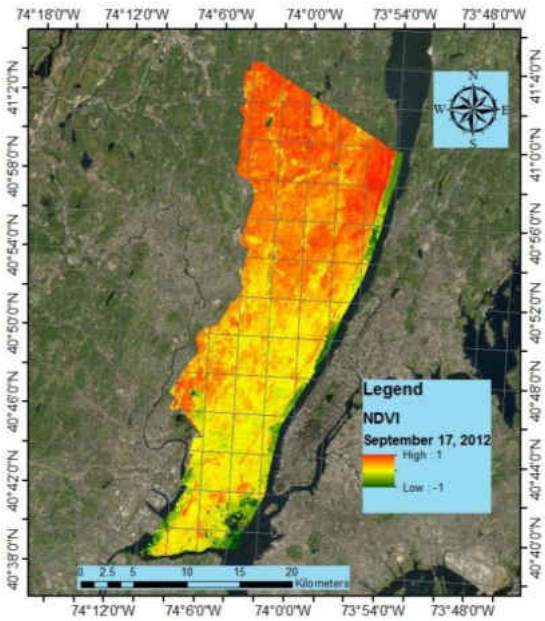

b) NDVI mapping for September 17, 2012

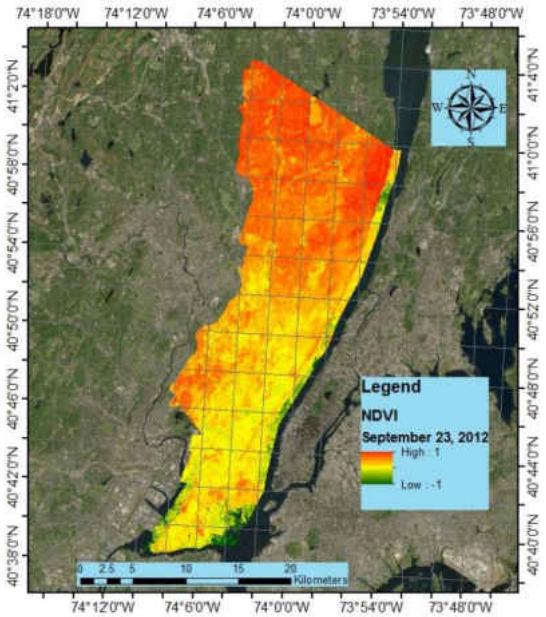

c) NDVI mapping for September 23, 2012

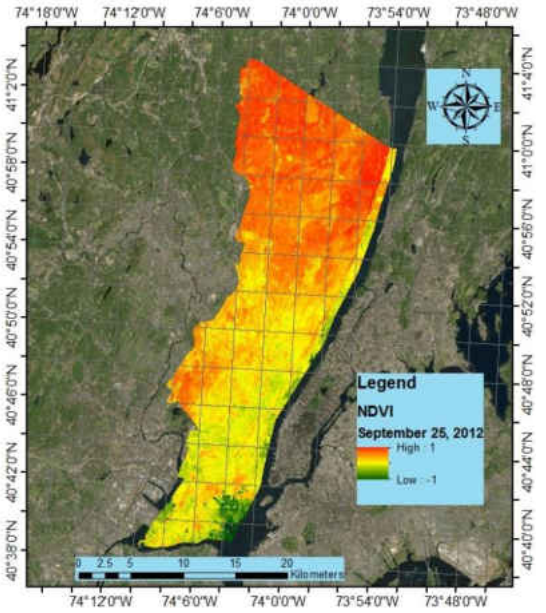

d) NDVI mapping for September 25, 2012

Figure 4-8: NDVI maps generated for observation of before impact of Hurricane Sandy on Hackensack and Pascack watershed. Figures (a) to (d) represent the NDVI maps derived from fused images for the respective dates.

Table 4-4: Mean values of NDVI before impact of Hurricane Sandy on Hackensack and Pascack watershed (Hurricane landfall date October 29, 2012).

Day	Mean NDVI
September 14, 2012	0.436
September 17, 2012	0.394
September 23, 2012	0.449
September 25, 2012	0.467

The NDVI maps for cloud free days for the month after Hurricane Sandy made landfall i.e. November is depicted in Fig. 4-9 below. The NDVI maps for the individual days were derived from images synthesized with the help of data fusion as mentioned earlier. These fused NDVI images will help us in the determination of the extent of damage the vegetation cover suffered after hurricane made landfall.

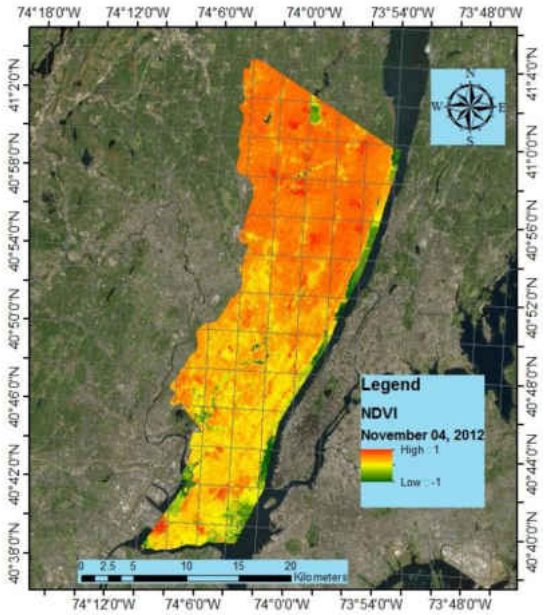

a) NDVI mapping for November 04, 2012

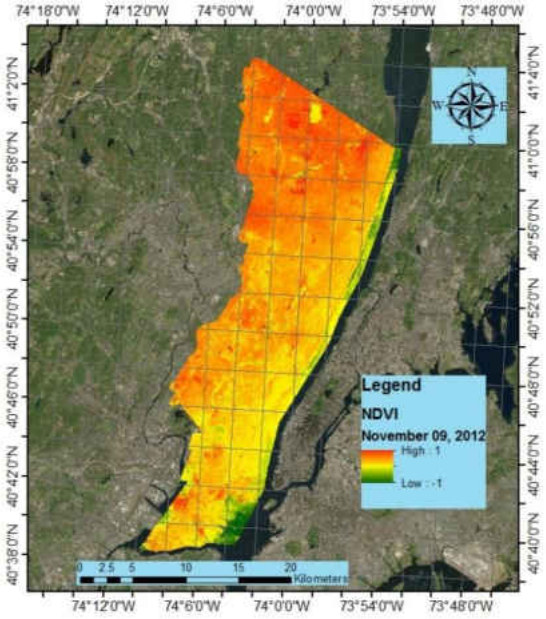

b) NDVI mapping for November 09, 2012

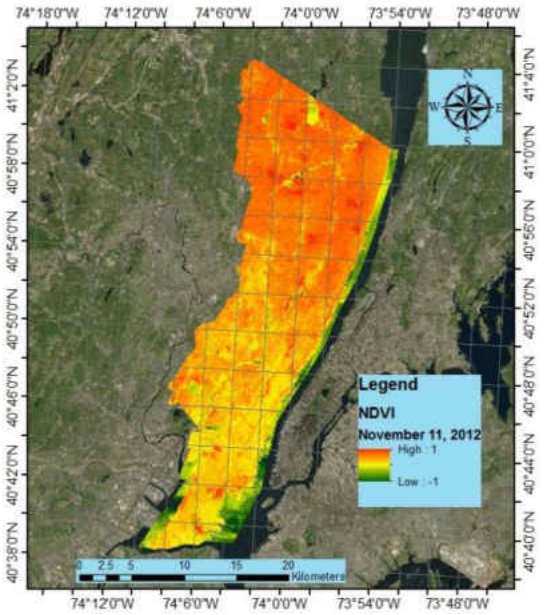

c) NDVI mapping for November 11, 2012

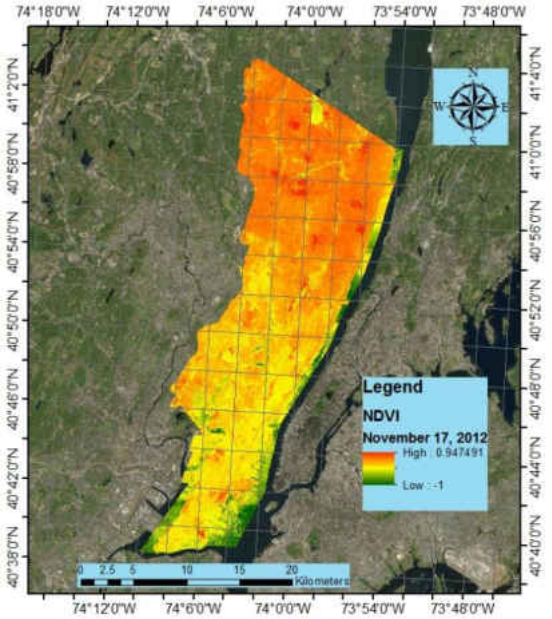

d) NDVI mapping for November 17, 2012

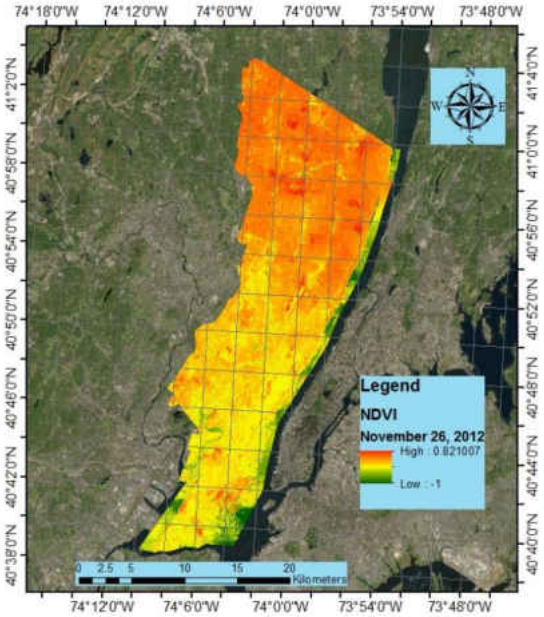

e) NDVI mapping for November 26, 2012

Figure 4-9: NDVI maps generated for observation of Hackensack and Pascack watershed after impact of Hurricane Sandy. Figures (a) to (e) represent the NDVI maps derived from fused images for the respective dates (Hurricane Sandy Landfall date is October 29, 2012).

Table 4-5: Mean values of NDVI after impact of Hurricane Sandy on Hackensack and Pascack watershed (Hurricane Sandy Landfall date is October 29, 2012).

Day	Mean NDVI
November 04, 2012	0.296
November 09, 2012	0.242
November 11, 2012	0.282
November 17, 2012	0.261
November 26, 2012	0.269

The NDVI maps for four cloud free days in September 2012, i.e. one month before the hurricane landfall shows that there is dense vegetation cover in the northern part of the watershed, especially in the northeastern part near the Hudson River (Fig 4-8a, 4-8b, 4-8c, 4-8d). The average NDVI values for the four days are also consistent (Table 4-4). However, the NDVI maps for five cloud-free images for November 2012, i.e. the month after hurricane landfall shows a decline in the NDVI average values compared to the values of September 2012 (Table 4-5). This is an indication of the impact of hurricane on the vegetative cover of the watershed. In addition, the NDVI maps also confirm the decline in the vegetative cover of the watershed. The dense colors as seen in the maps of Fig. 4-8 have become lighter in the same areas particularly in the northeastern region of the watershed. This is proof of effect of hurricane impact on the vegetative cover of the watershed. The NDVI maps for cloud free days for Mattapoisett River watershed when Hurricane Sandy made landfall is shown in Fig. 4-10 below

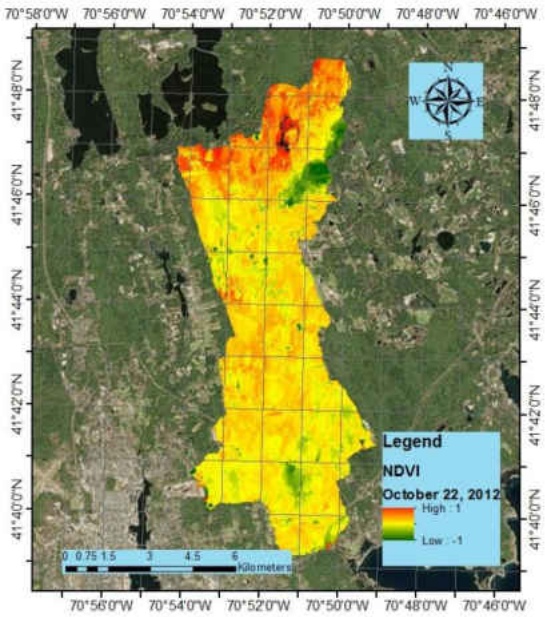

a) NDVI mapping for October 22, 2012

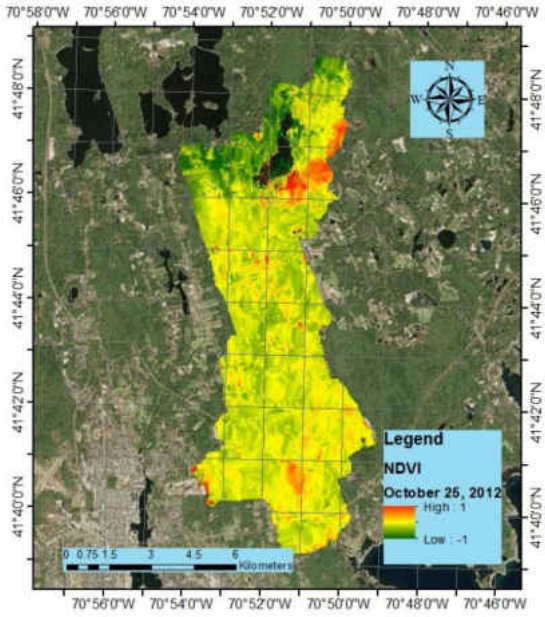

b) NDVI mapping for October 25, 2012

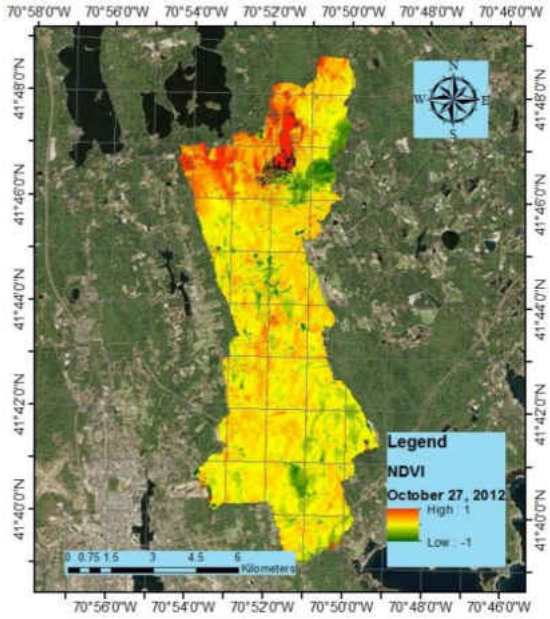

c) NDVI mapping for October 27, 2012

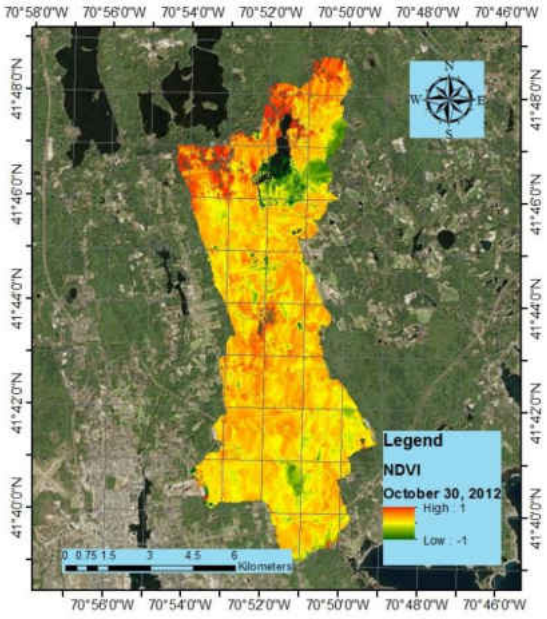

d) NDVI mapping October 30, 2012

Figure 4-10: NDVI maps generated for observation of impact of Hurricane Sandy on watershed that drains into the Mattapoisett River, which in turn, flows to the Mattapoisett Bay. Figure (a) is the NDVI map generated from cloud-free Landsat 7 and (b) to (d) represent the NDVI maps derived from fused images for the respective dates.

Table 4-6: Mean values of NDVI (Hurricane Landfall date October 29, 2012).

Day	Hurricane Condition	Mean NDVI
October 22, 2012	Before	0.663
October 25, 2012	Before	0.719
October 27, 2012	Before	0.625
October 30, 2012	After	0.627

The NDVI maps (Fig. 4-10) for four days show no significant changes in the vegetative cover during the hurricane event. This may be attributed to the fact that the hurricane did not make

landfall in the Mattapoisett harbor area unlike the Hurricane Bob event of 1991. The average NDVI value for the day of October 23; which is one day after hurricane formed, is 0.663 (Table 4-6). Although there is an increase in the value for October 27, the value again decreases to 0.625 for October 27 and holds steady at October 30 with a value of 0.627 (Table 4-6); a day after the hurricane made landfall in New Jersey. The low value indicates that there was some damage to the vegetative cover as there were reports of trees being uprooted. However, the damage seems to have been stabilized in the day following the hurricane.

4.5.2 Tasseled Cap Transformation Plots

The tasseled cap transformation plots for the Mattapoisett River watershed for before and after Hurricane Sandy made landfall is depicted in the Fig. 4-11 The before and after plots will help deduce the conditions of soil moisture, canopy cover and vegetation cover for the watershed area.

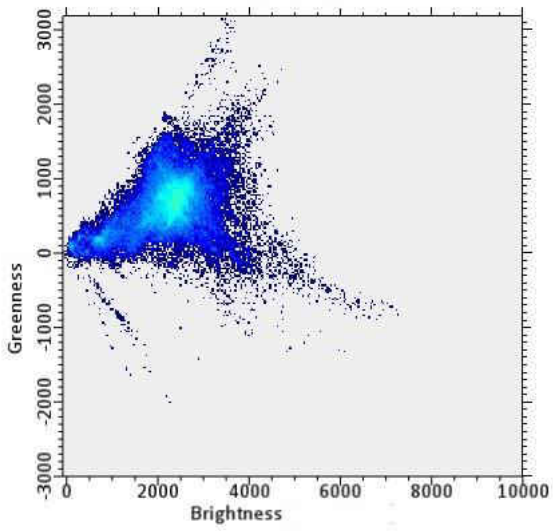

a) October 27, 2012 (Before hurricane)

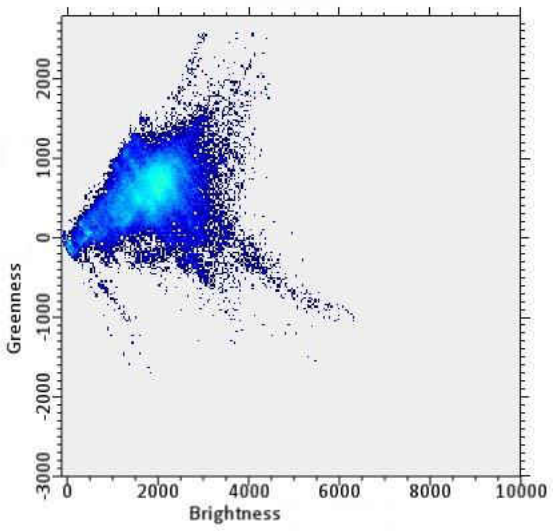

d) October 30, 2012 (After hurricane)

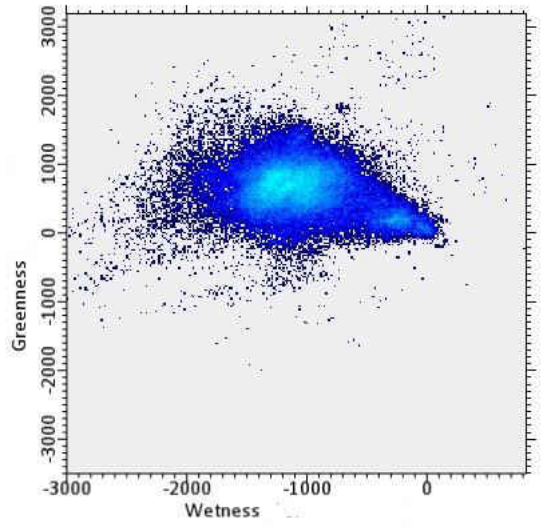

b) October 27, 2012 (Before hurricane)

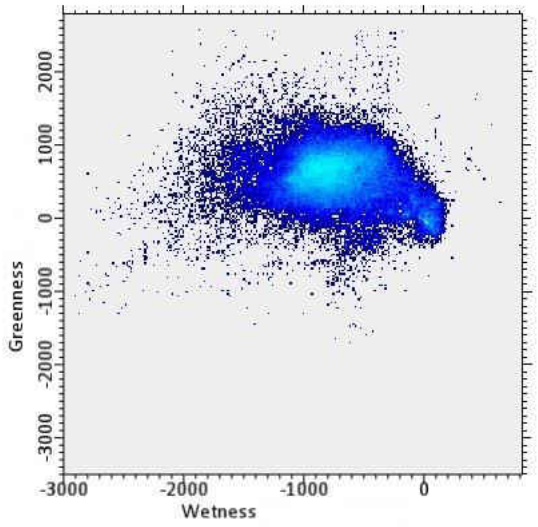

e) October 30, 2012 (After hurricane)

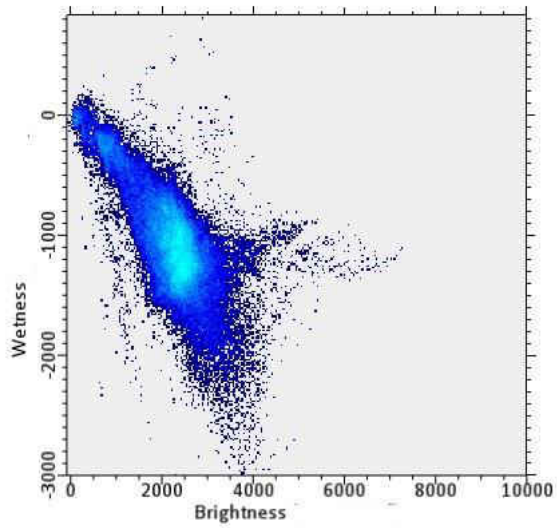

c) October 27, 2012 (Before hurricane)

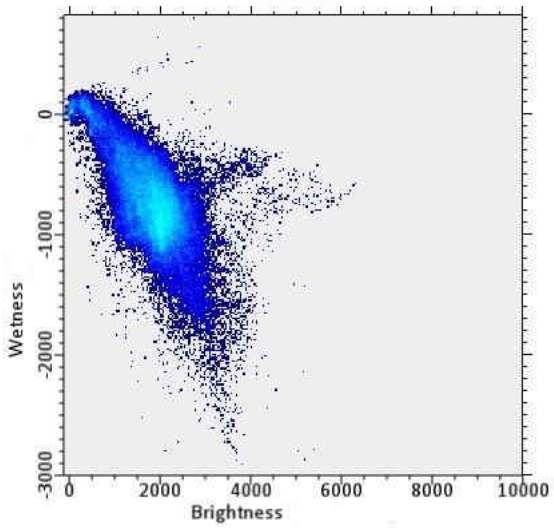

f) October 30, 2012 (After hurricane)

Figure 4-11: Tasseled cap plots (ENVI 5.3 software output) derived for Mattapoisett River watershed area depicting land cover conditions before and after Hurricane Sandy made landfall. The plots (a) to (c) depict conditions before hurricane landfall and (d) to (f) depict scenario after landfall

The tasseled cap transformation plots for Mattapoisett River watershed depicts the condition of the landscape before and after landfall in Fig. 4-11. The plots (a) to (c) are for October

27, 2012 i.e. before hurricane landfall and the plots (d) to (f) are for October 30, 2012 i.e. after hurricane landfall. From the plots, it is evident that there is no significant changes in the before and after conditions. This may be attributed to the fact that the Mattapoisett River watershed was not in the direct path of the hurricane. Therefore, the damages sustained were minimal of nature. This is reflected in the tasseled cap transformation plots as well. On the other hand, the areas that suffered the most devastating impact of the hurricane impact are New York and New Jersey areas. That is why we shall be looking at the before and after scenario of tasseled cap transformation plots for Hackensack and Pascack watershed.

The tasseled cap transformation plots for the Hackensack and Pascack watershed for before and after Hurricane Sandy made landfall are depicted in the Fig. 4-12. Here, plots for three days for the previous month of hurricane landfall i.e. for the month of September 2012 are depicted. In addition, plots for three days for the month after landfall i.e. for November 2012 are also included for comparison.

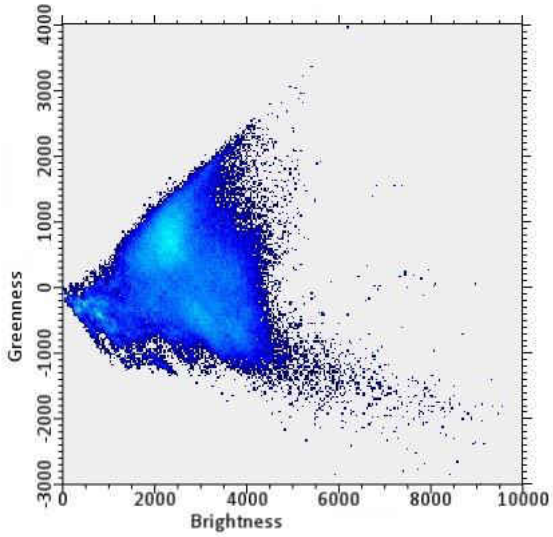

a) September 17, 2012 (Before hurricane)

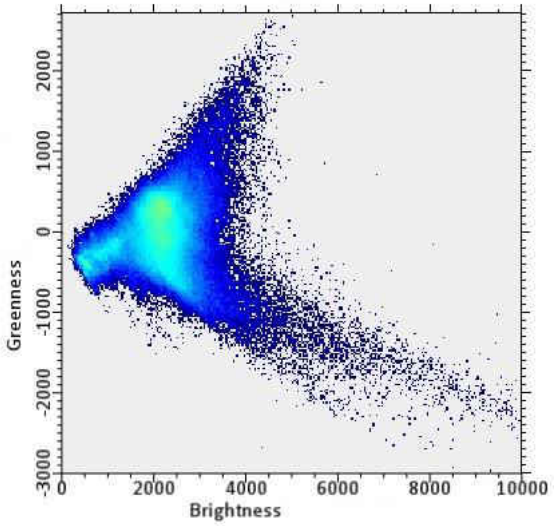

j) November 04, 2012 (After hurricane)

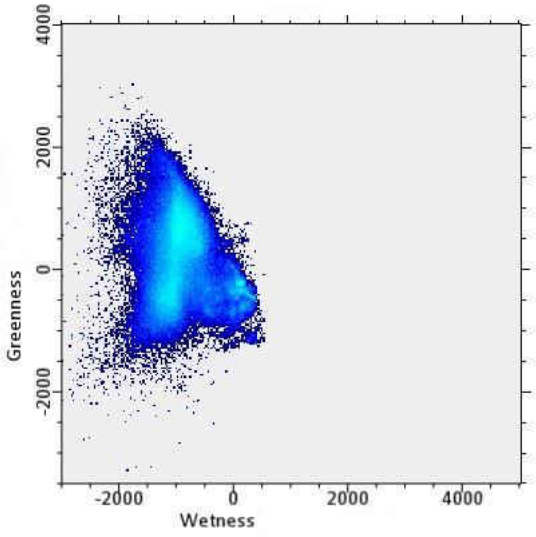

b) September 17, 2012 (Before hurricane)

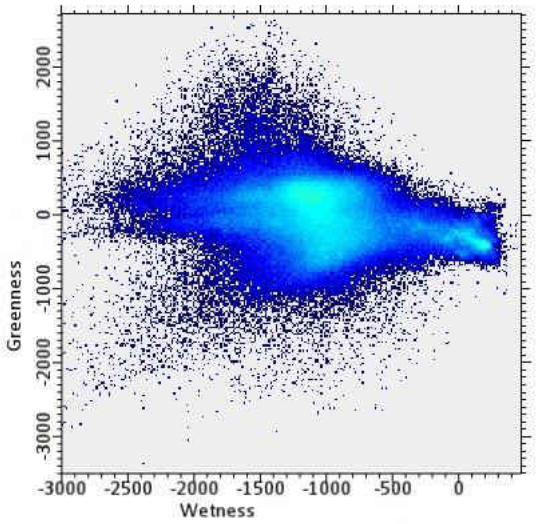

k) November 04, 2012 (After hurricane)

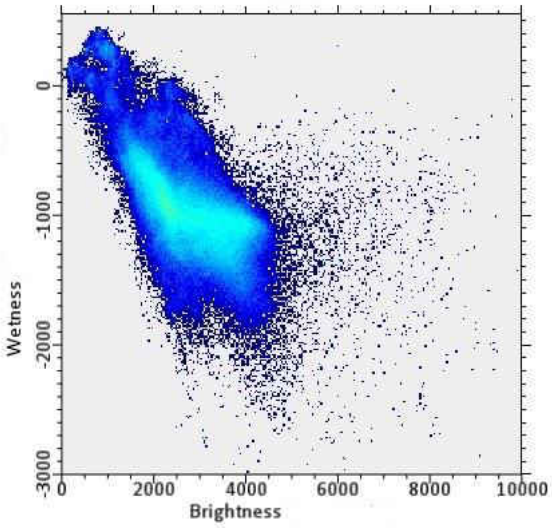

c) September 17, 2012 (Before hurricane)

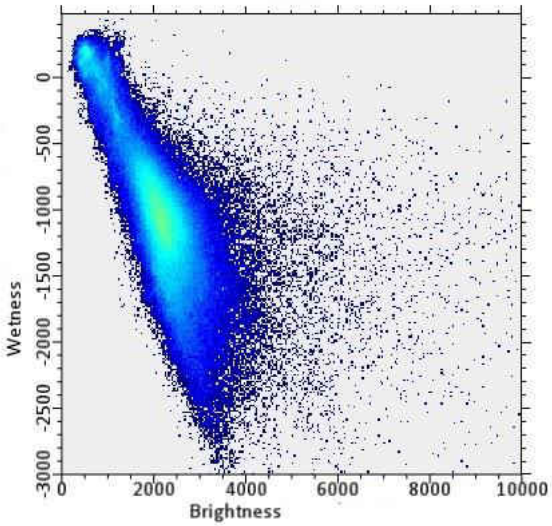

l) November 04, 2012 (After hurricane)

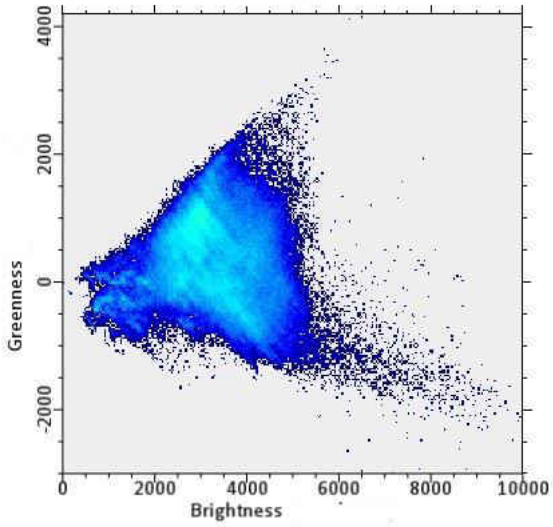

d) September 23, 2012 (Before hurricane)

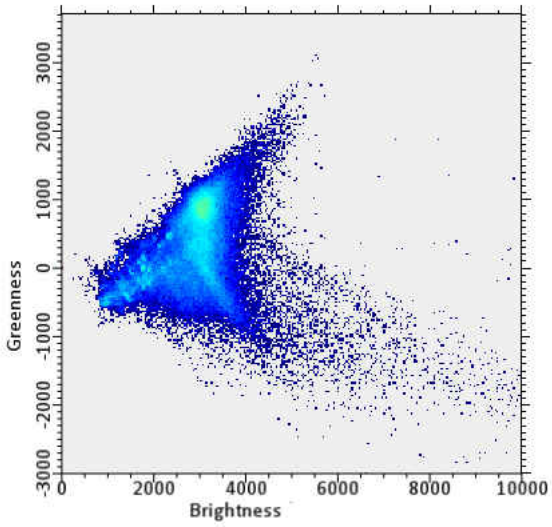

m) November 09, 2012 (After hurricane)

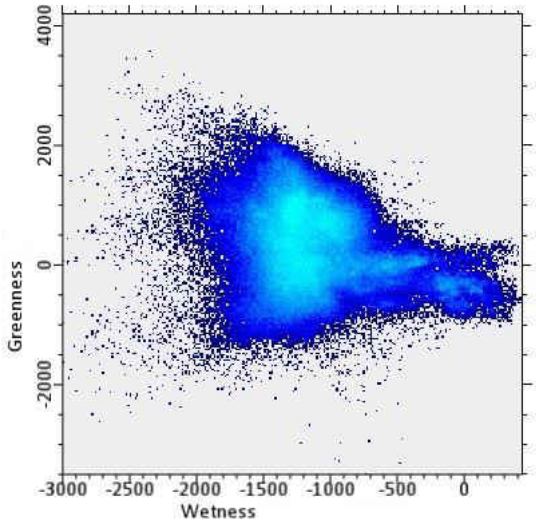

e) September 23, 2012 (Before hurricane)

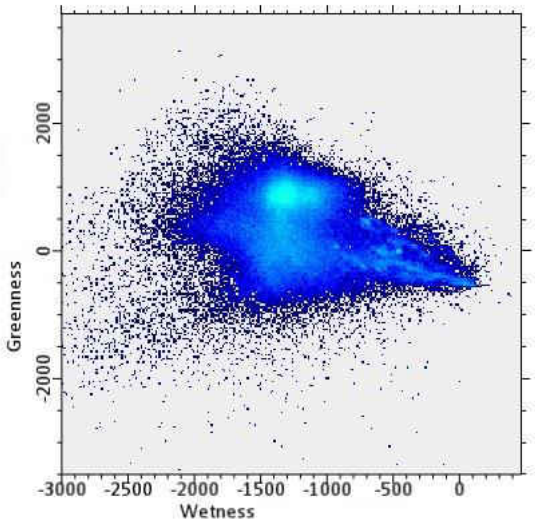

. n) November 09, 2012 (After hurricane)

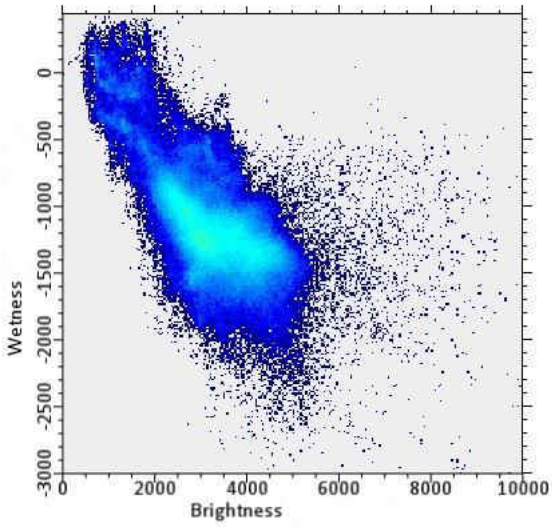

f) September 23, 2012 (Before hurricane)

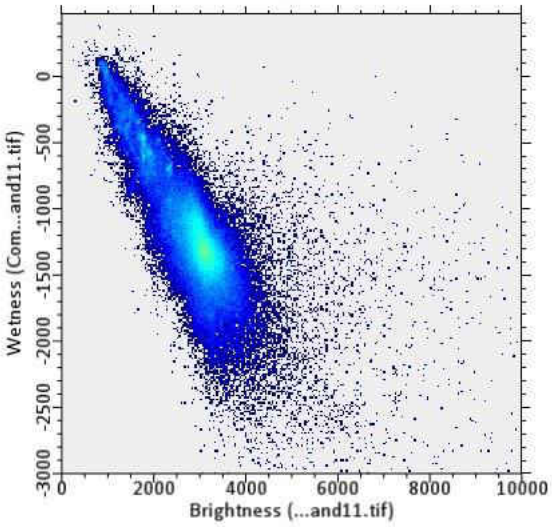

o) November 09, 2012 (After hurricane)

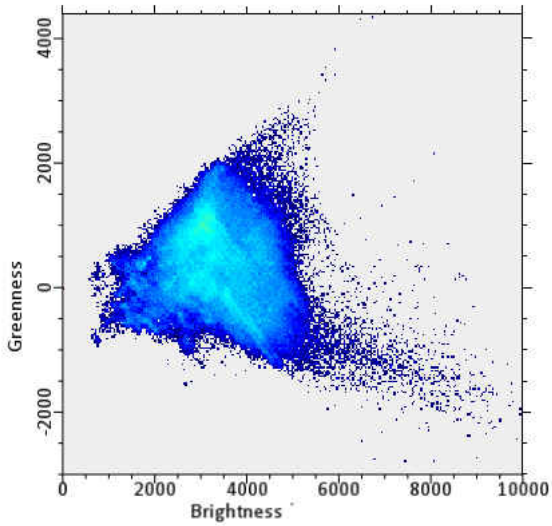

g) September 25, 2012 (Before hurricane)

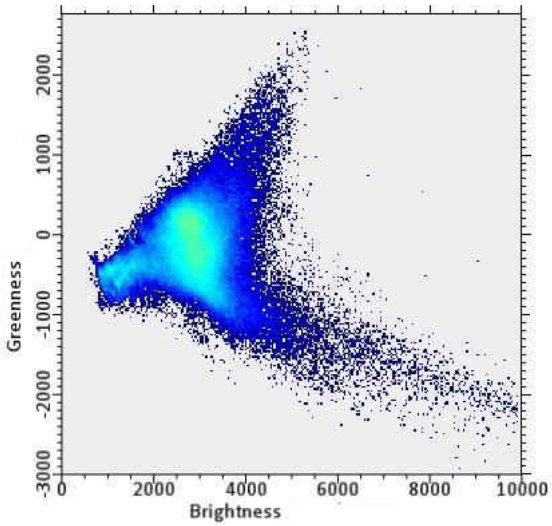

p) November 26, 2012 (After hurricane)

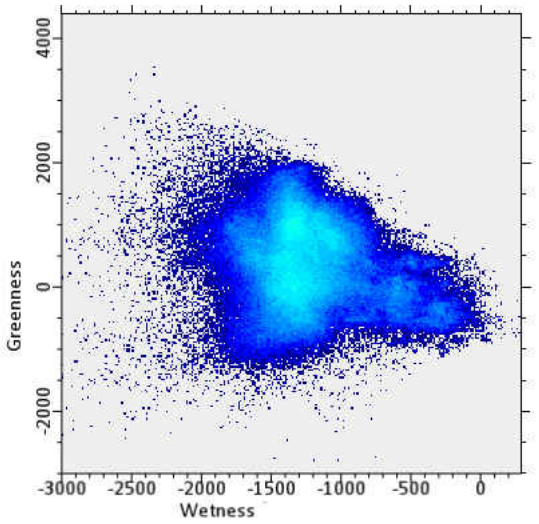

h) September 25, 2012 (Before hurricane)

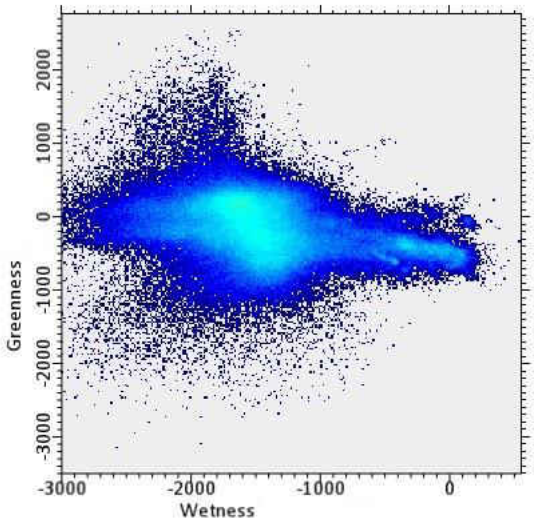

q) November 26, 2012 (After hurricane)

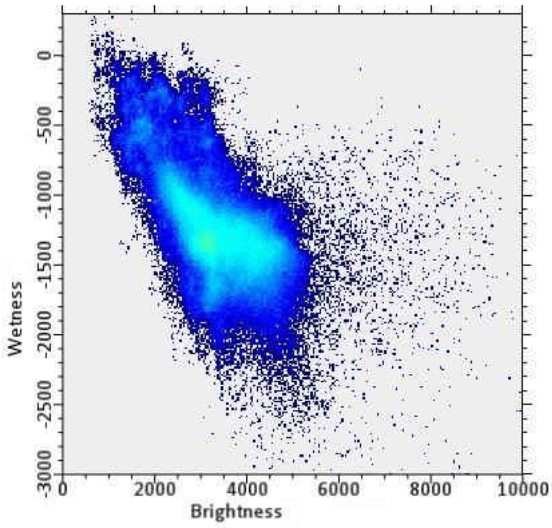

i) September 25, 2012 (Before hurricane)

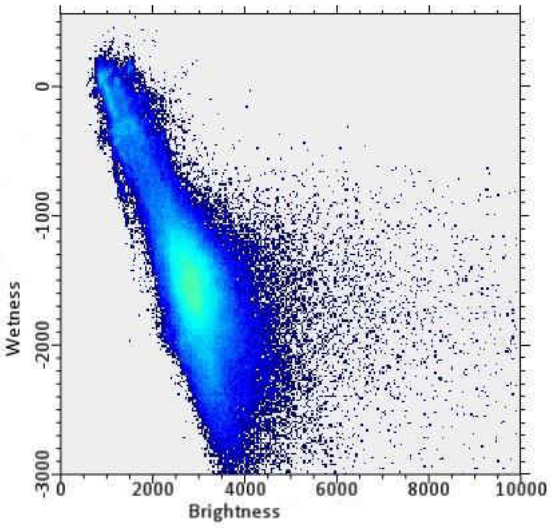

r) November 26, 2012 (After hurricane)

Figure 4-12: Tasseled cap plots (ENVI 5.3 software output) derived for Hackensack and Pascack watershed area depicting land cover conditions before and after Hurricane Sandy made landfall. The plots (a) to (f) depict conditions before hurricane landfall and (g) to (l) depict scenario after landfall.

The tasseled cap transformation plots in Fig. 4-12 represent the conditions of landscape of Hackensack and Pascack watershed of New Jersey, which is one of the hardest-hit areas due to landfall of Hurricane Sandy. This watershed was somewhat directly in the path of the hurricane when it made landfall, resulting in the devastation of the area. The significant changes in the tasseled cap transformation plots in the before and after scenario are an attestation to that. The figures (a) to (i) are the plots showing the land conditions before the hurricane landfall for three days in September; whereas the figures (j) to (r) demonstrates the land conditions after the hurricane made landfall for three days in November. Also, the figures (a) to (c), (d) to (f) and (g) to (i) display the tasseled cap plots for the dates September 17, September 23 and September 25 respectively. Concurrently, the figures (j) to (l), (m) to (o) and (p) to (r) portray the tasseled cap plots for the dates November 04, November 09 and November 26 respectively. The plots are so arranged so that the difference in the before and after scenarios are clearly visible and easily interpretable. In this arrangement, we have a three days before and three days after hurricane landfall scenario.

Let us look at the Greenness vs Brightness plots for the before and after scenarios. For September 17, the plot is quite similar to the standard plot depicted in Fig. 4-7 (a). This is true for the plots of September 23 and September 25 respectively. After hurricane made landfall, significant changes are noticed in the after landfall scenarios. The changes are noticeable in the clear water and turbid water sections. Huge waves made inland when the hurricane hit, which contributed to the changes in the turbid water sections. The change is noticeable for the plot of November 04 (Fig. 4-12 j); which is closer to the landfall date (October 29, 2012). The concrete section or the man-made section of the plot, if compared to Fig. 4-7 (a), shows that there is significant change in that section. The pixels are highly scattered compared to September 09 plot

(Fig. 4-12 a), indicating significant change in urban landscape after hurricane landfall. For the next two plots, it can be seen that the scattering effects are somewhat lessened; indicating the recovery of damages and cleanup conducted in the aftermath of the hurricane landfall.

For the Greenness vs Wetness plots for the days before the landfall, it can be seen that shape of the plots, although does not quite resemble to the standard plot depicted in Fig. 4-7 (b), they are consistent through the three days of September (Fig. 4-12 b, e, h). After hurricane made landfall, the plots for the three days of November show significant distortions. The distortions are especially clear for concrete urban areas and for vegetative areas (Fig. 4-12 k, n p).

For the last and final plot of wetness vs brightness plots, it can be seen that for the three days for the month of September, the patterns are almost the same (Fig. 4-12 c, f, i) when compared to the standard plot depicted in Fig. 4-7 (c). However, in the plots that depict the three days in November, i.e. after hurricane made landfall, there are significant changes in the areas of clear water, turbid water and concrete urban areas (Fig. 4-12 i, o, q). In addition, it can be seen from the plot of November 04 (Fig. 4-12 i) that the concrete urban areas faced significant distortions due to hurricane. This is exemplified by the scattering of the pixels in the area where concrete urban is depicted in the standard plot. After twenty-two days, the plot of November 26 (Fig. 4-12 r) shows that the pixels are less scattered that it was in the first. This indicates the effects of recovery operations

4.5.3 False Color Images and Tasseled cap transformation Maps

The tasseled cap transformation plots are useful in monitoring and assessing the damage sustained by a landscape in terms of vegetation cover, moisture urban areas etc. This usefulness of tasseled cap is reinforced further by analysis of false color images and tasseled cap transformation maps as depicted. The addition of false color images will add a new dynamic to the TCT analysis.

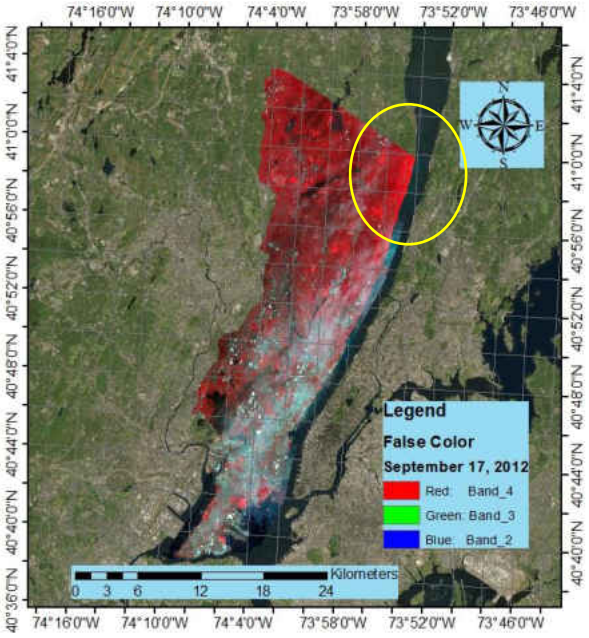

a) September 17, 2012 (Before hurricane)

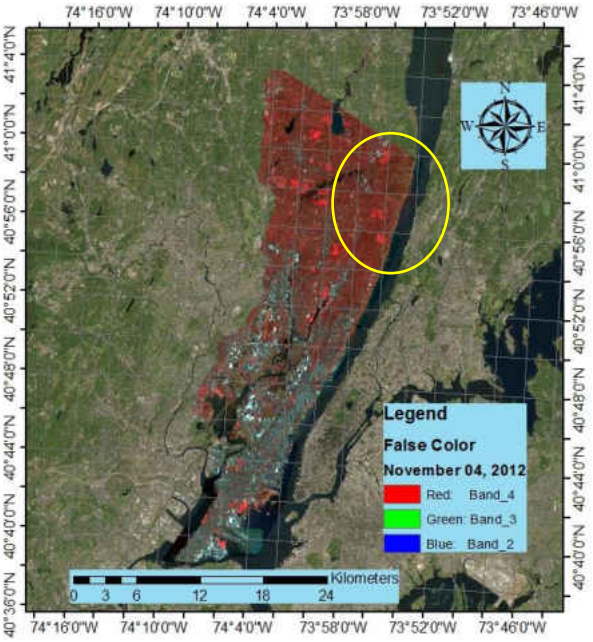

c) November 04, 2012 (After hurricane)

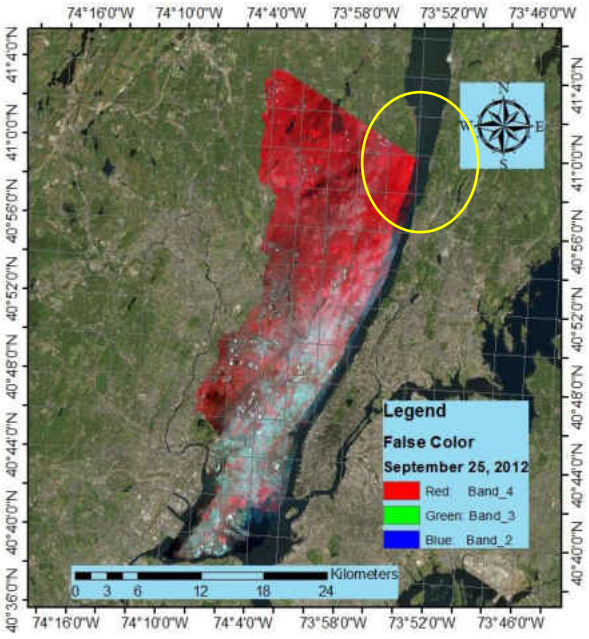

b) September 25, 2012 (Before hurricane)

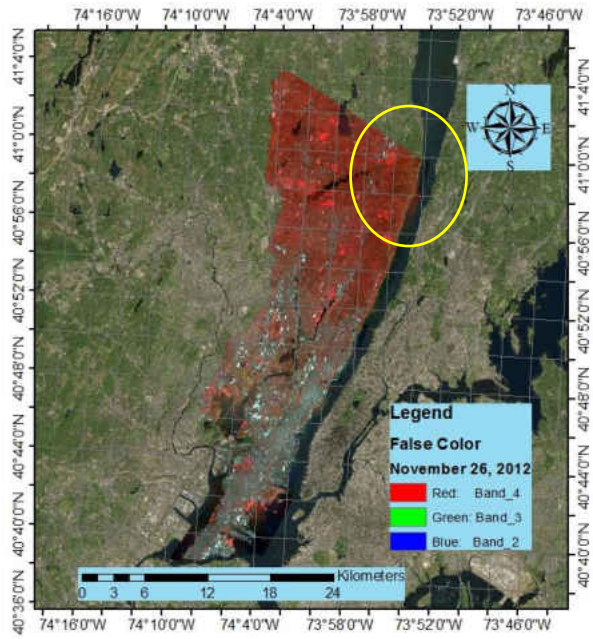

d) November 26, 2012 (After hurricane)

Figure 4-13: False color images of Hackensack and Pascack watershed showing before and after conditions of Hurricane Sandy landfall. (a) and (b) represent the conditions before landfall while (c) and (d) represent after landfall condition.

A multispectral Landsat-7 ETM+ image contains the bands of data obtained on board the sensors. Each of the bands may be displayed one at a time as a grey-scale image. The bands may also be displayed as a combination of three bands at a time (Crisp.nus.edu.sg, 2017). This combination of bands is known as color composite image. In color composite images, three primary colors red, green and blue (RGB) are combined in various proportions. This combination produces different colors in the visible spectrum. When bands are used in association with a separate primary color, the resulting image is a color composite image. Generally, two types of combinations are widely used. They are 1) Natural or True color composites and 2) False color composites.

The true color composite is a combination of visible red, green and blue spectrums to the red, green and blue channels in the software i.e. ArcGIS (Gsp, 2017). The composite image would be what the human eye naturally sees. The Landsat band combinations used for this purpose are Band 3, Band 2 and Band 1 for R, G, B channels respectively (Quinn, 2001). In this case, the healthy vegetation appears green, unhealthy vegetation appears brown and yellow, water blue to black, bare ground and impervious surfaces as light grey and brown. In true color composites, subtle differences in various features may be difficult to spot. The true color images may also be low in contrast that occurs due to scattering of blue light by atmosphere (Gsp, 2017).

This is where the false color composite images come into play. False color images are comprised of spectral bands other than red, green and blue. This helps in visualizing wavelengths that is not seen by the human eye. The use of bands such as near-infrared facilitates the spectral separation and this results in the increase of interpretability of the images (Gsp, 2017). The most commonly used false color combination for Landsat images is the combination of Band 4, Band 3 and Band 2 in the RGB channels. In this combination vegetation is depicted in red, urban areas in

cyan blue, soils in varying colors of dark to light brown and clouds, snow in whit or light cyan (Quinn, 2001). This false color combination is widely used in vegetative studies, drainage patterns, and crop growth monitoring. The deeper the red, the more likely of healthier vegetation. Since our study involves the observation of impact of hurricane Sandy on the vegetation as well as other land cover aspects in the Hackensack and Pascack watershed, we shall use the false color combination of Band 4, Band 3 and Band 2 in the RGB channels.

The changes in the vegetation due to hurricane impact can be seen in the false color images (Fig. 4-13). For both the days depicted, where the days are before hurricane made landfall, we can see there is presence of healthy vegetation in both the days (Fig. 4-13 a, 4-13 c). Especially in the northeastern corner of the watershed near the river (encircled in yellow), the vegetation is comparatively healthier than the rest of the watershed. After hurricane impact on October 29, if we observe the map for November 04 i.e six days after hurricane impact, we shall see that the healthy vegetation is no longer there (Fig. 4-13 b). Even after twenty-two days i.e. on the map of November 26, it can be seen that the vegetation has not yet recovered (Fig. 4-13 d). Overall, the color of vegetation is lighter in the maps after the hurricane than in the maps before the hurricane, suggesting that vegetation cover of the watershed has taken damage due to hurricane landfall

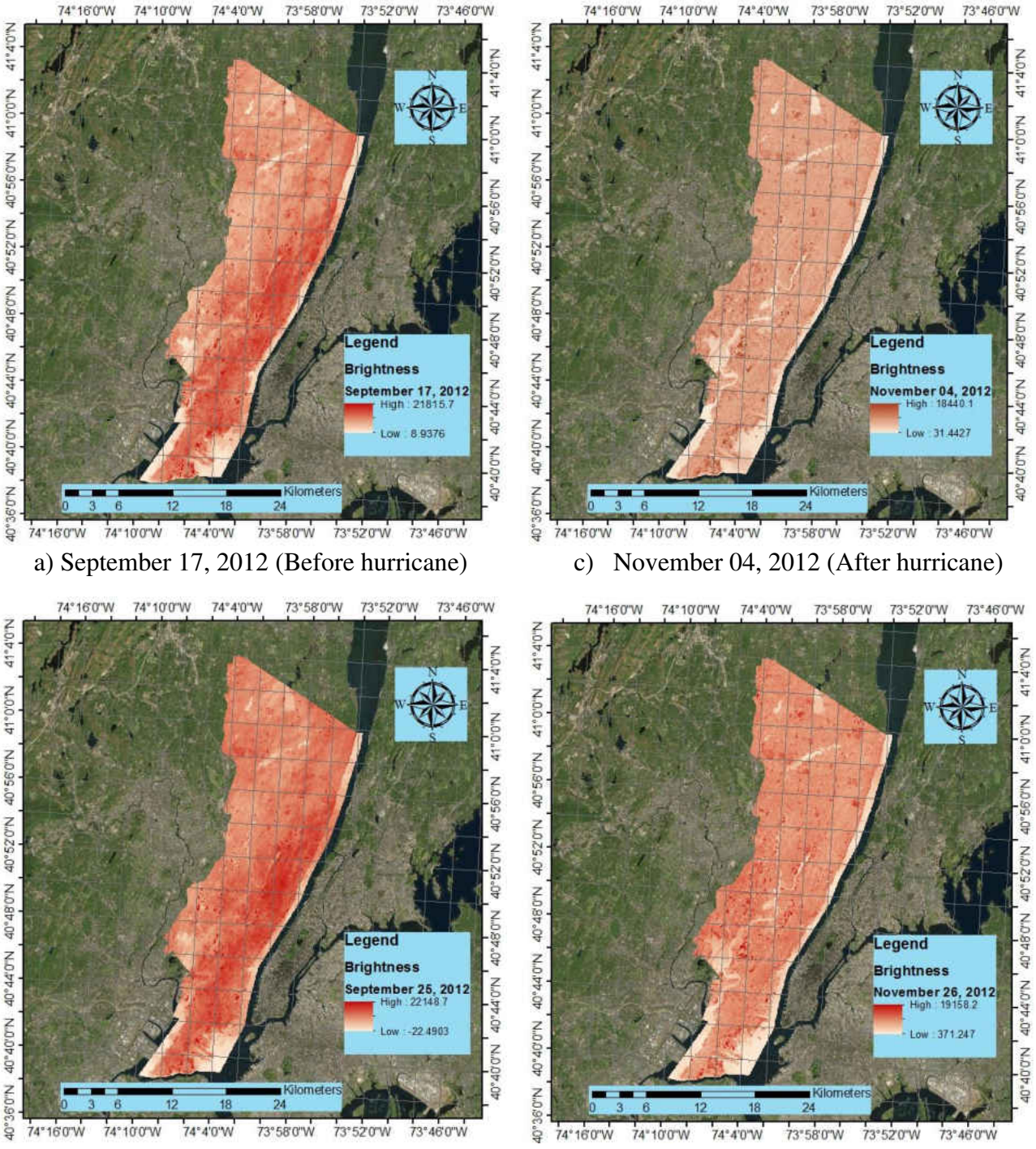

a) September 17, 2012 (Before hurricane)

c) November 04, 2012 (After hurricane)

b) September 25, 2012 (Before hurricane)

d) November 26, 2012 (After hurricane)

Figure 4-14: Brightness images of Hackensack and Pascack watershed showing before and after conditions of Hurricane Sandy landfall. (a) and (b) represent the conditions before landfall while (c) and (d) represent after landfall condition.

Similarly, the impact of hurricane can also be depicted in the brightness images of the watershed. Brightness images represent the variation in the soil background reflectance. The lower the vegetation cover, the more prominent soil reflectance is. However, the soil reflectance may also vary due to urban conditions and the presence of water in the soil (Ciesin, 2017). It has been found that as wetness increases, the brightness decreases (Ciesin, 2017). In case of our watershed, the impact of hurricane on the soil of watershed is clearly seen as the soil reflectance is lighter in both the maps depicting the conditions after the hurricane (Fig. 13b, 13d) than that of the previous conditions (Fig. 4-14a, 4-14c). Heavy rains and flooding associated with the hurricane landfall contributed to the increase in soil moisture resulting in the decrease of soil reflectance.

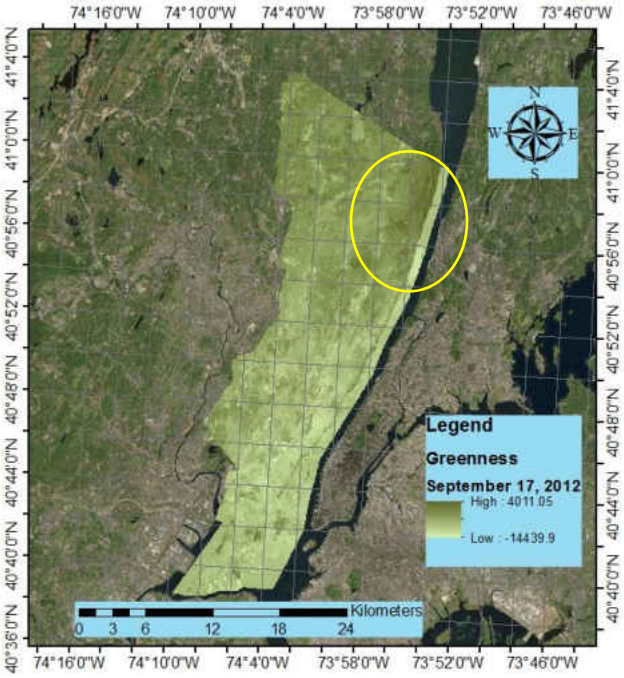

a) September 17, 2012 (Before hurricane)

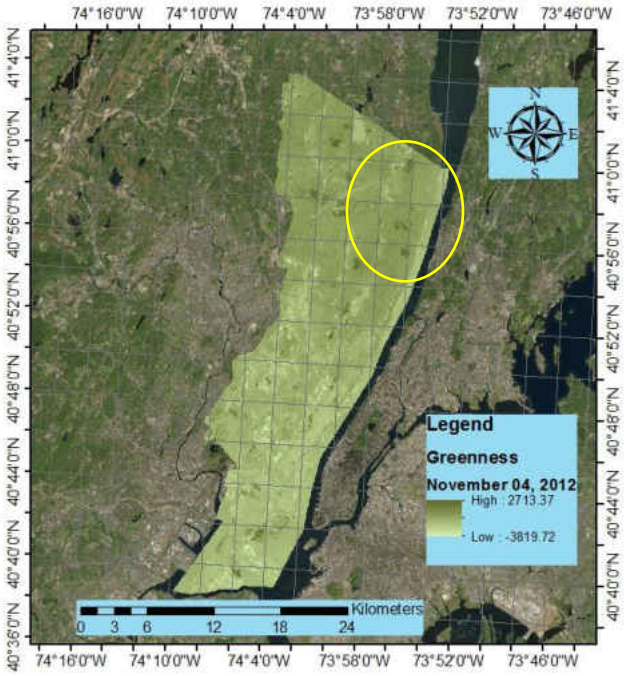

c) November 04, 2012 (After hurricane)

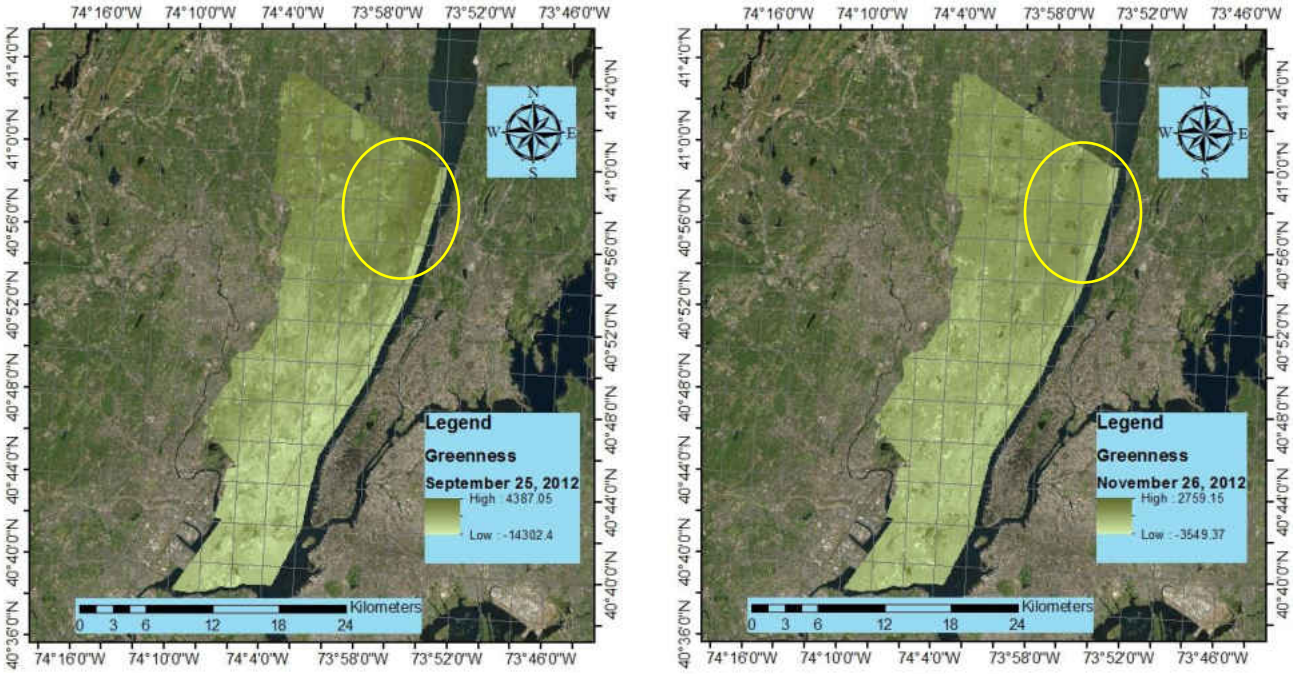

b) September 25, 2012 (Before hurricane)

d) November 26, 2012 (After hurricane)

Figure 4-15: Greenness images of Hackensack and Pascack watershed showing before and after conditions of Hurricane Sandy landfall. (a) and (b) represent the conditions before landfall while (c) and (d) represent after landfall condition.

The greenness index in tasseled cap transformation depicts the presence and density of the green vegetation (Ciesin, 2017). Before the hurricane impact, the maps indicate a healthy vegetation presence in the watershed, particularly in the northeastern side (encircled in yellow) (Fig. 4-15a, 4-15c). After hurricane made landfall, the density of the vegetation is lower six days after the hurricane (Fig. 4-15b). The vegetation density remained lower on November 26, 2012; indicating slower recovery or no recovery at all (Fig. 4-15d). This observation is consistent with the observation of the false color images depicted before.

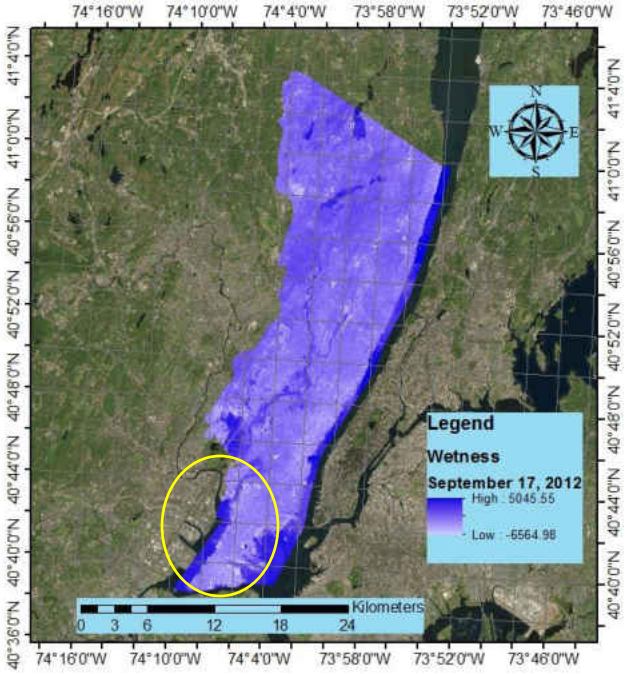

a) September 17, 2012 (Before hurricane)

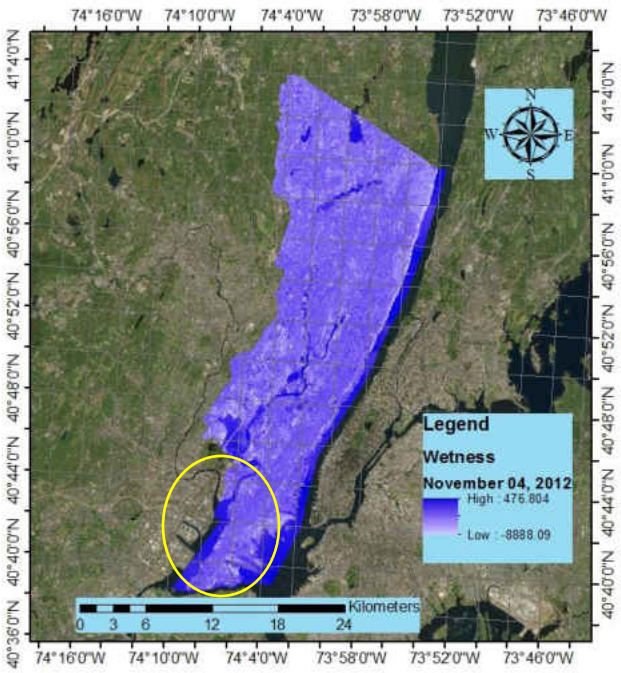

c) November 04, 2012 (After hurricane)

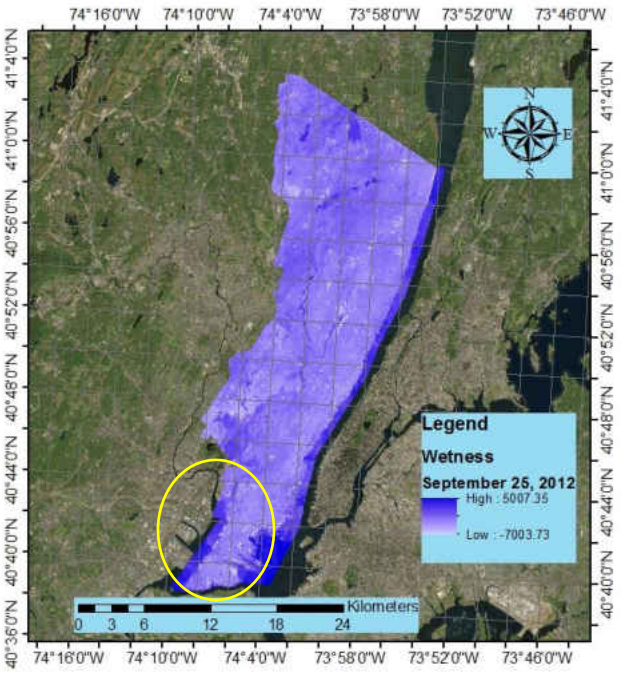

b) September 25, 2012 (Before hurricane)

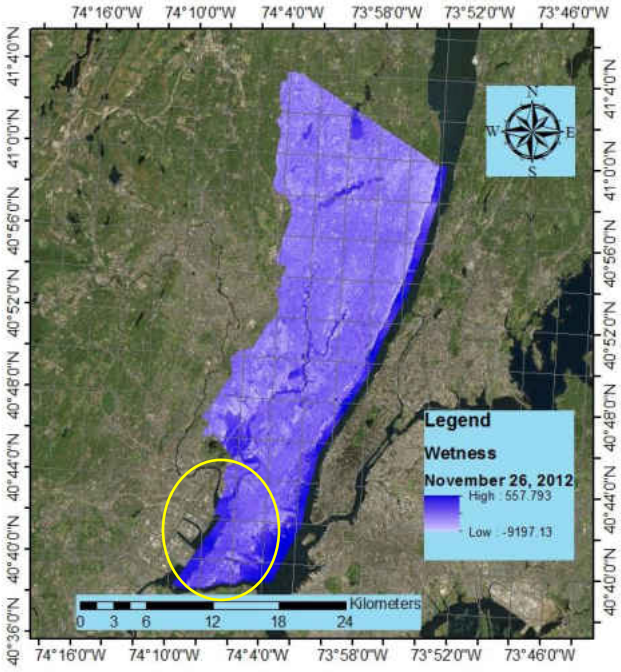

d) November 26, 2012 (After hurricane)

Figure 4-16: Greenness images of Hackensack and Pascack watershed showing before and after conditions of Hurricane Sandy landfall. (a) and (b) represent the conditions before landfall while (c) and (d) represent after landfall condition.

Tasseled cap wetness is an indication of sensitivity towards soil and plant moisture. More particularly, wetness is sensitive to plant canopy moisture (Ciesin, 2017). Before the hurricane impact, the wetness maps show that there is lower wetness in the entire watershed as the reflectance is situated in the lower end of the band (Fig. 4-16a, 4-16c). After hurricane made impact, the heavy rains and the subsequent flooding caused by tidal surges have contributed to the increase in the soil moisture and decrease in plant canopy moisture content as depicted in the maps (Fig. 4-16b, 4-16d). The southwest part of the watershed (encircled in yellow) shows an increase in moisture content six days after hurricane landfall (Fig. 4-16b). The moisture content looked largely unchanged on November 26, 2012; almost one month after hurricane landfall (Fig. 4-16d). In the northeastern corner of the watershed, where the density of vegetation is highest as indicated in the false color and greenness maps, the plant canopy moisture is greater in the maps before the hurricane landfall. After landfall, due to damage suffered by plant canopy, the wetness or moisture content of plant canopy shows lower reflectances (Fig. 4-16b, 4-16d)

4.5.4 NDVI Difference Maps

Vegetation of a watershed area undergoes change when hurricane landfall occurs. This change can be more pronounced when it can e shown in a difference map. The difference map is created by subtracting the before map from after map in ArcGIS. This difference map will help show where the vegetation cover was most impacted.

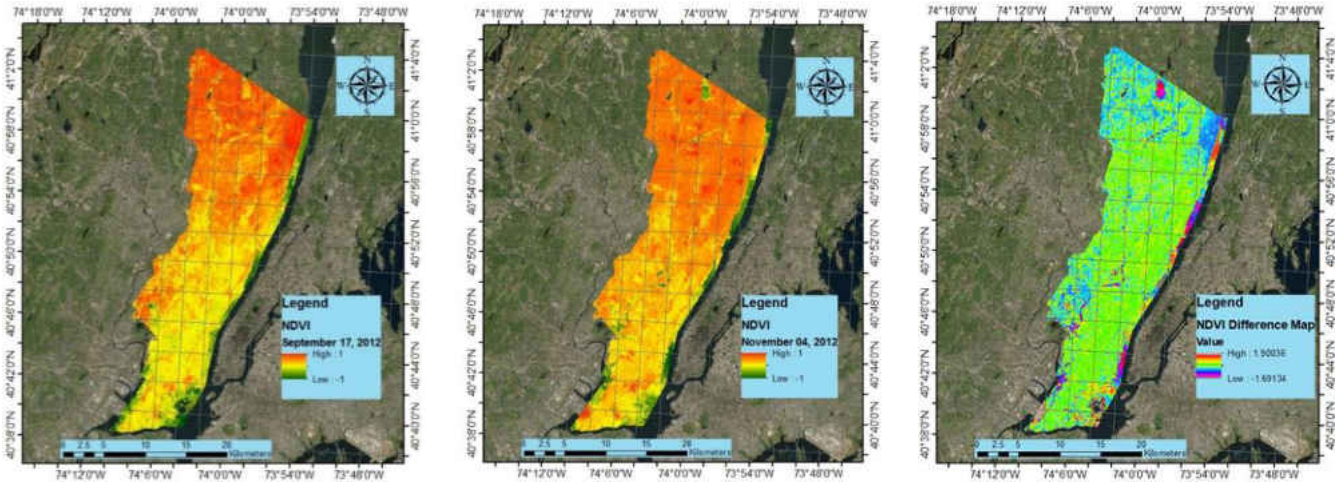

a) Before Landfall b) After Landfall c) NDVI Difference

Figure 4-17: NDVI maps for Hackensack and Pascack Watershed area. Fig. 4-17a is the map for before landfall. Fig. 4-17b is the map after landfall and Fig. 4-17c is the NDVI difference map.

The NDVI difference of the watershed is shown in Fig. 4-17. It accounts for the change in before and after scenario. The vegetation cover in the before landfall scenario shows concentration of vegetative cover on the northern half of the watershed (Fig. 4-17a). After landfall, the changes are evident especially in the northern half (Fig. 4-17b). The difference map clearly shows the change in vegetation in the northern part. The difference in cover is also quite high in the northeastern part of the watershed. In the difference map, the negative values imply more severe change. The difference map was created by subtracting the before-landfall raster from after-landfall raster. Therefore, in the after-landfall raster, if a particular pixel had negative value before and positive value after-landfall, the resulting difference will be negative as the negative value of NDVI indicates diminishing of vegetation cover

4.6 Conclusion

The incorporation of tasseled cap transformation with data fusion is helpful to gain a better understanding of the impact of hurricane on a coastal watershed. This is also a cost effective way to monitor the recovery progress of the vegetation cover of the watershed on a daily basis, provided there are cloud-free satellite images are available. The individual tasseled cap transformation finding can be correlated to the false color renderings of the study area. This provides strong evidence about the ability of the tasseled cap transformation tool as well as the reliability of the data fusion technique to obtain crucial information in a cost effective and time saving manner for environmental monitoring in the event of a natural hazard especially hurricanes.

4.7 References

Adam, E., Mutanga, O., Odindi, J., & Abdel-Rahman, E. M. (2014). Land-use/cover classification in a heterogeneous coastal landscape using RapidEye imagery: evaluating the performance

of random forest and support vector machines classifiers. *International Journal of Remote Sensing*, *35*(10), 3440-3458.

Anderson, G. L., Hanson, J. D., & Haas, R. H. (1993). Evaluating Landsat Thematic Mapper derived vegetation indices for estimating above-ground biomass on semiarid rangelands. *Remote sensing of Environment*, *45*(2), 165-175.

Ban, Y., Hu, H., & Rangel, I. M. (2010). Fusion of Quickbird MS and RADARSAT SAR data for urban land-cover mapping: Object-based and knowledge-based approach. *International Journal of Remote Sensing*, *31*(6), 1391-1410.

Blake, E. S., Kimberlain, T. B., Berg, R. J., Cangialosi, J. P., & Beven II, J. L. (2013). Tropical cyclone report: Hurricane sandy. *National Hurricane Center*, *12*, 1-10.

Carlson, T. N., & Ripley, D. A. (1997). On the relation between NDVI, fractional vegetation cover, and leaf area index. *Remote sensing of Environment*, *62*(3), 241-252.

Chandrasekar, K., Sesha Sai, M. V. R., Roy, P. S., & Dwevedi, R. S. (2010). Land Surface Water Index (LSWI) response to rainfall and NDVI using the MODIS Vegetation Index product. *International Journal of Remote Sensing*, *31*(15), 3987-4005.

Chang, N. B., Vannah, B. W., Yang, Y. J., & Elovitz, M. (2014). Integrated data fusion and mining techniques for monitoring total organic carbon concentrations in a lake. International Journal of Remote Sensing, 35(3), 1064-1093.

Chen, B., Huang, B., & Xu, B. (2015). Fine land cover classification using daily synthetic Landsat-like images at 15-m resolution. *IEEE Geoscience and Remote Sensing Letters*, *12*(12), 2359-2363.

Ciesin.org. (2017). *VEGETATION AND SOILS INFORMATION CONTAINED IN TRANSFORMED THEMATIC MAPPER DATA*. [online] Available at: http://www.ciesin.org/docs/005-419/005-419.html [Accessed 24 Jun. 2017].

Crisp.nus.edu.sg. (2017). *Principles of Remote Sensing - Centre for Remote Imaging, Sensing and Processing, CRISP*. [online] Available at: http://www.crisp.nus.edu.sg/~research/tutorial/opt_int.htm [Accessed 24 Jun. 2017].

Crist, E. P., Laurin, R., & Cicone, R. C. (1986, September). Vegetation and soils information contained in transformed Thematic Mapper data. In *Proceedings of IGARSS'86 Symposium* (pp. 1465-1470). Paris: European Space Agency Publications Division.

Dousset, B., & Gourmelon, F. (2003). Satellite multi-sensor data analysis of urban surface temperatures and landcover. *ISPRS journal of photogrammetry and remote sensing*, *58*(1), 43-54.

Friedl, M.A.; McIver, D.K.; Hodges, J.C.F.; Zhang, X.Y.; Muchoney, D.; Strahler, A.H.; Woodcock, C.E.; Gopal, S.; Schneider, A.; Cooper, A.; *et al*. Global land cover mapping from MODIS: Algorithms and early results. *Remote Sens. Environ.* **2002**, *83*, 287–302.

Fu, B., & Burgher, I. (2015). Riparian vegetation NDVI dynamics and its relationship with climate, surface water and groundwater. *Journal of Arid Environments*, *113*, 59-68.

Gao, F., Masek, J., Schwaller, M., & Hall, F. (2006). On the blending of the Landsat and MODIS surface reflectance: Predicting daily Landsat surface reflectance. *Geoscience and Remote Sensing, IEEE Transactions on*, *44*(8), 2207-2218.

Gong, P.; Wang, J.; Yu, L.; Zhao, Y.C.; Zhao, Y.Y.; Liang, L.; Niu, Z.G.; Huang, X.M.; Fu, H.H.; Liu, S.; *et al*. Finer resolution observation and monitoring of global land cover: First

mapping results with Landsat TM and ETM+ data. *Int. J. Remote Sens.* **2013**, *34*, 2607–2654.

Gsp.humboldt.edu. (2017). *Composites*. [online] Available at: http://gsp.humboldt.edu/olm_2015/Courses/GSP_216_Online/lesson3-1/composites.html [Accessed 24 Jun. 2017].

"Highest Winds from Sandy in Massachusetts". WCVB.com. Retrieved 2017-05-15.

"High winds, rain knock out power to thousands in Mass.". Boston.com. Archived from the original on October 30, 2012. Retrieved 2017-05-15.

Hilker, T., Wulder, M. A., Coops, N. C., Linke, J., McDermid, G., Masek, J. G., & White, J. C. (2009). A new data fusion model for high spatial-and temporal-resolution mapping of forest disturbance based on Landsat and MODIS. *Remote Sensing of Environment*, *113*(8), 1613-1627.

Holm, A. M., Burnside, D. G., & Mitchell, A. A. (1987). The development of a system for monitoring trend in range condition in the arid shrublands of Western Australia. *The Rangeland Journal*, *9*(1), 14-20.

Huang, B., Wang, J., Song, H., Fu, D., & Wong, K. (2013). Generating high spatiotemporal resolution land surface temperature for urban heat island monitoring. *IEEE Geoscience and Remote Sensing Letters*, *10*(5), 1011-1015.

Jia, K., Liang, S., Wei, X., Yao, Y., Su, Y., Jiang, B., & Wang, X. (2014). Land cover classification of Landsat data with phenological features extracted from time series MODIS NDVI data. *Remote Sensing*, *6*(11), 11518-11532.

Jia, K., Liang, S., Zhang, N., Wei, X., Gu, X., Zhao, X., ... & Xie, X. (2014). Land cover classification of finer resolution remote sensing data integrating temporal features from

time series coarser resolution data. *ISPRS Journal of Photogrammetry and Remote Sensing*, *93*, 49-55.

Jia, K., Liang, S., Zhang, L., Wei, X., Yao, Y., & Xie, X. (2014). Forest cover classification using Landsat ETM+ data and time series MODIS NDVI data. *International Journal of Applied Earth Observation and Geoinformation*, *33*, 32-38.

Kauth, R. J., & Thomas, G. S. (1976, January). The tasselled cap--a graphic description of the spectral-temporal development of agricultural crops as seen by Landsat. In *LARS Symposia* (p. 159).

Lukina, E. V., Stone, M. L., & Raun, W. R. (1999). Estimating vegetation coverage in wheat using digital images. *Journal of Plant Nutrition*, *22*(2), 341-350.

"Massachusetts Event Reports for October 29–30, 2012". National Climatic Data Center. National Oceanic and Atmospheric Administration. 2013. Retrieved May 15, 2017.

Mkhabela, M. S., Bullock, P., Raj, S., Wang, S., & Yang, Y. (2011). Crop yield forecasting on the Canadian Prairies using MODIS NDVI data. *Agricultural and Forest Meteorology*, *151*(3), 385-393.

Olexa, E. M., & Lawrence, R. L. (2014). Performance and effects of land cover type on synthetic surface reflectance data and NDVI estimates for assessment and monitoring of semi-arid rangeland. *International Journal of Applied Earth Observation and Geoinformation*, *30*, 30-41.

Penuelas, J., Filella, I., & Gamon, J. A. (1995). Assessment of photosynthetic radiation‐use efficiency with spectral reflectance. *New Phytologist*, *131*(3), 291-296.

Pettorelli, N., Vik, J. O., Mysterud, A., Gaillard, J. M., Tucker, C. J., & Stenseth, N. C. (2005). Using the satellite-derived NDVI to assess ecological responses to environmental change. *Trends in ecology & evolution*, *20*(9), 503-510.

Prasad, A. K., Chai, L., Singh, R. P., & Kafatos, M. (2006). Crop yield estimation model for Iowa using remote sensing and surface parameters. *International Journal of Applied Earth Observation and Geoinformation*, *8*(1), 26-33.

Pohl, C., & Van Genderen, J. L. (1998). Review article multisensor image fusion in remote sensing: concepts, methods and applications. *International journal of remote sensing*, *19*(5), 823-854.

Quarmby, N. A., Milnes, M., Hindle, T. L., & Silleos, N. (1993). The use of multi-temporal NDVI measurements from AVHRR data for crop yield estimation and prediction. *International Journal of Remote Sensing*, *14*(2), 199-210.

Quinn, J. W. Band Combinations.–2001. *Access mode: http://web. pdx. edu/emch/ip1/bandcombinations. html*.

Ran, Y. H., Li, X., & Lu, L. (2009). China land cover classification at 1 km spatial resolution based on a multi-source data fusion approach. *Advances in Earth Science*, *24*(2), 192-203.

Rao, Y., Zhu, X., Chen, J., & Wang, J. (2015). An improved method for producing high spatial-resolution NDVI time series datasets with multi-temporal MODIS NDVI data and Landsat TM/ETM+ images. *Remote Sensing*, *7*(6), 7865-7891.

Rouse Jr, J., Haas, R. H., Schell, J. A., & Deering, D. W. (1974). Monitoring vegetation systems in the Great Plains with ERTS.

Scanlon, T. M., Albertson, J. D., Caylor, K. K., & Williams, C. A. (2002). Determining land surface fractional cover from NDVI and rainfall time series for a savanna ecosystem. *Remote Sensing of Environment*, *82*(2), 376-388.

Shimoni, M., Borghys, D., Heremans, R., Perneel, C., & Acheroy, M. (2009). Fusion of PolSAR and PolInSAR data for land cover classification. *International Journal of Applied Earth Observation and Geoinformation*, *11*(3), 169-180.

Singh, K. K., Vogler, J. B., Shoemaker, D. A., & Meentemeyer, R. K. (2012). LiDAR-Landsat data fusion for large-area assessment of urban land cover: Balancing spatial resolution, data volume and mapping accuracy. *ISPRS Journal of Photogrammetry and Remote Sensing*, *74*, 110-121.

Solaiman, B., Pierce, L. E., & Ulaby, F. T. (1999). Multisensor data fusion using fuzzy concepts: application to land-cover classification using ERS-1/JERS-1 SAR composites. *IEEE Transactions on Geoscience and Remote Sensing*, *37*(3), 1316-1326.

Van Genderen, J. L., & Pohl, C. (1994). Image fusion: Issues, techniques and applications. In *Intelligent Image Fusion, Proceedings EARSeL Workshop, Strasbourg, France* (Vol. 11, pp. 18-26).

Vermote, E. F., Kotchenova, S. Y., & Ray, J. P. (2008). MODIS surface reflectance user's guide. *MODIS Land Surface Reflectance Science Computing Facility, version*, *1*.

Vorovencii, I. (2007). Use of the "Tasseled Cap" transformation for the interpretation of satellite images. *Cadastre J. RevCAD*, *7*, 75-82.

Wang, Q., Adiku, S., Tenhunen, J., & Granier, A. (2005). On the relationship of NDVI with leaf area index in a deciduous forest site. *Remote sensing of environment*, *94*(2), 244-255.

Watkins, T. (2005). The Tasseled Cap transformation in remote sensing. *Available online ataccessed*, *14*.

Weng, Q., Fu, P., & Gao, F. (2014). Generating daily land surface temperature at Landsat resolution by fusing Landsat and MODIS data. *Remote Sensing of Environment*, *145*, 55-67.

Wu, P., Shen, H., Ai, T., & Liu, Y. (2013). Land-surface temperature retrieval at high spatial and temporal resolutions based on multi-sensor fusion. *International Journal of Digital Earth*, *6*(sup1), 113-133.

Wu, P., Shen, H., Zhang, L., & Göttsche, F. M. (2015). Integrated fusion of multi-scale polar-orbiting and geostationary satellite observations for the mapping of high spatial and temporal resolution land surface temperature. *Remote Sensing of Environment*, *156*, 169-181.

Yengoh, G. T., Dent, D., Olsson, L., Tengberg, A. E., & Tucker, C. J. (2014). The use of the normalized difference vegetation index (NDVI) to assess land degradation at multiple scales: A review of the current status, future trends, and practical considerations. *Lund University Center for Sustainability Studies (LUCSUS), and the Scientific and Technical Advisory Panel of the Global Environment Facility (STAP/GEF)*.

Zhang, B., Zhang, L., Xie, D., Yin, X., Liu, C., & Liu, G. (2015). Application of synthetic NDVI time series blended from Landsat and MODIS data for grassland biomass estimation. *Remote Sensing*, *8*(1), 10.

Zhu, X., Chen, J., Gao, F., Chen, X., & Masek, J. G. (2010). An enhanced spatial and temporal adaptive reflectance fusion model for complex heterogeneous regions. *Remote Sensing of Environment*, *114*(11), 2610-2623.

CHAPTER 5: FINAL REMARKS AND CONCLUSION

5.1 Summary of Current Work

The research presented in this thesis proves that remote sensing technologies are a useful and reliable tool in the reconstruction of water quality maps of an estuary to monitor the situation of the parameters before and after hurricane landfall. The satellite images provided the necessary data that helped link the derived data with the ground truth data. This linkage helped create the parameter derivation models the end result of which were the water quality concentration maps. These concentration maps demonstrated the condition of TOC and SSS in the Mattapoisett Harbor bay area, including the mouth of the Mattapoisett River where it discharges out to bay. The before and after hurricane landfall conditions show that the levels of TOC and SSS were not high; in fact they were low. This helped allay fears about salt water intrusion into the drinking water supply wells that is in the Mattapoisett river watershed area. The TOC levels were also low which indicates that there is low chance of disinfection by-products formation when the water is treated.

In the second phase of the research, the effect of hurricane landfall on coastal watershed was explored in detail. The remote sensing tools used for this purpose were tasseled cap transformation and NDVI. The tasseled cap transformation provided information on the soil moisture, canopy cover and vegetation cover of the Mattapoisett river watershed. In addition, the tasseled cap plots for after landfall demonstrated phenomenal changes in the watershed cover conditions. The qualitative findings were backed up quantitate proofs in form of statistical analysis and box plots. To give a certain level of credibility to this research, the same works were done for the very recent Hurricane Irma that made landfall in Big Cypress Swamp watershed of Florida. The qualitative and quantitative results confirm the use of TCT plots as a land cover monitoring tool in the event of a hurricane.

The previous two studies were done with the help of Landsat satellite images, which did prove to of great use. However, Landsat satellites have an inherent disadvantage. That is these satellites have low temporal resolution. The revisit time of Landsat satellites for a given area is 16 days. In order to effectively monitor a change in landscape after a hurricane landfall, it is desirable to have higher temporal resolution. MODIS satellites solve the problem of low temporal resolution although the spatial resolution is compromised due to this. Data fusion provides solution to this dilemma by providing high spatial and temporal resolution images for the missing Landsat revisit days. This advantage was utilized for Hackensack and Pascack watershed where Hurricane Sandy made landfall in 2012. Fused images were generated for cloud-free days and combination of TCT, NDVI and false color observations were made to observe the effects of hurricane landfall. The results from this research proved that data fusion is an effective tool for landscape monitoring in combination with TCT. If these monitoring systems can be implemented on a large scale basis, then this will help if effective disaster management.

5.2 Scope of Future Work

- Water quality prediction models may be improved using non-linear regression technique such as polynomial regression, logistic regression etc.
- The prediction models may be further improved by using machine learning techniques such as Artificial Neural Networks, Extreme Learning Machine, Convoluted Neural Networks etc. for calibration and validation purposes.
- In addition to data fusion, data merging may be used for improvement and comparison of fused images in monitoring land cover changes. Other data fusion algorithms such as ESTARFM and other satellite sensors such as MERIS, ASTER, Sentinel etc. may also be utilized for improvement and comparison studies.

- Further studies and research to develop models for other water quality parameters such as chlorophyll, suspended matters etc. may be undertaken to have a greater understanding of the effect of hurricane landfall on estuaries.